(NASA-CR-128607) EVALUATION OF NONDESTRUCTIVE TESTING D.A. Tiede (McDonnell-Douglas Astronautics Co.) Jul. 1972 136 p CSCL 22B

N73-10893

Unclas
G3/31 45732

EVALUATION OF NONDESTRUCTIVE TESTING TECHNIQUES FOR THE SPACE SHUTTLE NONMETALLIC THERMAL PROTECTION SYSTEM

by D. A. Tiede

Prepared under Contract NAS9-12180
McDonnell Douglas Astronautics Company
5301 Bolsa Avenue, Huntington Beach, California 92647

JULY 1972

For

Manned Spacecraft Center
Houston, Texas 77058

NATIONAL AERONAUTICS AND SPACE ADMINISTRATION

MDC G3678

CR-128607

EVALUATION OF NONDESTRUCTIVE TESTING TECHNIQUES FOR THE SPACE SHUTTLE NONMETALLIC THERMAL PROTECTION SYSTEM

by D. A. Tiede

Prepared under Contract NAS9-12180
McDonnell Douglas Astronautics Company
5301 Bolsa Avenue, Huntington Beach, California 92647

JULY 1972

Details of illustrations in this document may be better studied on microfiche

For

Manned Spacecraft Center
Houston, Texas 77058

NATIONAL AERONAUTICS AND SPACE ADMINISTRATION

ABSTRACT

A program was conducted to evaluate nondestructive analysis techniques for the detection of defects in rigidized surface insulation (a candidate material for the Space Shuttle thermal protection system). Uncoated, coated, and coated and bonded samples with internal defects (voids, cracks, delaminations, density variations, and moisture content), coating defects (holes, cracks, thickness variations, and loss of adhesion), and bondline defects (voids and unbonds) were inspected by x-ray radiography, acoustic, microwave, high-frequency ultrasonic, beta backscatter, thermal, holographic, and visual techniques. Additional uncoated samples with density variations were inspected using x-ray radiography and microwave reflection techniques and subsequently tested to determine their tensile strength. The detectability of each type of defect was determined for each technique (when applicable). A possible relationship between microwave reflection measurements (or x-ray-radiography density measurements) and the tensile strength was established. A possible approach for in-process inspection using a combination of x-ray radiography, acoustic, microwave, and holographic techniques was recommended.

ACKNOWLEDGMENTS

This program was conducted with the cooperation and support of the Space Shuttle program and the rigidized surface insulation material development program at McDonnell Douglas Astronautics Company – East.

The author wishes to acknowledge the early work performed on this program by Mr. J. S. Evangelides.

PRECEDING PAGE BLANK NOT FILMED

CONTENTS

Preceding page blank

PRECEDING PAGE BLANK NOT FILMED

FIGURES

Preceding page blank

TABLES

Section 1
INTRODUCTION

The thermal protection system (TPS) is one of the most vital systems of the Space Shuttle vehicle. The TPS will carry aerodynamic loads and protect the crew, cargo, propulsion system, and other critical systems from reentry heating. A local failure in this system might cause catastrophic failure and loss of an entire vehicle. Consequently, techniques are required for determining the integrity of the TPS. Nondestructive testing (NDT) techniques are particularly suited for inspection of TPS integrity.

The application of nondestructive analysis techniques for in-process monitoring or initial qualification differs somewhat from that for reuse qualification. The use of these techniques for in-process monitoring may be a cost-effective tool for material screening, fabrication, and characterization. These techniques can also measure the effectiveness of the processing methods by application after specific processing steps. Identification of processing difficulties can lead to more effective process specifications and procedures. The initial qualification of a TPS component may be considerably simplified through the in-process detection of defects and measurement of material properties. Prior to assembly, the components are accessible for detailed inspection. Selection of techniques for reuse qualification will be influenced by the accessibility of the components on the Space Shuttle and the detection capabilities of each technique.

Rigidized surface insulation (RSI) is an attractive material for the Shuttle TPS because of its availability, low cost, temperature overshoot capability, and potential weight savings. The prime effort of this program is the identification and evaluation of NDT techniques as applied to RSI material. This program includes:

A. Experimental evaluation using laboratory-controlled samples of RSI with and without various realistic defects to determine the sensitivity and resolution of each NDT technique.

B. Application of selected NDT techniques to natural in-process defects.

C. Application of selected techniques for in-process material evaluation and subsequent correlation of NDT data with mechanical properties.

D. Recommendations of NDT techniques for an in-process quality control program.

E. Identification of NDT techniques for the requalification of the RSI thermal protection system.

Section 2
TECHNICAL APPROACH AND RESULTS

The purpose of this program was to identify and evaluate NDT techniques to ensure the uniformity of rigidized surface insulation materials. The major portion of the program treats the nondestructive evaluation of samples containing artificial defects at various points in the fabrication sequence. In addition, an in-process inspection was conducted on material screening and natural defect samples to establish a relationship between NDT data and mechanical properties. The approach used in this program is described in the following sections.

2.1 BACKGROUND

The thermal protection system for the Space Shuttle must protect the primary vehicle structure and other vehicle subsystems during ascent and reentry. This system requires a lightweight, cost-effective, temperature-resistant material with low thermal conductivity and high emissivity to protect the metallic structure from the thermal environment of reentry. Nonmetallic, rigidized, external-surface ceramic insulation materials are primary candidates for filling these requirements. An RSI panel consists of a waterproof coating, RSI, elastomeric bond between the RSI and support structure, and support structure, as shown in Figure 2-1. During a typical Shuttle mission, various loads (vibration, acoustic, and heating during launch; push-off during staging; heating during reentry; vibration, and rain or dust erosion during landing; and ground landing) may cause damage and possible failures. Possible failure modes during a mission are also shown in Figure 2-1.

A number of possible defects, material variations, and discrete discontinuities may be introduced into an RSI TPS system during fabrication, during installation on the vehicle, during the mission, or during ground handling. A local failure in this critical system before or during reentry may have catastrophic results. To avoid this, the RSI panels should be evaluated, inspected, and qualified to make sure they are free of critical material anomalies.

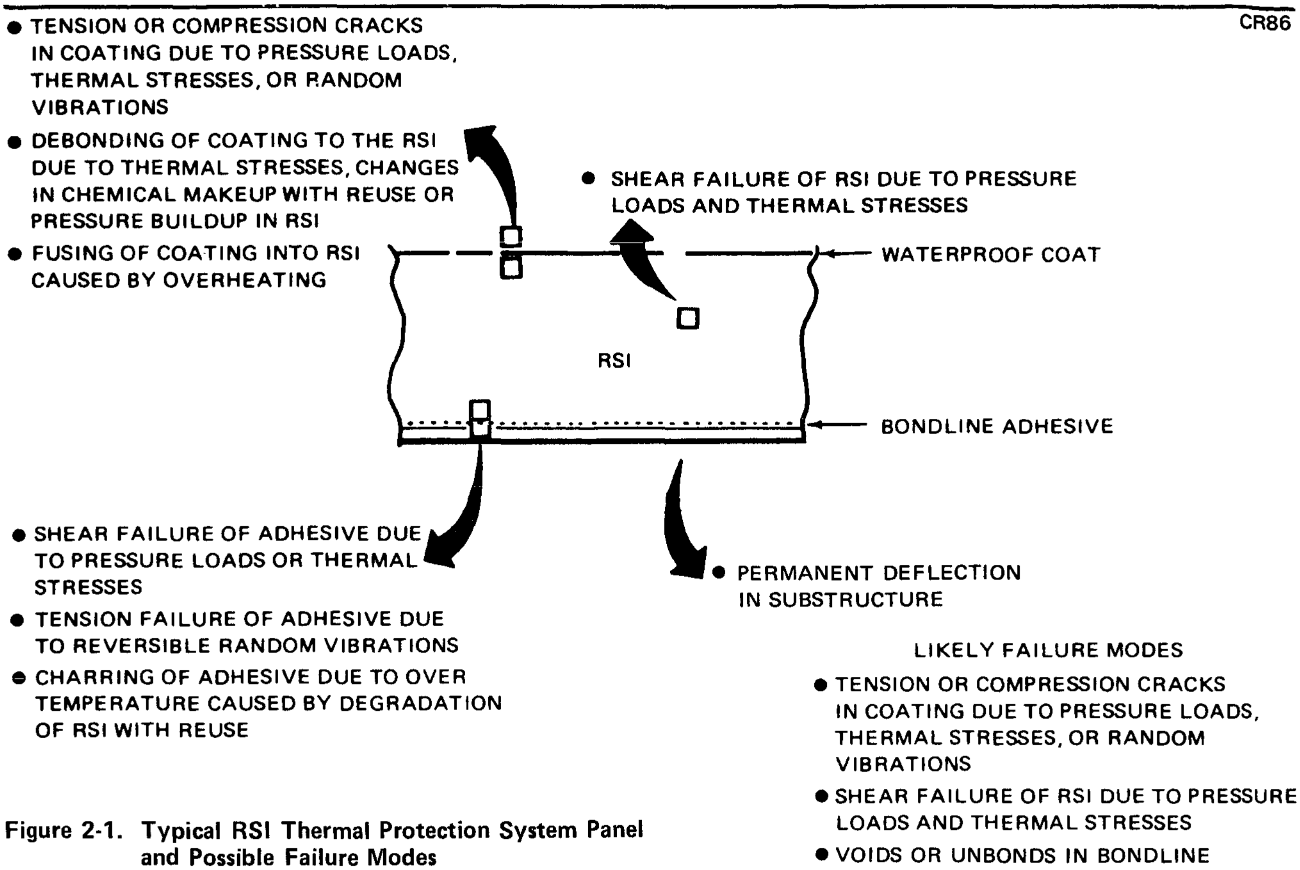

Figure 2-1. Typical RSI Thermal Protection System Panel and Possible Failure Modes

The various RSI defects, material variations, and discrete discontinuities of interest are presented in Table 2-1. Eight techniques—x-ray radiography, acoustic, microwave, high-frequency ultrasonics, beta backscatter, thermal, holographic, and visual—were evaluated for detection of these defects, as described in the following sections.

2.2 SPECIMEN DESCRIPTION

Currently, several varieties of RSI are being developed utilizing different precursor materials, fibers (mullite or silica), binders, and processes. Since all the end products are essentially low-density ceramics, NDT techniques developed for one type should be applicable to the others.

The material used for this program consists of mullite fibers, fillers, and binders, which are fired to obtain a ceramic having a high microvoid content. The material was obtained from current production runs of a materials-development program (NASA Contract NAS9-12082) at McDonnell Douglas Astronautics Company—East (MDAC-E). The material was obtained in three material conditions—uncoated RSI; coated RSI; and coated RSI bonded to a metallic substrate.

Table 2-1

VARIOUS RSI DEFECTS, MATERIAL VARIATIONS, AND DISCRETE DISCONTINUITIES

Material	Processing Step	Possible Defects
Uncoated RSI material	Firing	RSI Defects Voids Cracks Delaminations Inclusions Density variations Moisture (absorbed after firing)
Coated RSI	Coating and firing	Coating Defects Cracks Holes Inclusions Delaminations Thickness variations Adhesion to RSI Coated RSI defects Similar to uncoated RSI material
Adhesive bond	Bonding to support structure	Bond Defects Void Unbond

Three material thicknesses were used—2, 1, and 1/4 in. These thicknesses are representative of those being considered for Orbiter use. Three coating thicknesses were used—0.022, 0.015, and 0.010 in.

The metallic substrate (0.020-inch-thick aluminum plate) and adhesive (General Electric RTV560 Silicone Adhesive) were selected in cooperation with NASA as a cost-effective method of simulating an RSI bonded panel.

Since initiation of this program, several different design options for attachment of RSI to structure have been proposed. Each of these designs will have an impact upon the type of NDT required for the bonded assembly.

A series of samples was fabricated from the material obtained, as shown in Table 2-2. This table provides the material condition, dimensions, types of defects, defect dimensions, density, and NDT techniques employed for each sample. The defect dimensions are listed for each type of defect in the order shown in Figure 2-2. The void defects in the RSI were made using flat-bottomed drills of various sizes as required. The crack and delamination defects in the RSI were made using shim stock of various dimensions as required. Holes in the coating were made using drills of various sizes as required. The holes were drilled just deep enough to penetrate the coating. Several methods (thermal shock, machining) were employed in an attempt to create controlled coating crack defects. It was not possible to create controlled crack defects without damaging the material. Consequently, natural cracks were employed whenever possible. The bondline void defects were made by applying no adhesive to the two adherends in the region desired to be a void. The final dimensions of defects created in this manner depended upon the amount of adhesive flow as the two adherends were placed in contact. The bondline unbond condition was simulated by placing a piece of 0.001-in.-thick Mylar of the desired dimensions in the bondline. Whether this method actually simulated an unbond condition is debatable.

2.3 PROGRAM PLAN

Eight NDT techniques (x-ray radiography, acoustic, microwave, high-frequency ultrasonic, beta backscatter, thermal, holographic, and visual) were employed on samples fabricated from material at different stages in the processing cycle (uncoated, coated, and coated and bonded) as shown in Table 2-3. This table identifies, by sample number, the samples used in the evaluation of each technique.

Each NDT technique was evaluated in detail to establish a critical and thorough inspection technique. An attempt was made to determine the sensitivity and resolution of each technique capable of detecting a given

Table 2-2

SAMPLE DESCRIPTION

Sample No.	Material Condition	Dimensions (in.) L	W	T	Description	Defect Dimensions (in.) (See Figure 2-2)	Density (lb/ft^3)	Technique X	A	M	U	B	T	H	V
1	Uncoated	3.5	3.5	2	Control, moisture		13.5		A	M					V
2	Uncoated	3.5	3.5	2	Void	1.0 dia x 0.75 deep	15.0		A	M					
3	Uncoated	3.5	3.5	2	Void	0.5 dia x 2.25 deep side drilled	15.0		A						
5	Uncoated	3.5	3.5	2	Density		16.1		A						
6	Uncoated	5	1	2	Control	$t = 2.0$, $a_1 = 0.075$, $a_2 = 0.150$, $h_1 = 0.195$, $h_2 = 0.200$, $\ell = 5.0$ slots	17.9	X							
7	Uncoated	2	2	2	Void	(0.016, 0.032, 0.064, 0.128) dia x 0.5 deep, (0.018, 0.032, 0.064) dia x 1 deep side drilled	16.7	X							V
8	Uncoated	2	2	2	Crack	0.5 x 0.5 x (0.002, 0.006, 0.012, 0.020)	15.5	X							V
9	Uncoated	2	2	2	Delamination	0.5 x 0.5 x (0.012, 0.025, 0.048)	17.0	X							V
10	Uncoated	3	1	1	Control	$t = 1.0$, $a_1 = 0.245$, $a_2 = 0.270$, $h_1 = 0.130$, $h_2 = 0.125$, $\ell = 3.0$ slots	14.7	X							
11	Uncoated	2	1	1/4	Control	$t = 0.26$, $a_1 = 0.90$, $a_2 = 0.17$, $h_1 = 0.10$, $h_2 = 0.095$, $\ell = 2.97$ slots	12.6	X							
13	Uncoated	3.5	3.5	1	Delamination	1.5 x 2.5 x 0.025	14.5		A						
14	Uncoated	3.5	3.5	1/4	Control, moisture		13.7		A	M					V
15	Uncoated	3.5	3.5	1/4	Delamination	1.5 x 2.5 x 0.005	14.9		A						
16	Uncoated	3.5	3.5	1	Density, moisture		11.8	X	A	M					
17	Uncoated	2	2	1	Void	(0.016, 0.032, 0.064, 0.128) dia x 0.5 deep, (0.016, 0.022, 0.032) dia x 5 deep side drilled	18.5	X							V
18	Uncoated	2	2	1/4	Void	(0.016, 0.032, 0.064, 0.128) dia x 0.125 deep, (0.016, 0.072, 0.032) dia x 0.125 deep side drilled	16.2	X							V
19	Uncoated	2	2	1	Delamination	0.5 x 0.5 x (0.013, 0.022, 0.035)	12.8	X							V
20	Uncoated	2	2	1/4	Delamination	0.5 x 0.5 x (0.012, 0.018, 0.022)	16.7	X							V
21	Coated	3.5	3.5	2	Control, coating thickness, moisture	0.015 coating	11.1	X		M					
22	Coated	3.5	3.5	2	Control, coating thickness	0.022 coating	12.4	X		M					
23	Coated	3.5	3.5	2	Control, coating thickness	0.010 coating	16.2	X		M					
24	Coated	6	1	2	Control, coating hole, crack	0.013, 0.016, 0.032, 0.064 dia holes in coating	17.2	X				B	T		V
26	Coated	3.5	3.5	2	Coating loss of adhesion	1.5 x 2.0 x 0.015	12.1	X	A	M			T		

Key
X = X-ray Radiography; A = Acoustic; M = Microwave; U = High-Frequency Ultrasonic; B = Beta Backscatter; T = Thermal; H = Holography; V = Visual.

Table 2-2

SAMPLE DESCRIPTION (Continued)

Sample No.	Material Condition	Dimensions (in.) L	W	T	Description	Defect Dimensions (in.) (See Figure 2-2)	Density (lb/ft^3)	Technique X	A	M	U	B	T	H	V
27	Coated	3.5	3.5	1/4	Control, coating thickness, moisture		19.7		A	M					
28	Coated	3.5	3.5	1/4	Coating loss of adhesion	1.5 x 3.5 x 0.005	20.0		A	M					
29	Coated	12	6	1	Control		14.9							H	
30	Coated	12	6	1	Coating loss of adhesion, cracks	4 x 1/4 x 0.005, miscellaneous cracks	16.4							H	
32	Coated	5	1	1/4	Control, coating hole,	0.013, 0.016, 0.032, 0.064 dia holes in coating	22.6	X							V
34	Coated	5	1	2	Control	t = 2.031, a = 0.060, h = 0.200, ℓ = 5.062 slot	18.1	X							
36	Coated	6	1	2	Void, crack	(0.016, 0.032, 0.064) dia x 0.5 deep, (0.016, 0.020, 0.032, 0.064) dia x 0.5 deep side drilled	18.7	X							
37	Coated	3.5	3.5	2	Control		14.6		A						
38	Coated	3.5	3.5	2	Void	0.5 dia x 2.5 deep side drilled	13.4		A	M					
39	Coated	3.5	3.5	2	Delamination	1.5 x 2.5 x 0.048	14.9		A	M					
41	Coated and Bonded	3.5	3.5	2	Bondline void	3/4-in. dia, previously Sample No. 22	----	X	A	M	U		T		
42	Coated and Bonded	3.5	3.5	2	Control, moisture		----	X	A	M	U		T		
43	Coated and Bonded	3.5	3.5	2	Bondline void	1-1/2 in. dia, previously Sample No. 23	----	X	A	M	U		T		
44	Coated and Bonded	3.5	3.5	2	Unbond	3/4-in. dia, previously Sample No. 37	----	X	A	M	U		T		
45	Coated and Bonded	3.5	3.5	2	Unbond	1-1/2-in. dia,	----	X	A	M	U		T		
46	Coated and Bonded	3.5	3.5	1/4	Control, moisture		----	X	A	M	U				
47	Coated and Bonded	3.5	3.5	1/4	Bondline void	1-1/2-in. dia	----	X	A	M	U				
48	Coated and Bonded	3.5	3.5	1/4	Unbond	1-1/2-in. dia	----	X	A	M	U				
50	Coated and Bonded	3.5	3.5	1	Control, moisture		----			M					
57	Uncoated	3.5	3.5	2	Delamination	1.5 x 2.5 x 0.048	14.3		A	M					
58	Uncoated	3.5	3.5	1	Control		15.3		A	M					V

Key

X = X-ray Radiography; A = Acoustic; M = Microwave; U = High-Frequency Ultrasonic; B = Beta Backscatter; T = Thermal; H = Holography; V = Visual.

Table 2-2
SAMPLE DESCRIPTION (Continued)

Sample No.	Material Condition	Dimensions (in.) L	W	T	Description	Defect Dimensions (in.) (See Figure 2-2)	Density (lb/ft^3)	Technique X	A	M	U	B	T	H	V
D	Coated and Bonded	12	6	1	Bondline void	1-1/2-in. dia	----							H	
E	Coated and Bonded	12	6	1	Unbond	1-1/2-in. dia	----							H	
F	Coated and Bonded	12	6	1	Unbond	3/4-in. dia	----							H	
G	Coated and Bonded	12	6	1	Bondline void	3/4-in. dia	----							H	
25-3	Uncoated	9-in. dia x 2-in. thick			Material screening		----	X	A	M					
ND-1	Uncoated	3	2-3/4	3-1/4	Natural defect		13.9	X		M					
ND-2	Uncoated	3	2-3/4	3-1/4	Natural defect		13.5	X		M					
ND-3	Uncoated	3	2-3/4	3-1/4	Natural defect		13.2	X							
ND-4	Uncoated	3	2-3/4	3-1/4	Natural defect		13.8	X							
ND-5	Uncoated	3	2-3/4	3-1/4	Natural defect		13.3	X							
ND-6	Uncoated	3	2-3/4	3-1/4	Natural defect		12.8	X							
ND-7	Uncoated	3	2-3/4	3-1/4	Natural defect		12.7	X		M					
ND-8	Uncoated	3	2-3/4	3-1/4	Natural defect		13.3	X							
ND-9	Uncoated	3	2-3/4	3-1/4	Natural defect		13.4	X							
ND-10	Uncoated	3	2-3/4	3-1/4	Natural defect		13.1	X		M					
ND-11	Uncoated	3	2-3/4	3-1/4	Natural defect		13.1	X							
ND-12	Uncoated	3	2-3/4	3-1/4	Natural defect		13.4	X							
ND-13	Uncoated	3	2-3/4	3-1/4	Natural defect		14.3	X							
ND-14	Uncoated	3	2-3/4	3-1/4	Natural defect		14.3	X							
ND-15	Uncoated	3	2-3/4	3-1/4	Natural defect		14.4	X							
ND-16	Uncoated	3	2-3/4	3-1/4	Natural defect		14.5	X		M					

Key

X = X-ray Radiography; A = Acoustic; M = Microwave; U = High-Frequency Ultrasonic; B = Beta Backscatter; T = Thermal; H = Holography; V = Visual.

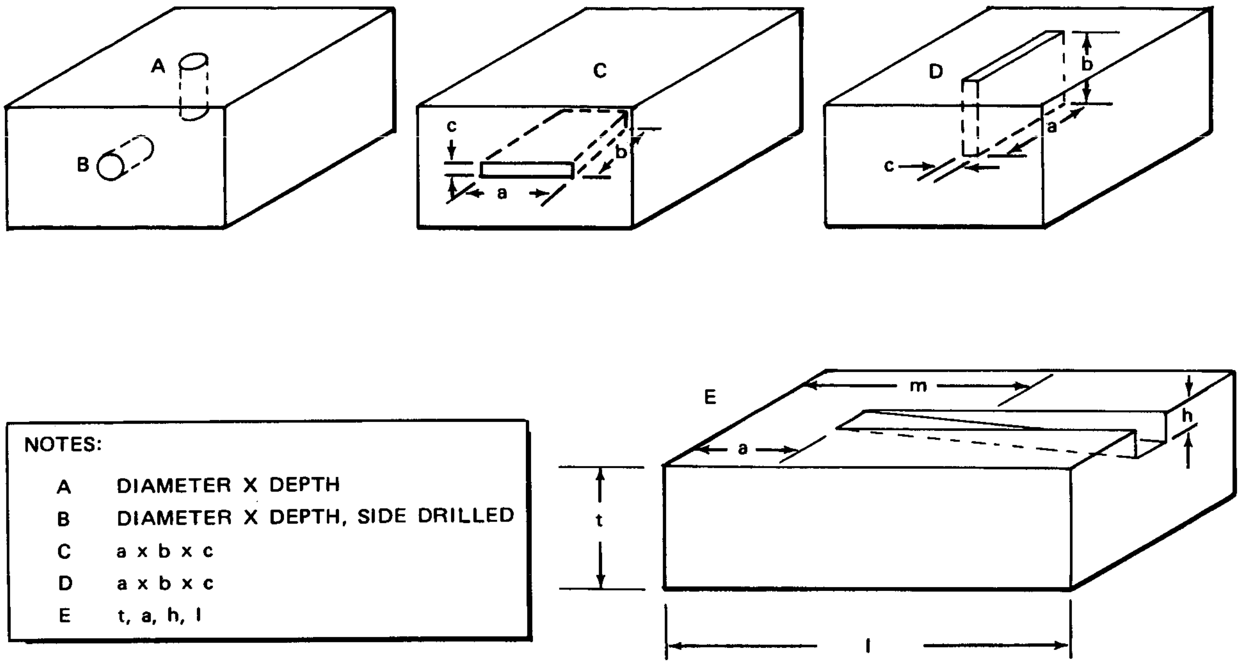

Figure 2-2. Defect Dimensions

defect type. The sensitivity refers to the smallest possible defect detectable while resolution refers to the ability to distinguish between two defects. Emphasis was placed on developing those techniques applicable from the coated surface since access from the metallic substructure side will probably not be possible.

After the NDT techniques were evaluated for the basic RSI material, selected techniques were applied to samples containing natural defects (density variations) to verify the ability of the technique to detect an actual production defect. These techniques were also applied to another sample to verify the ability of the techniques to be used for material screening. Selected portions of the natural defect and material screening samples were then tensile tested to determine if in-process analysis can be correlated with mechanical properties.

Table 2-3

IN-PROCESS APPLICATION OF NDT TECHNIQUES TO SPECIFIC DEFECTS

Uncoated RSI

NDT Technique	Material Thickness (in.)	Control	Void	Cracks	Delamination	Density Variation	Moisture
X-Ray Radiography	2	6	7	8	9		
	1	10	17		19	16	
	1/4	10 11	17 18		19 20	16	
Acoustic	2	1	(2,3)		57	5	
	1	58			13	16	
	1/4	14			15		
Microwave	2	1	2		57		1
	1	58				16	(16, 58)
	1/4	14					14
High Frequency Ultrasonic							
Beta Backscatter							
Thermal							
Holography							
Visual	2	1	7	8	9		
	1	58	17		19		
	1/4	14	18		20		

RSI Coating

NDT Technique	Material Thickness (in.)	Control	Hole	Cracks	Thickness Variation	Loss of Adhesion
X-Ray Radiography	2-RSI 0.022-Coating 0.015-Coating 0.010-Coating	22 21 23	24	24	22 21 23	26
	1/4-RSI 0.015-Coating		32	32		
Acoustic	2-RSI 0.015-Coating	37				26
	1/4-RSI 0.015-Coating	27				28
Microwave	2-RSI 0.022-Coating 0.015-Coating 0.010-Coating	22 21 23			22 21 23	26
High Frequency Ultrasonic						
Beta Backscatter	2-RSI 0.015-Coating	24	24	24		
Thermal	2-RSI 0.015-Coating	24	24	24		26
Holography	1-RSI 0.015 Coating	29		30		30
Visual	2-RSI 0.015-Coating	24	24	24		
	1/4-RSI 0.015-Coating	32	32	32		

Coated RSI

NDT Technique	Material Thickness (in.)	Control	Void	Cracks	Delamination	Moisture
X-Ray Radiography	2-RSI 0.015 Coating	34	36	36		
Acoustic	2-RSI 0.015-Coating	37	38		39	
Microwave	2-RSI 0.015-Coating	21	38		39	21
	1/4-RSI 0.015-Coating	27				27
High Frequency Ultrasonic						
Beta Backscatter						
Thermal						
Holography						
Visual						

Coated and Bonded RSI Panels

NDT Technique	Material Thickness (in.)	Control	Void	Unbond	Moisture
X-Ray Radiography	2-RSI 0.015-Coating 0.020-Aluminum plate	42	(41, 43)	(44, 45)	
	1/4-RSI 0.015-Coating 0.020-Aluminum plate	46	47	48	
Acoustic	2-RSI 0.015-Coating 0.020-Aluminum plate	42	(41. 43)	(44. 45)	
	1/4-RSI 0.015-Coating 0.020-Aluminum plate	46	47	48	
Microwave	2-RSI 0.018-Coating 0.020-Aluminum plate	42	(41, 43)	(44, 45)	42
	1-RSI 0.015-Coating 0.020-Aluminum plate	50			50
	1/4-RSI 0.015-Coating 0.020-Aluminum plate	46	47	48	46
High Frequency Ultrasonic	2-RSI 0.015-Coating 0.020-Aluminum plate	42	(41. 43)	(44, 45)	
	2-RSI 0.015-Coating 0.020-Aluminum plate	46	47	48	
Beta Backscatter					
Thermal	2-RSI 0.015-Coating	42	(41, 43)	(44 45)	
Holography	1-RSI 0.015-Coating 0.020-Aluminum plate		(D, G)	(E, F)	
Visual					

2.4 NONDESTRUCTIVE ANALYSIS TECHNIQUES AND RESULTS

2.4.1 X-ray Radiography

X-ray-radiographic techniques have been applied to RSI materials for the detection of voids, cracks, delaminations, and density variations (Reference 1). Visual inspection of the RSI material alone can be extremely misleading, and internal flaws can go undetected.

The basic evaluation of the x-ray-radiography technique was to optimize the exposure parameters to obtain good contrast and image sharpness (resolution and definition) at the lowest beam voltage consistent with adequate penetration of the material (Reference 2). This was accomplished by conducting a series of radiographs at various voltages in the region of 10 to 50 kV. In addition to voltage, the exposure parameters examined were time, film-to-source distance, and the use of screens to absorb the low-evergy, air-scattered x-rays that can reduce sensitivity. The use of a helium chamber to reduce this air scattering was also evaluated. Kodak Type M film was used throughout the program for this technique. In a previous program, the use of finer grained film (Type R) and coarser grained film (Type AA) was found either to offer no additional advantage or greatly to reduce sensitivity (Reference 3). Major emphasis was placed on developing a clear understanding of the information contained in the x-ray radiograph.

A Penetrex 50-kV x-ray machine was used for the majority of the x-ray exposures. First, a check was made to determine the effective focal-spot size. A 0.010-in.-thick lead screen with a 0.040-in.-dia hole was placed half-way between the source and film using a 24-in. source-to-film distance. This arrangement produces a pinhole picture of the x-ray tube focal spot. The result of a 1-min, 10-ma, 52.5-kV exposure was a square spot of approximately 3.5 mm on a side. Subtracting twice the hole diameter from this to correct for the finite size of the pinhole (Reference 4), the focal spot size was found to be 1.5 mm. This figure will be used later in calculations of geometric unsharpness.

2.4.1.1 Uncoated Samples

Next, selected exposure parameters were determined for 2-in.-, 1-in.-, and 1/4-in.-thick uncoated material through the use of slotted test samples. The current was kept at 10 ma throughout. The parameters investigated were:

A. Source to film distance: 24, 29, 34 in.

B. Voltage: 22.5, 25, 35, 37.5, 45, 47.5 kV.

C. Time: 30 to 180 sec.

D. Screens: 0.008-, 0.004-in.-thick polyethylene.

E. Helium chamber: only for 2-in. material.

The exposure duration was limited to a maximum of 180 sec in order to keep production inspection time within a reasonable value. Exposures were made for various combinations of these parameters, as shown in Table 2-4 for the 2-in.-thick material; Table 2-5 for the 1-in.-thick material; and Table 2-6 for the 1/4-in.-thick material. The sensitivity of each radiograph was then determined. The sensitivity is the size of the smallest detail that can be seen in a radiograph. A typical radiograph is shown

Table 2-4

EXPOSURE PARAMETERS FOR TWO-INCH MATERIAL

Exposure No.	Voltage (kV)	Time (sec)	Distance (in.)	Screen
1	47.5	90	29	None
2		120	29	None
3		150	29	None
4		90	24	None
5		150	24	None
6		150	34	None
7		180	34	None
8	47.5	120	34	None
9	45	180	29	None
10	45	150	29	None
11	47.5	90	29	0.008
12		120	29	0.008
13		150	29	0.008
14		90	29	0.004
15		120	29	0.004
16		120	34	He
17		150	34	He
18	47.5	180	34	He

Table 2-5

EXPOSURE PARAMETERS FOR ONE-INCH MATERIAL

Exposure No.	Voltage (kV)	Time (sec)	Distance (in.)	Screen
1	37.5	60	29	None
2		90	29	None
3		120	29	None
4		30	24	None
5		60	24	None
6		90	24	None
7		90	34	None
8		120	34	None
9	37.5	150	34	None
10	35	150	29	None
11		180	29	None
12		120	29	None
13		150	29	0.008
14	35	150	29	0.004

Table 2-6

EXPOSURE PARAMETERS FOR QUARTER-INCH MATERIAL

Exposure No.	Voltage (kV)	Time (sec)	Distance (in.)	Screen
1	25	60	29	None
2		90	29	None
3		105	29	None
4		30	24	None
5		60	24	None
6		75	24	None
7		90	34	None
8		120	34	None
9		150	34	None
10	22.5	120	29	None
11		150	29	None
12		180	29	None
13		150	29	None
14		180	29	None
15		150	29	0.008
16	22.5	180	29	0.004

in Figure 2-3. The position at which the slot can be barely detected provides a measure of the sensitivity. A formula for the sensitivity percentage is

$$S = 100\frac{s}{t} = 100\,\frac{h(m-a)}{t(l-a)}$$

where t, a, h, l, and m are measured from the sample as shown in Figure 2-2.

The experimental sensitivities obtained using this formula are shown in Table 2-7.

The following conclusions were made based on the measured sensitivities:

A. Two-inch material:
   1. Best sensitivity for 29-in. source-to-film distance.
   2. Best sensitivity for 45 kV (47.5 kV very good).
   3. Polyethylene screen slightly reduces sensitivity.
   4. He chamber provides no advantage.

CR86

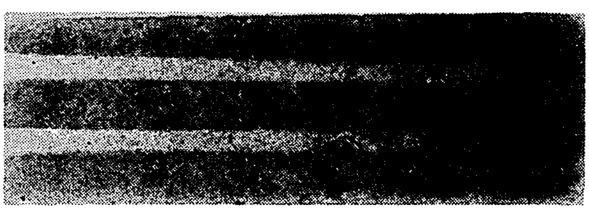

Figure 2-3. Radiograph of 1-In.-Thick Sample No. 10 (Top View)

Table 2-7

AVERAGE SENSITIVITY

Two Inch		One Inch		Quarter Inch	
Exposure (No.)	Sensitivity	Exposure (No.)	Sensitivity	Exposure (No.)	Sensitivity
1-3	1.75	1-3	2.30	1-3	8.7
4-5	1.62	4-6	2.59	4-6	10.8
6-8	1.63	7-9	2.23	7-9	8.8
9-10	1.57	10-12	1.87	10-12	8.4
11-13	1.62	13	2.14	13-14	8.5
14-15	1.71	14	2.09	15-16	8.5
16-18	1.62				

5. Recommended exposure parameters:

$$\left.\begin{array}{c}45\text{ kV}\\150\text{ sec}\\29\text{ in.}\\10\text{ ma}\end{array}\right\}\text{ or }\left\{\begin{array}{c}47.5\text{ kV}\\90\text{ sec}\\29\text{ in.}\\10\text{ ma}\end{array}\right.$$

6. Realistic sensitivity is 1.6 percent.

B. One-inch material:

1. Best sensitivity for 29-in. source-to-film distance.
2. Best sensitivity for 35 kV.
3. Polyethylene screen provides no advantage.
4. Recommended exposure parameters:

   35 kV
   120 sec
   29 in.
   10 ma

5. Realistic sensitivity is 2.2 percent.

C. Quarter-inch material:

1. Best sensitivity for 29-in. source-to-film distance.
2. Best sensitivity at 22.5 kV with 0.004-in.-thick polyethylene screen.

3. Polyethylene screen 0.008 in. thick provides no advantage.
4. Recommended exposure parameters:
   22.5 kV
   150 sec
   29 in.
   10 ma
   0.004-in.-thick polyethylene
5. Realistic sensitivity 8.6 percent.

Using the selected exposure parameters, the void, crack, and delamination samples were evaluated. The void samples contained both top- and side-drilled holes. All the top-drilled holes were detected. These holes ranged in diameter from 0.016 to 0.128 in. and were 0.5 in. deep for the 2- and 1-in.-thick material and 0.125 in. deep for the 1/4-in.-thick material. A resolution of 0.020-in. separation between diameters was easily observed. The results for the side-drilled holes were:

Two-inch material (Sample No. 7)
- 0.018 in. not detected
- 0.032 in. detected—sensitivity of 1.6 percent
- 0.064 in. detected

One-inch material (Sample No. 17)
- 0.016 in. not detected
- 0.022 in. detected—sensitivity of 2.2 percent
- 0.032 in. detected

Quarter-inch material (Sample No. 18)
- 0.016 in. detected—sensitivity of 6.4 percent
- 0.022 in. detected
- 0.032 in. detected

The crack sample contained slots of various widths 0.5 in. deep by 1/4 in. long in material 2 in. thick. The sample was evaluated with the slot oriented parallel to the x-ray beam. All the slots were detected down to a width of 0.003 in. The delamination samples were evaluated with the delamination perpendicular to the x-ray beam. The results were:

Two-inch material (Sample No. 9)

- 0.012 in. wide not detected
- 0.025 in. wide not detected
- 0.048 in. wide just barely detectable—sensitivity of 2.4 percent

One-inch material (Sample No. 19)

- 0.013 in. wide not detected
- 0.022 in. wide detected—sensitivity of 2.2 percent
- 0.035 in. wide detected

Quarter-inch material (Sample No. 20)

- 0.012 in. wide just barely detectable—sensitivity of 4.8 percent
- 0.018 in. wide detected
- 0.022 in. wide detected

In some cases, powder remaining in the slot made the detection more difficult. Successful detection is dependent upon a minimum opening, as determined by the sensitivity for the material thickness.

These results compare favorably with the previous results. The radiographs were difficult to interpret due to the mottled pattern of density variations. The effect became more pronounced as the sample thickness was reduced.

Having experimentally determined the sensitivities for uncoated material, theoretical calculations were made for comparison. Derivation of the necessary equations and the assumptions involved in applying them for RSI material are presented in the Appendix. The theoretical sensitivities obtained were:

Material Thickness (in.)	Sensitivity (%)
2	2.2
1	2.1
1/4	2.6

These values compare favorably with the experimentally determined sensitivities except for the 1/4-in.-thick material. As would be expected for equivalent exposures of a homogeneous material, the theoretical sensitivities were nearly the same for the different material thicknesses. The reason the experimentally determined sensitivity is different for the 1/4-in.-thick material is that the sensitivity is limited by the size of the naturally occurring pores in the material. The pore size is on the order of 0.020 in., which would account for sensitivities of 8 percent in the 1/4-in.-thick material and 2 percent in the 1-in.-thick material. For material thicknesses greater than 1 in., the experimental sensitivity should approach the theoretical value as the effect of pore size becomes negligible.

All the holes in the coating were detected from through-thickness exposures of the hole and crack samples. The holes ranged from 0.013 in. to 0.064 in. in diameter. Edge exposures were taken on the coating-thickness control samples. Measurements of the full coating thickness were then taken from the radiographs. The thicknesses were 0.025 in. for Sample No. 25, 0.030 in. for Sample No. 21, and 0.030 in. for Sample No. 22. For best results, the coating surface must be along the direction of the x-ray beam. These values are somewhat larger than the values obtained from visual measurement of the coating thickness. An edge exposure of the loss-of-adhesion defect showed the coating separation from the RSI to be approximately 0.030 in.

2.4.1.2 Coated Samples

All exposures of coated samples were taken with the coated surface next to the film. A series of different exposures for the control sample containing slots yielded the best sensitivity for the following parameters:

29 in.
45 kV
165 sec
10 ma

The best sensitivity obtained for these parameters was 1.1 percent. These parameters were used to evaluate the void-and-crack coated sample. All the drilled holes were detected with the x-ray beam parallel to the holes. The hole sizes ranged from 0.016 in. to 0.064 in. in diameter. A resolution of 0.0125 in. between hole diameters was obtained. The smallest detectable hole size for an edge exposure was 0.032 in., which leads to a sensitivity of 1.6 percent for 2-in.-thick material, as before.

Through-thickness exposures were taken of all the bonded samples other than those used for the holography evaluation. A typical radiograph is shown in Figure 2-4. All the voids and simulated unbonds using Mylar film were detected. The selected parameters for these radiographs were:

29 in.
50 kV
120 sec for 2-in.-thick material
30 sec for 1/4-in.-thick material
10 ma

CR86

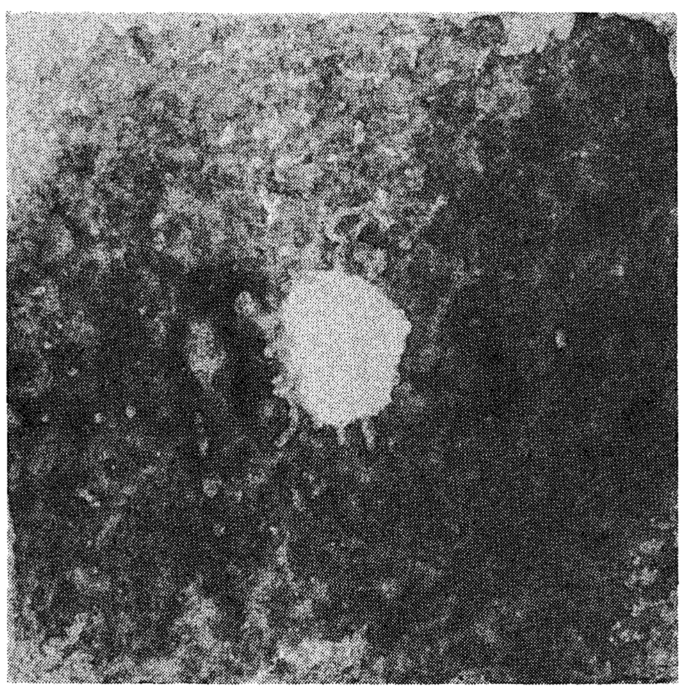

Figure 2-4. Radiograph of 2-In. - Thick Sample No. 41 (Top View)

2.4.2 Acoustic

The interaction of acoustic waves with RSI material may provide a means of nondestructively detecting the presence of defects. This may be accomplished by monitoring the degree to which the RSI absorbs, reflects, or transmits sound as a function of the frequency. Previous work has shown that detection of changes in the vibrational characteristics of low-density foam materials provides a means of identifying internal defects (References 5 and 6). In this work, transmitted and reflected acoustic waves in the 100 to 10,000 Hz ranges were successfully monitored for the detection of unbonds in the adhesive bond between foam and an aluminum plate. Electromagnetically inducing vibrations in the aluminum plate were also shown to be a feasible method of generating acoustic waves in the foam. This work found that direct contact coupling and a small receiving microphone were required for inspection of low-density foam.

In this program, a detailed experimental program was conducted to evaluate transmitted, reflected, and electromagnetically induced vibrations as a means of detecting defects in RSI materials. Frequencies from 500 to 16,000 Hz were employed. Three coupling methods--air coupling, RSI material direct contact coupling, and contact microphone coupling--were evaluated for their effectiveness. Two different diameters (1 and 1/2 in.) for the receiving microphone were evaluated for their sensitivity. The experimental approach used to evaluate the sensitivity of the acoustic technique to intentional defects is described in the following subsections.

2.4.2.1 Acoustic Transmission

The sensitivity of the acoustic transmission technique was evaluated by comparing the transmission of sound from a defect-free RSI control sample with that of similar samples containing known artificial defects. A schematic of the setup used for the transmission measurements is shown in Figure 2-5. A Hewlett-Packard Model 200CD signal generator was used to generate signals from 500 to 16,000 Hz. This signal was amplified by a McIntosh Type A116-B power amplifier until the signal was 4 V from

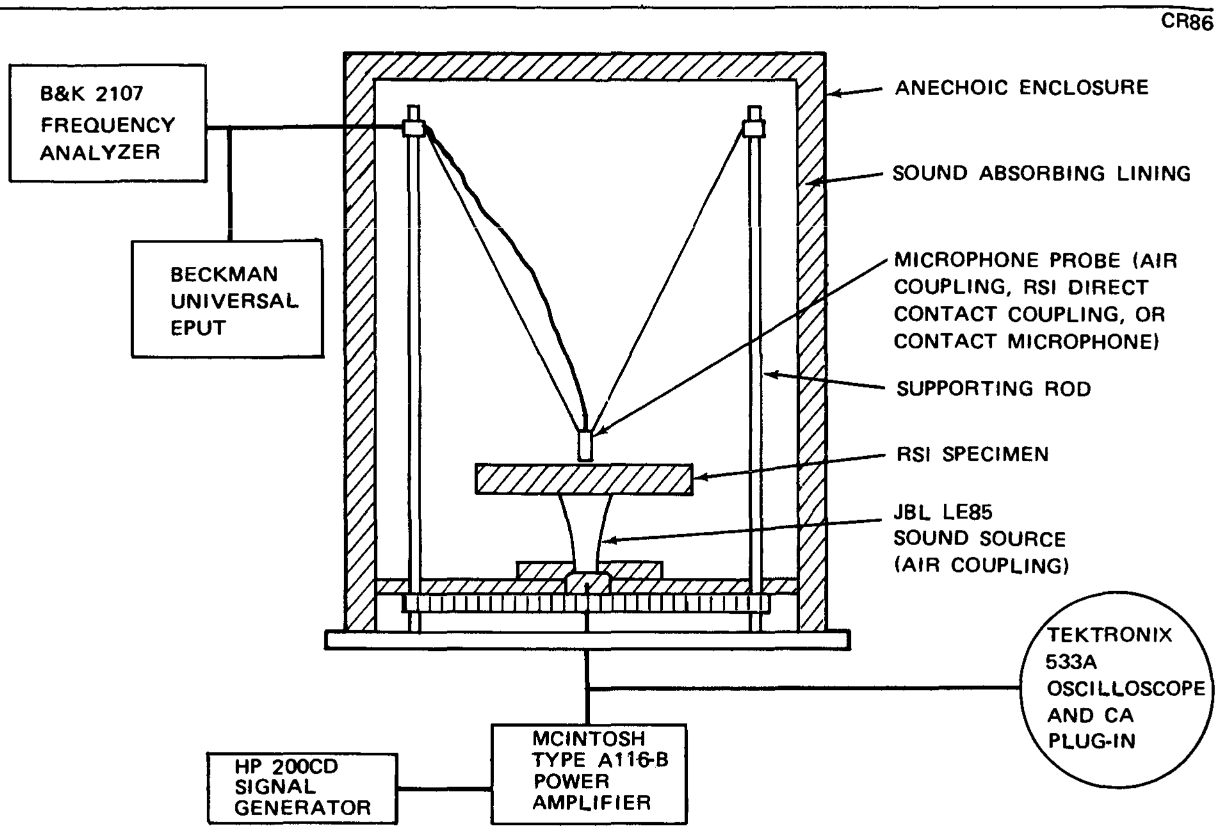

Figure 2-5. Acoustic Transmission Apparatus

peak-to-peak. A Tektronix Model 533A oscilloscope with a Type CA plug-in was used to check the amplitude of the amplified signal. The signal was then introduced into a James B. Lansing Model LE85 horn speaker. The receiving probe was either a Bruel and Kjaer Model 4133 1/2-in. dia condenser microphone, a Bruel and Kjaer Model 4131 1-in. -dia condenser microphone, or an Electro-Voice Model 805 contact crystal microphone. The received signal was then amplified and analyzed using a Bruel and Kjaer Model 2107 Frequency Analyzer. The speaker, material, and microphone were enclosed in an anechoic chamber.

The experimental procedure was as follows. First, the signal generator was set for the desired frequency. The power amplifier was then adjusted to provide the correct signal strength as displayed on the oscilloscope. The output of the signal generator changed as a function of the frequency. The Beckman counter was used to check the frequency output of the signal generator. This procedure was repeated, if necessary, to obtain the desired frequency. Next, the strength of the received signal at the given frequency was measured using the frequency analyzer. This figure was then recorded as the signal amplitude. This entire procedure was repeated for each frequency of interest from 500 to 16,000 Hz in steps of 100 Hz from 500 to 12,000 Hz, and then in steps of 125 Hz from 12,125 to 16,000 Hz.

2.4.2.2 Choice of Coupling

The initial step in the evaluation of the coupling techniques was to run a series of measurements for each frequency with no RSI material between the speaker and the microphone. This air calibration could be used to subtract the response of the speaker, microphone, and electronic equipment from the response obtained with a sample between the speaker and microphone. Since the response from a sample containing a defect was always compared to the response from a defect free control sample, the effect of the overall system response should cancel out. The system response for air using the 1/2-in.-dia microphone is presented in Figure 2-6 merely to show how flat the response was even though the information was not needed for further analysis. A check of the response from the 1/2-in.-dia microphone with the speaker off showed the background noise within the anechoic chamber to be negligible.

Next, the response from a defect free RSI control (Sample No. 1) was obtained using the 1/2-in.-dia microphone. The sample was centered directly on the horn and the microphone was placed approximately 1/64 in. from the back surface of the sample. The results for Control Sample No. 1 are shown in Figure 2-7. As the figure shows, the higher frequencies are more highly attenuated than the lower frequencies. Also, the material clearly introduces some resonances of its own. That is, some frequencies are more readily transmitted than others. The resonances appear to be fairly evenly spaced with a separation of approximately 550 Hz. There was also a prominent resonance at approximately 6,300 Hz. This resonance is definitely due to the material since the resonance was not present in the air calibration.

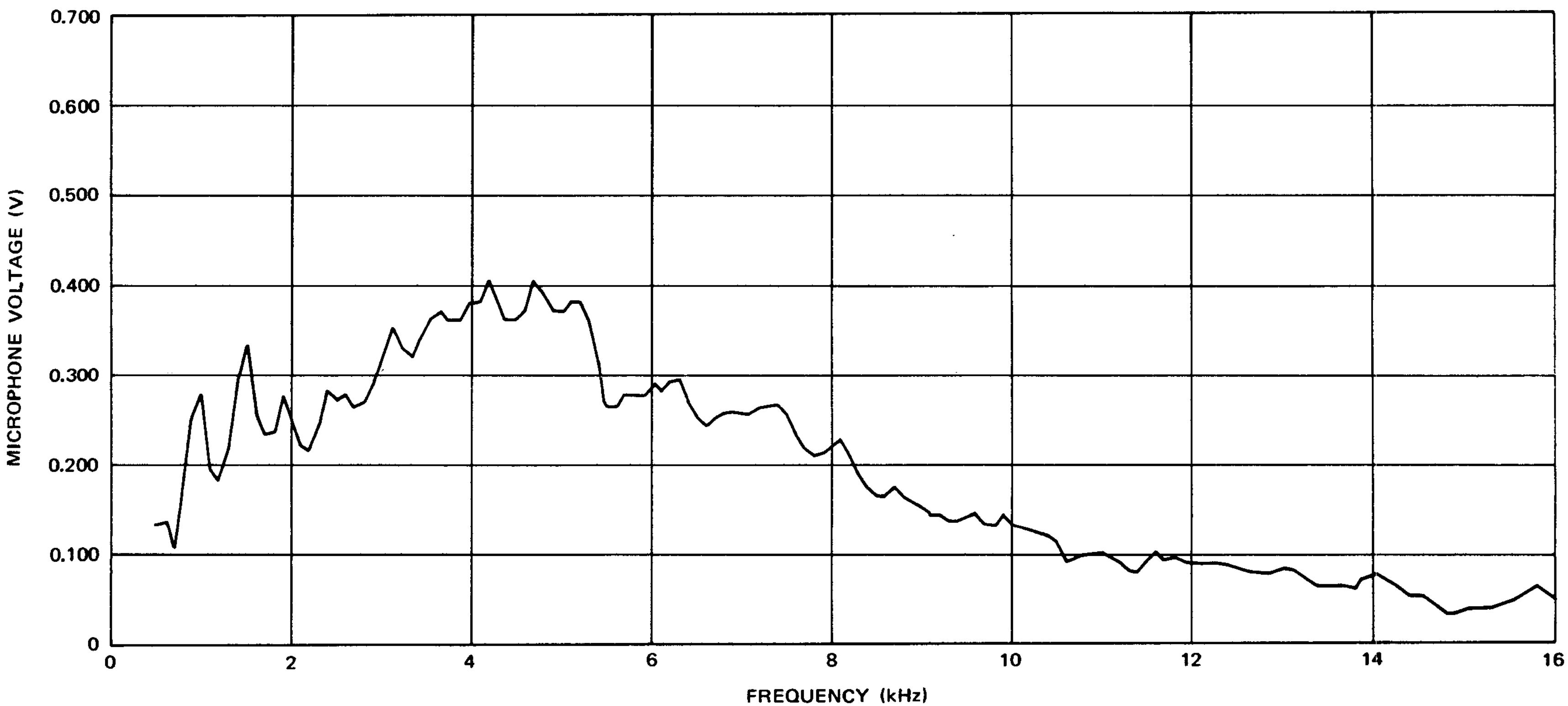

Figure 2-6. Air Calibration

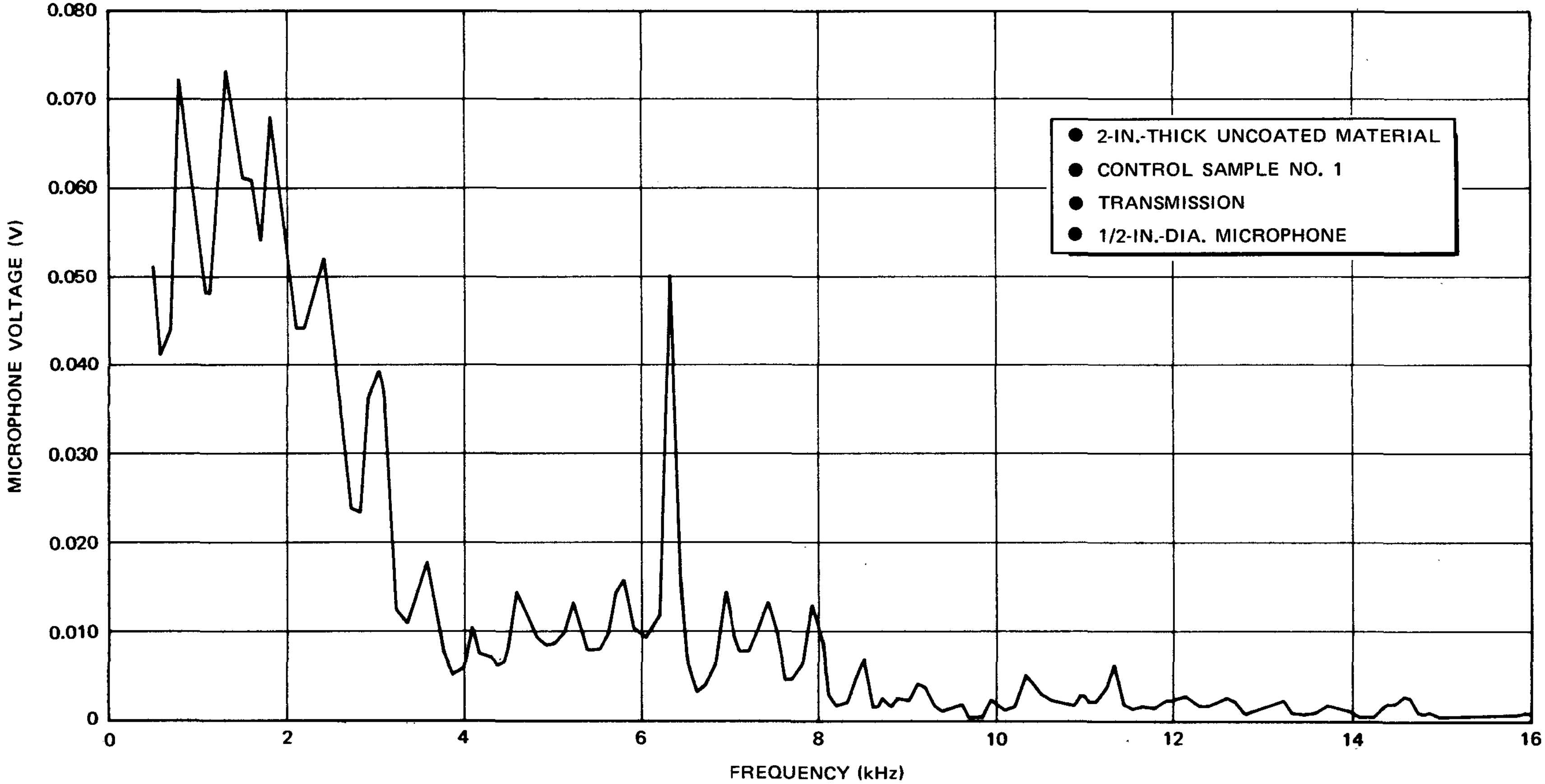

Figure 2-7. Air-Coupling Response for Sample No. 1 (Transmission)

Measurements were also taken using the same procedure for uncoated material containing voids and delaminations. The response from each sample was compared to that of the control by subtracting the response of the defective sample from the corresponding response of the control. A change in response as compared to that of the control is then represented by a deviation from zero. The results for Void Sample No. 2 and Delamination Sample No. 57 are shown in Figure 2-8. As the figure shows, deviations from the control response were obtained from these samples. The greatest change in the response occurred at approximately 6,300 Hz. This is the frequency at which the control sample had a large resonance. Since the difference in the responses at this frequency is positive, this means that the defective samples did not have as large a resonance at this frequency as did the control sample. Generally, the deviations from the control response were greater for the sample containing a delamination defect than they were for the sample containing the void defect. A possible explanation is that two RSI-to-air interfaces are involved for the delamination defect, whereas only one RSI-to-air interface is involved for the void defect since the void defect was simply a hole drilled in the thickness direction.

Measurements were then taken using RSI contact coupling for the same control, void, and delamination samples. The RSI coupling consisted of a block of RSI into which a hole had been drilled. The hole was drilled slightly smaller than the diameter of the 1/2-in.-dia microphone. The microphone was then placed inside this hole and the RSI placed in contact with the sample being evaluated. The response from the control sample using RSI coupling was different from that using air coupling in that a resonance was not present at 6,300 Hz and that the response fell off sharply with increasing frequency. The results for Void Sample No. 2 and Delamination Sample No. 57 are shown in Figure 2-9. Most of the deviations occurred for frequencies below 5,000 Hz.

Next, measurements were taken using contact microphone coupling for the same control, void, and delamination samples as before. A 100-g mass was used to hold the microphone in contact with the sample. Since this mass was observed to move during the test due to vibration, the mass was increased to 200 g, which resulted in a significant increase in the signal response.

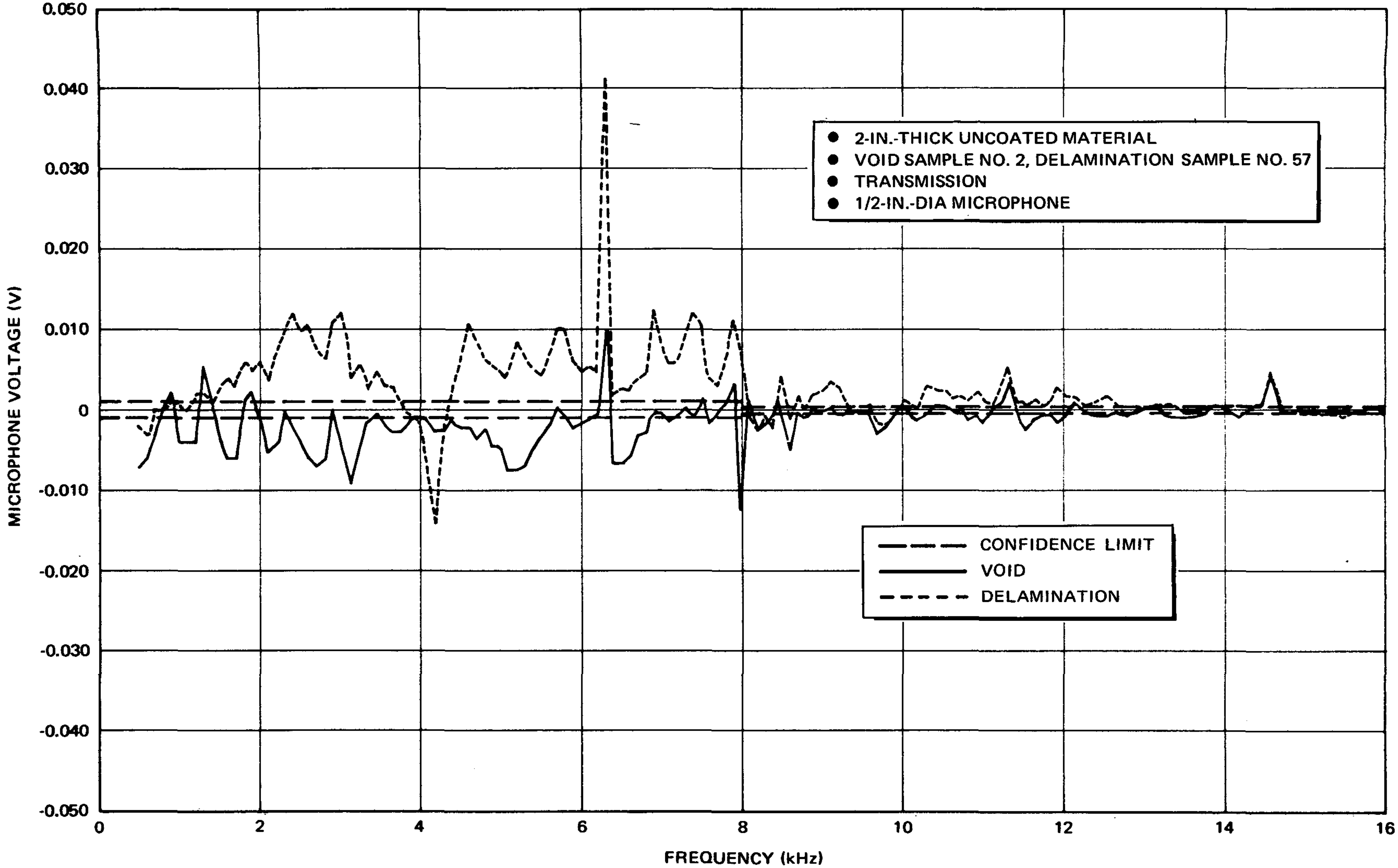

Figure 2-8. Difference in Air-Coupling Response for Samples 2 and 57 (Control Sample No. 1)

CR86

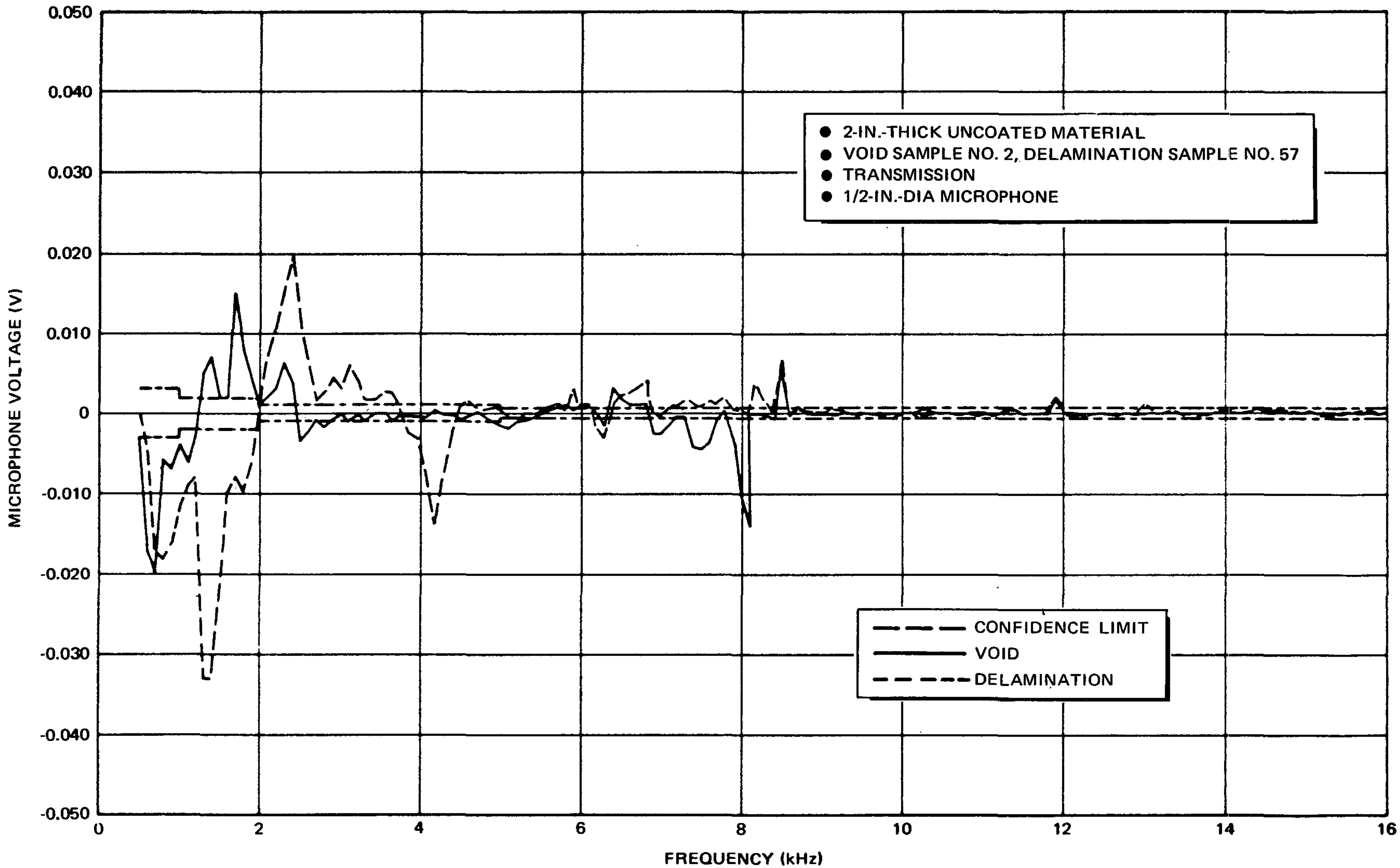

Figure 2-9. Difference in RSI-Coupling Response for Samples 2 and 57 (Control Sample No. 1)

Furthermore, with a total mass of 200 g, the signal response was observed to increase with time. This suggests that the vibration of the contact microphone abrades the high points of the RSI and increases the total effective area in contact with the microphone. Since application of pressure resulted in fluctuations of the response, no mass was used for the final measurements made. The results for Void Sample No. 2 and Delamination Sample No. 57 are shown in Figure 2-10. The difference in response for the void sample was less than the accuracy with which the measurements could be made. The difference in the response for the delamination sample, on the other hand, showed a very large difference at approximately 440 Hz, thus appearing to provide a good criterion for detection of a delamination defect. Unfortunately, the effect of pressure on the contact microphone makes this coupling method difficult to use. This problem and the lack of response to the void defect left the choice of coupling method between air coupling and RSI contact coupling. Contact microphone coupling, however, should provide a good check for any delamination defects revealed by another coupling method.

In an attempt to decide between air coupling and RSI contact coupling, measurements using both techniques were taken on another control sample whose density differed significantly from that of the previous control, but which was still within specifications. Sample No. 5 with a density of 16.1 lb/ft^3 was used for this purpose. The density of Sample No. 1 was 13.5 lb/ft^3. The results for air and RSI coupling are shown in Figure 2-11. It would be desirable if the response from defect-free samples of different densities within the allowable ranges were similar. In this regard, the difference in response was smaller over a larger frequency range for the air coupling than for the RSI coupling. The difference in air coupling responses still showed a resonance at approximately 6,300 Hz. This suggests that perhaps the response from Control Sample No. 1 is not typical.

A better procedure would be to perform many such measurements on as many control samples as possible, and then to prepare an average response which would minimize the deviation of any one particular control sample from the average. In this case, a measure of a significant deviation from the average

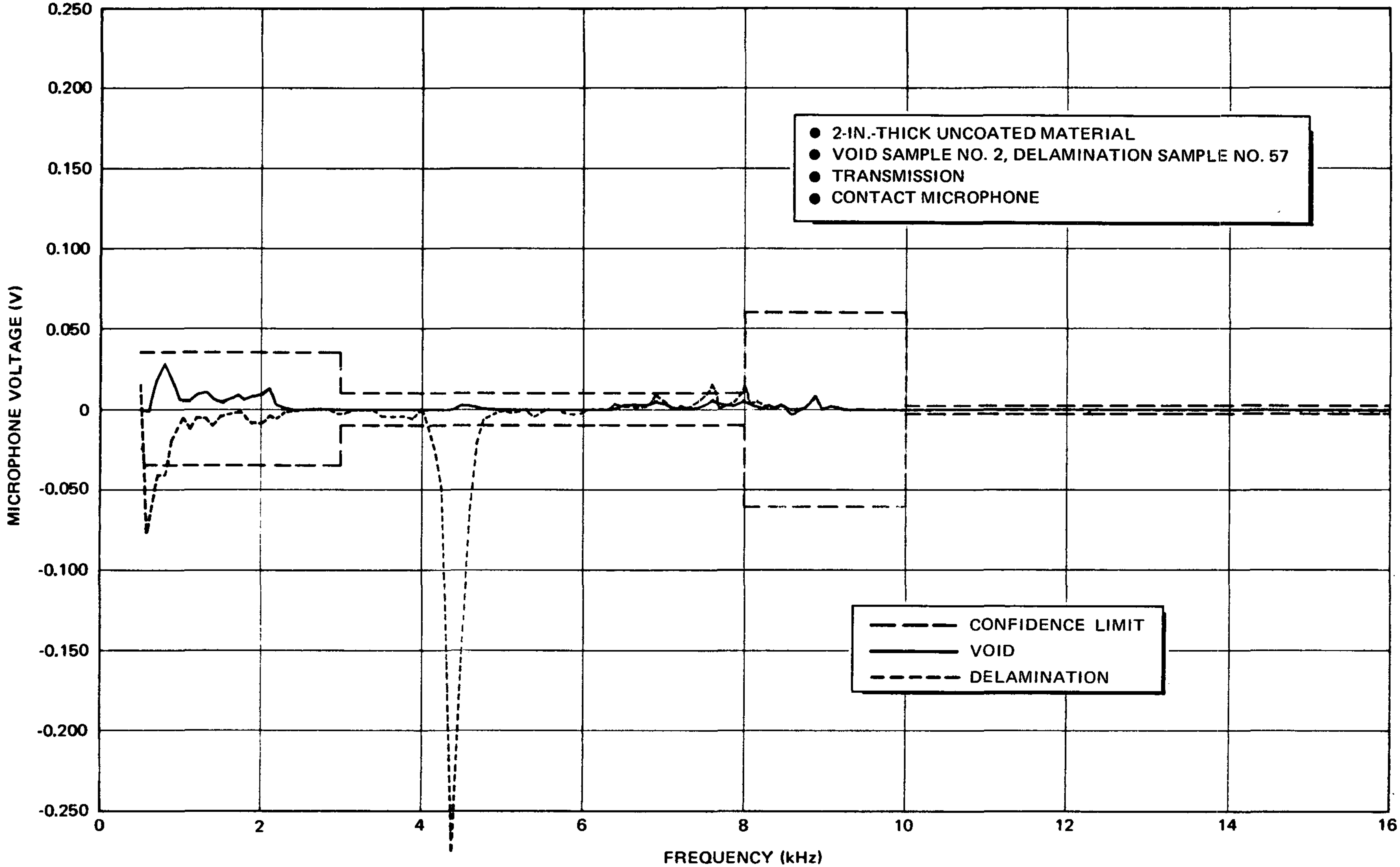

Figure 2-10. Difference in Contact-Microphone Response for Samples 2 and 57 (Control Sample No. 1)

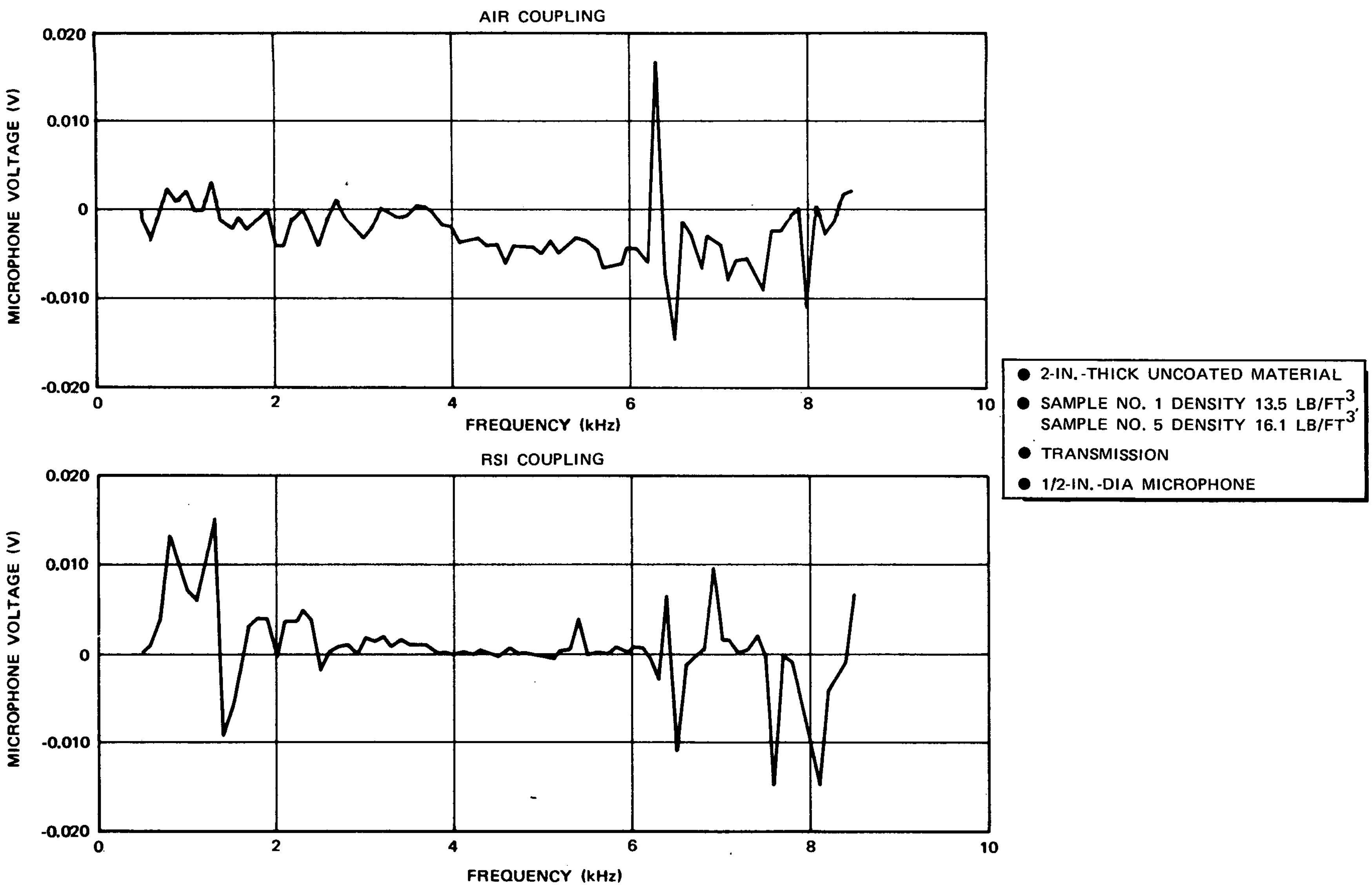

Figure 2-11. Difference in Response (Sample 1 - Sample 5)

would be provided by the largest deviation seen within the various control samples. These largest deviations then could be used to create bands within which the response of a sample must fall in order to be considered defect-free. Similarly, if the difference in response is larger than these limits, the sample could be considered to contain a defect. For air coupling and the two samples used, such a band would be ±0.0075 V for the response below 6,000 Hz.

Conceptually, RSI contact coupling introduces a new interface as compared to air coupling. The interfaces between RSI-to-air and air-to-RSI for the region between the RSI couplant and the RSI sample is similar to the interfaces present in a delamination defect. To investigate the possibility that RSI coupling introduces a delamination defect between the couplant and sample for all such measurements taken, air-coupling measurements were taken for two control samples placed together. Sample No. 58 and Sample No. 13 (a delamination defect was introduced into the latter sample later) were placed together for a total sample thickness of 2 in. for this purpose. The results are shown in Figure 2-12. Comparing this figure with the results for the void and delamination samples using RSI coupling, we see that all three response curves initially become negative for the first 2,000 Hz and then become positive for the next 2,000 Hz and then decrease in amplitude with increasing frequency. In short, all three responses have similar form. This may be due to differences in the delamination defects introduced during RSI contact coupling from one sample to the next. Thus, for example, the difference from one delamination defect to the other may not cancel out completely when comparing the response from a control sample with that from a defective sample using RSI contact coupling.

Air coupling was chosen for all further measurements. This choice was based upon the higher signal strength, more uniform response for different density control samples, and the fact that no additional delaminations are introduced during inspection. Air coupling also has the advantages over RSI contact coupling in that scanning may be more easily accomplished without the possibility of any abrasion between RSI surfaces.

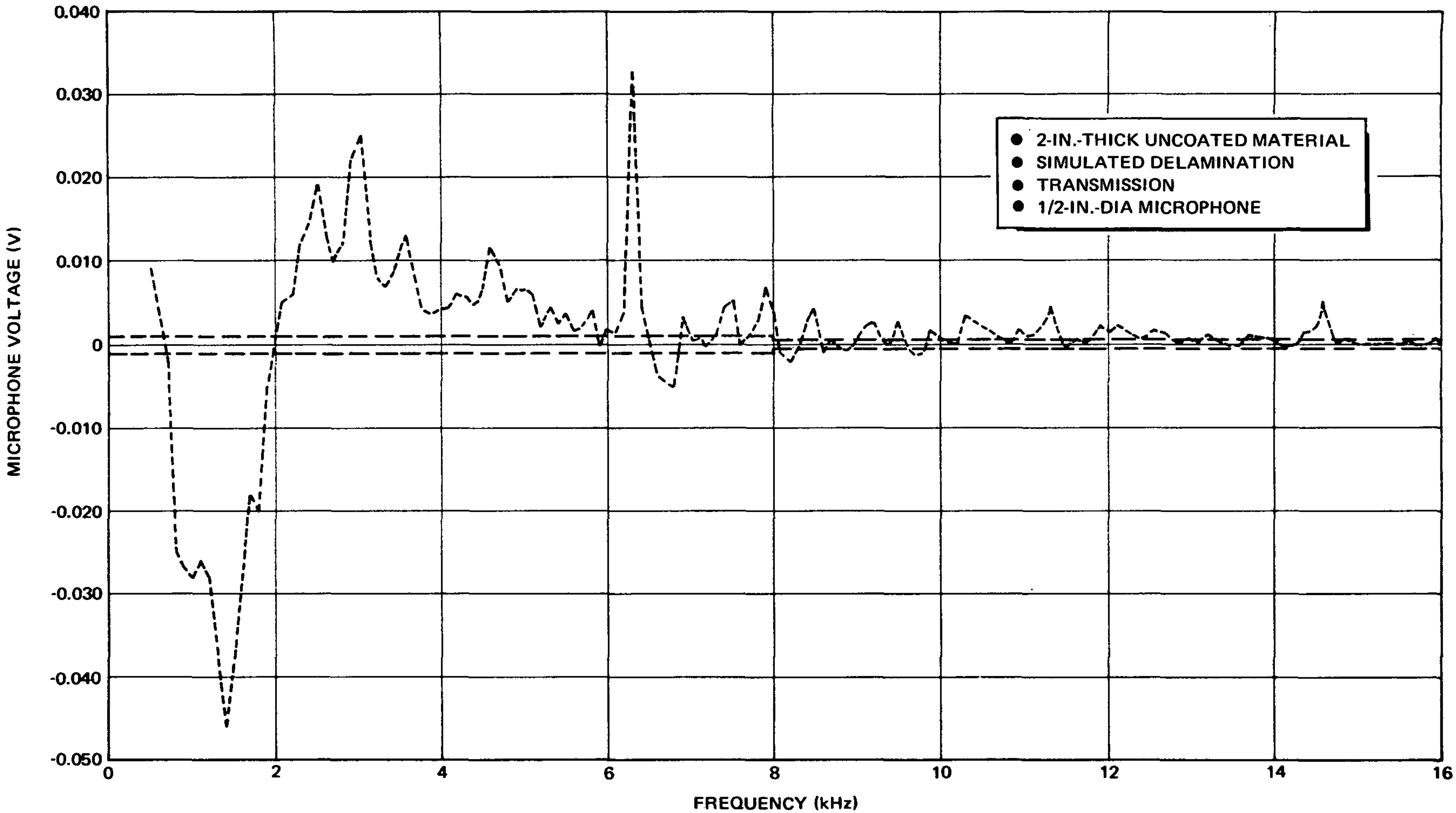

Figure 2-12. Difference in Air-Coupling Response for Simulated Delamination (Sample 13 + Sample 58) (Control Sample No. 1)

Accordingly, additional measurements were taken on 2-in.-thick Void Sample No. 3, 1-inch thick Delamination Sample No. 13, and 1/4-in.-thick Delamination Sample No. 15. The results are shown in Figures 2-13 through 2-15. All these figures show differences from the defective samples as compared to the controls. The larger differences obtained for Void Sample No. 3 (Figure 2-13) as compared to those obtained for Void Sample No. 2 (Figure 2-8) may be due to the fact that the void in Sample No. 3 was a side-drilled hole which introduces an additional interface as compared to the hole drilled in the thickness direction for Sample No. 2. Generally, air coupling was successful for detection of void and delamination defects in 2-in.-thick uncoated material and delamination defects in both 1- and 1/4-in.-thick uncoated material.

Confidence limits are shown on some of the figures discussed previously. Values for these confidence limits were obtained for each of the three different coupling methods investigated by determining the effect of experimental variations in the microphone placement and the input voltage to the speaker. These effects were determined for selected frequencies throughout the frequency range of interest. Changes of 1/64 in. in the microphone position resulted in small changes in the response, as compared to changes of ±0.1 V in the voltage applied to the speaker. The confidence limits associated with the possible experimental variations in the speaker voltage were used for the figures mentioned. For air coupling, changes in the response due to control sample density are greater than the errors associated with the actual measurements. The extremes of this variation should be used as the actual confidence limits.

The final parameter decided upon before continuing with further measurements was the microphone size. As mentioned earlier, previous work had shown that small-diameter microphones were required of small bondline defects. A 1-in.-dia microphone was evaluated for its sensitivity in addition to the 1/2-in.-dia microphone used up to this point. The results obtained for air coupling using a 1-in.-dia microphone for Void Sample No. 2, Void Sample No. 3, and Delamination Defect Sample No. 57 are shown in Figures 2-16

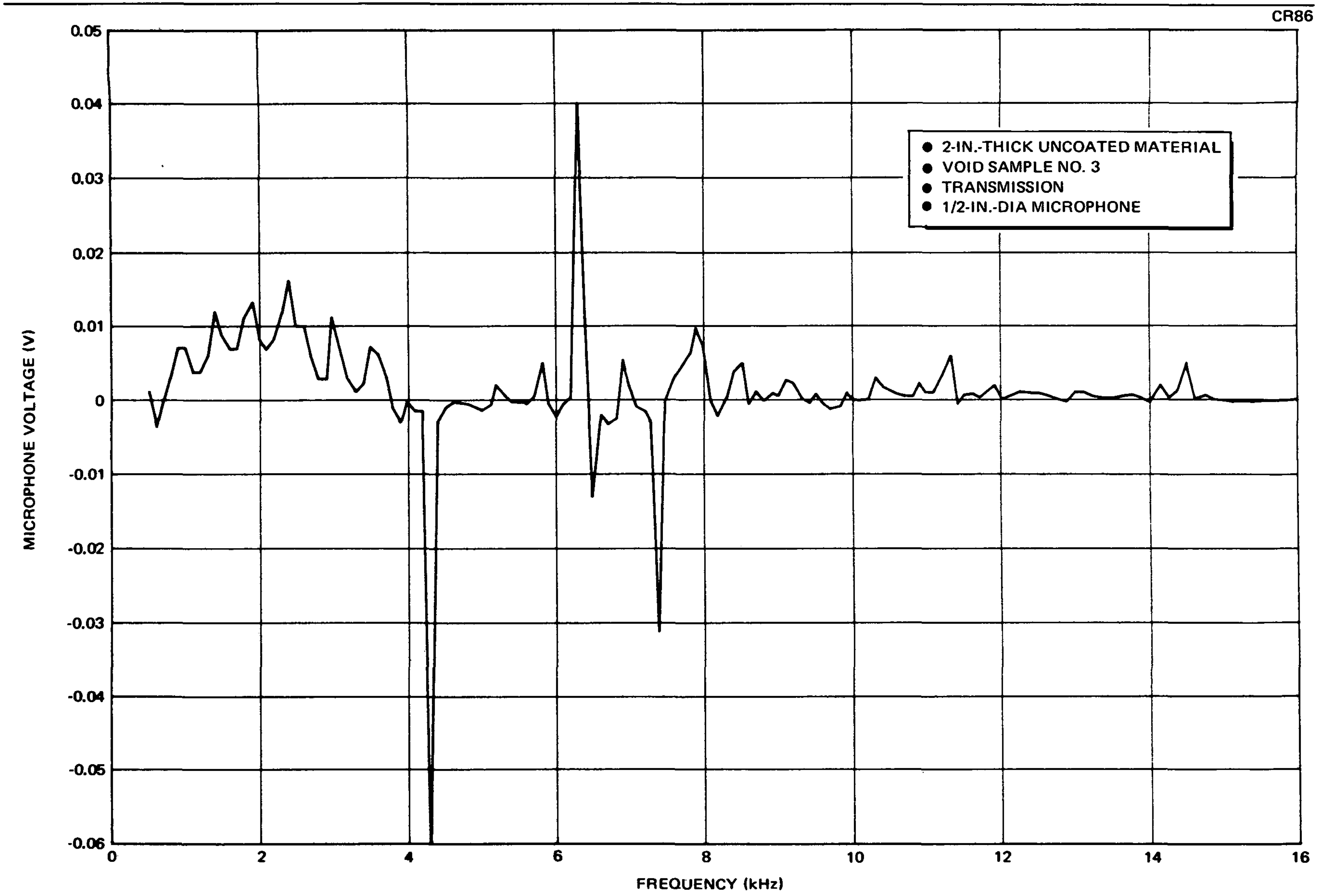

Figure 2-13. Difference in Air-Coupling Response for Sample No. 3 (Control Sample No. 1)

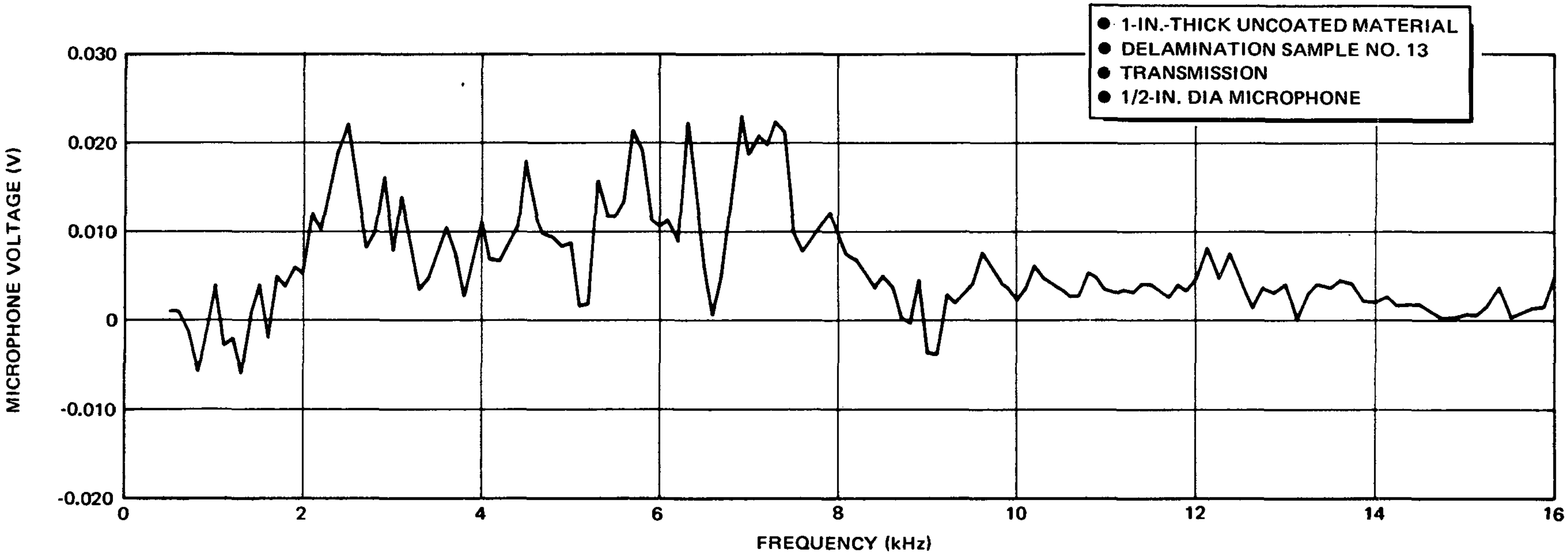

Figure 2-14. Difference in Air-Coupling Response for Sample No. 13 (Control Sample No. 58)

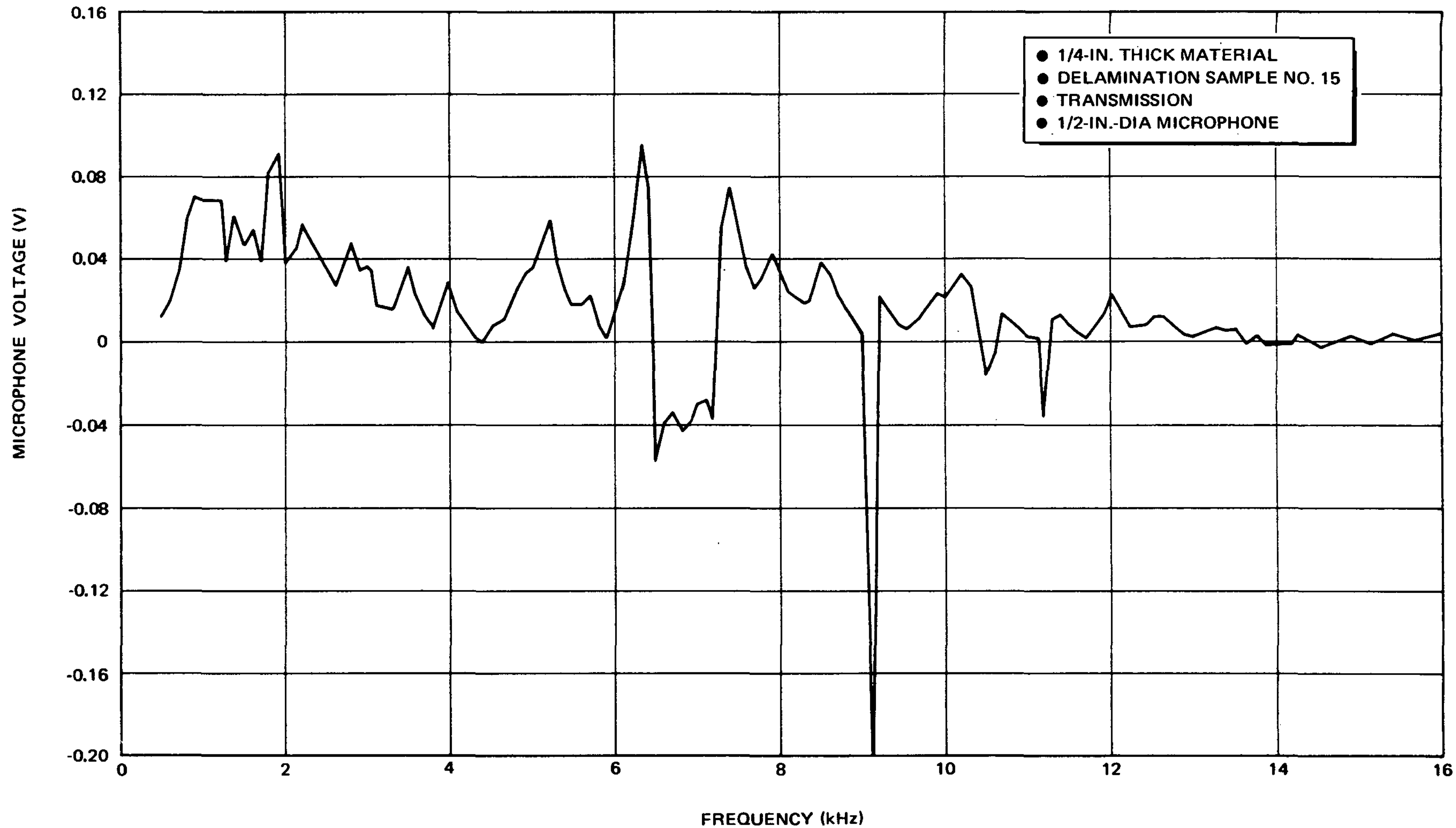

Figure 2-15. Difference in Air-Coupling Response for Sample No. 15 (Control Sample No. 58)

through 2-18. As shown by these figures, the sensitivity of the 1-in.-dia microphone was greater than that of the 1/2-in.-dia microphone. That is, the voltage output of the 1-in.-dia microphone was larger. Consequently, the 1-in.-dia microphone was used for all further air coupling measurements.

2.4.2.3 Acoustic Reflection

The sensitivity of the acoustic reflection technique was evaluated by comparing the reflection of sound from a defect-free RSI control sample with that of similar samples containing known artificial defects. The equipment setup used for the reflection measurements was similar to that used for the transmission measurements, the only difference being the introduction and reception of the sound from the same surface. The samples were suspended on a small piece of cloth 2 in. from the edge of the horn. A fixture was used to hold the microphone within the opening of the horn so the microphone was approximately 1/4 in. from the bottom surface of the sample. Air coupling and the 1-in.-dia microphone were used.

2.4.2.4 Uncoated Samples

Acoustic transmission and reflection measurements were made for void, delamination, and density samples and then compared to the response from control samples. The results for the transmission measurements were described in the preceding discussion of coupling methods. The corresponding results for the acoustic reflection measurements are shown in Figures 2-19 through 2-24.

Figure 2-19 shows the response from the control sample alone. The amplitude of the response was quite small. In fact, the largest reflected amplitude was approximately 0.010 V, whereas the largest transmitted amplitude for the same sample was approximately 0.075 V. As the figure shows, the response was very small for low frequencies, increasing to a maximum of 5,000 Hz and then slowly decreasing with increasing frequency. The response from the control sample displayed a series of peaks fairly evenly spaced, with a separation of approximately 820 Hz. It appeared that such a series of peaks might be due either to the occurrence of standing waves or to interference

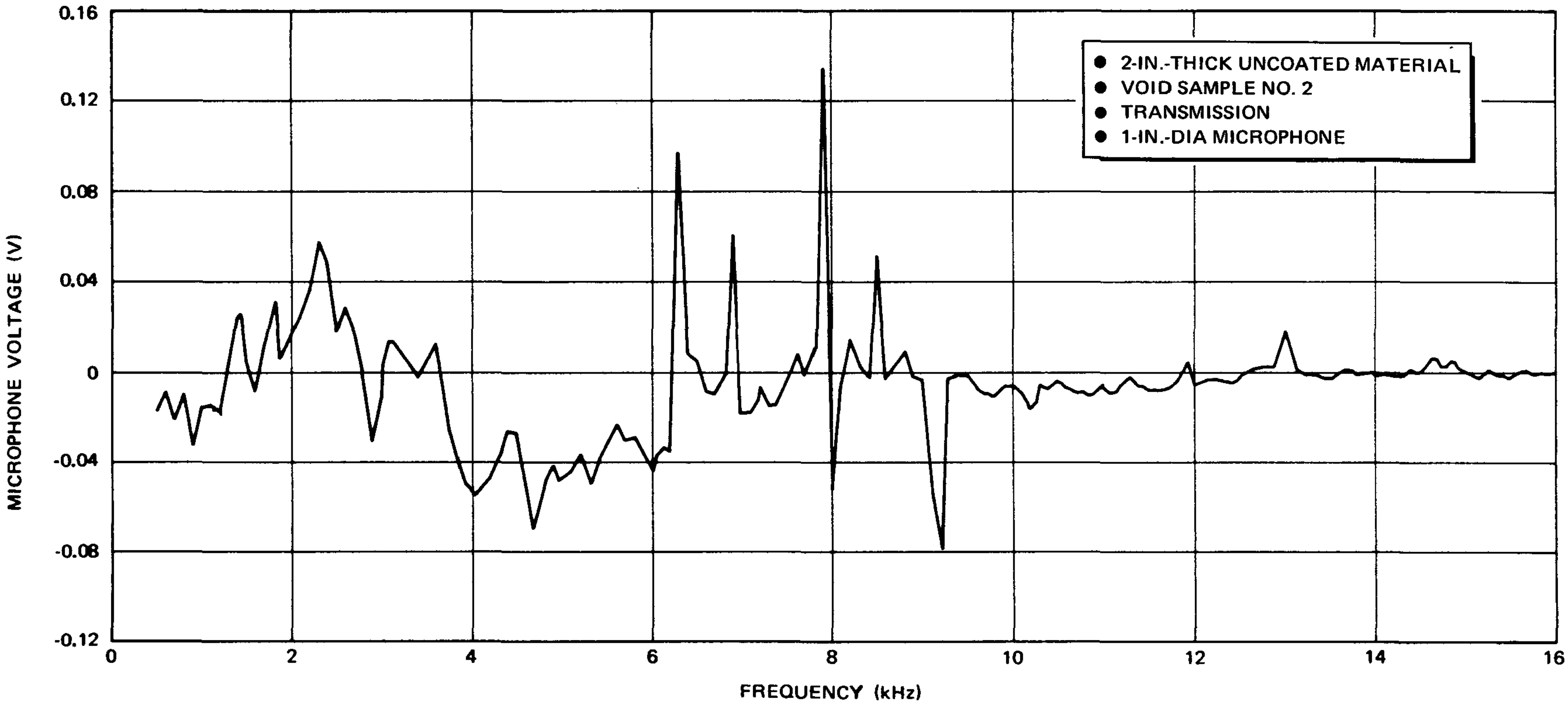

Figure 2-16. Difference in Air-Coupling Response for Sample No. 2 (Control Sample No. 1)

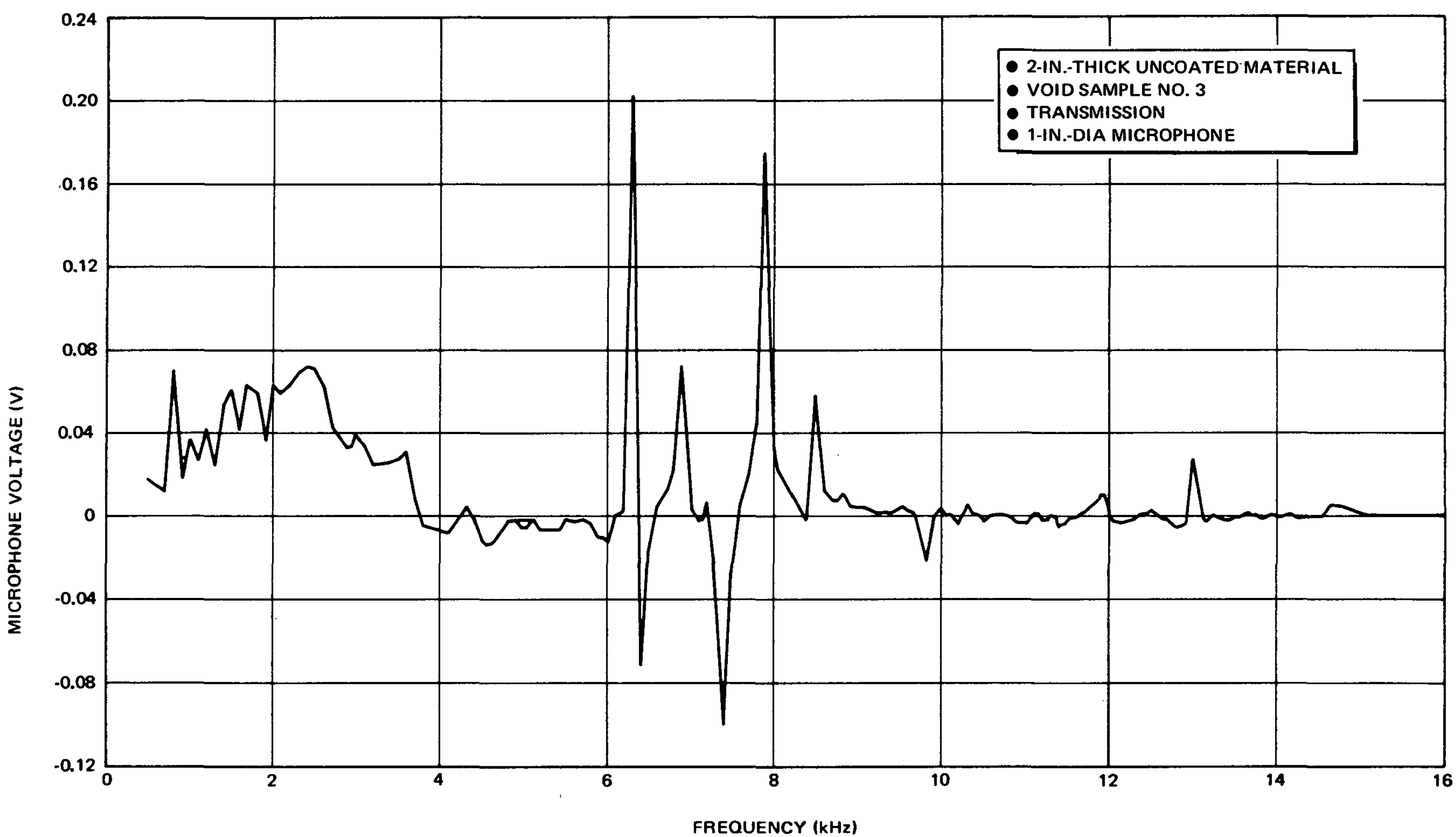

Figure 2-17. Difference in Air-Coupling Response for Sample No. 3 (Control Sample No. 1)

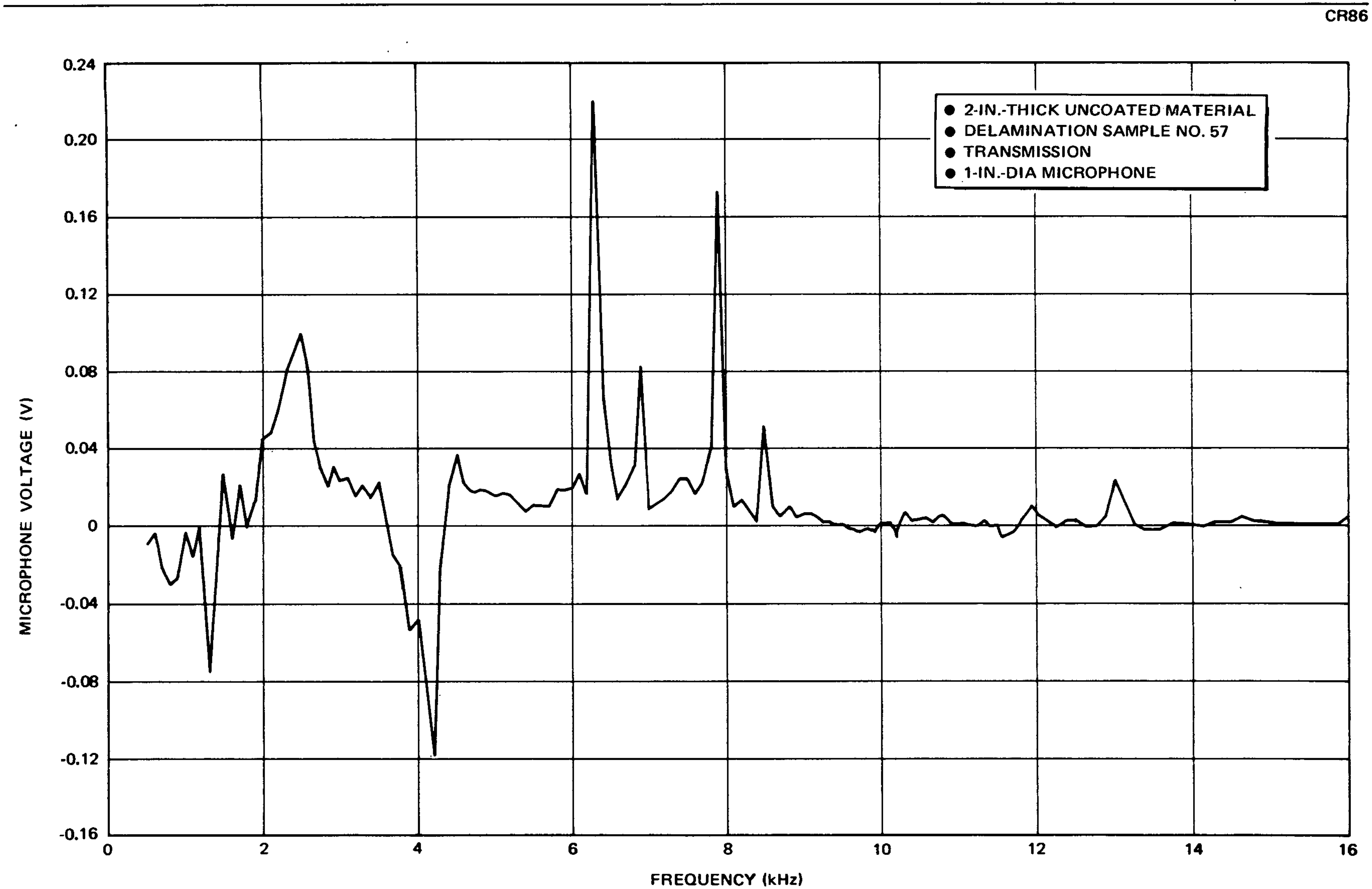

Figure 2-18. Difference in Air-Coupling Response for Sample No. 57 (Control Sample No. 1)

CR86

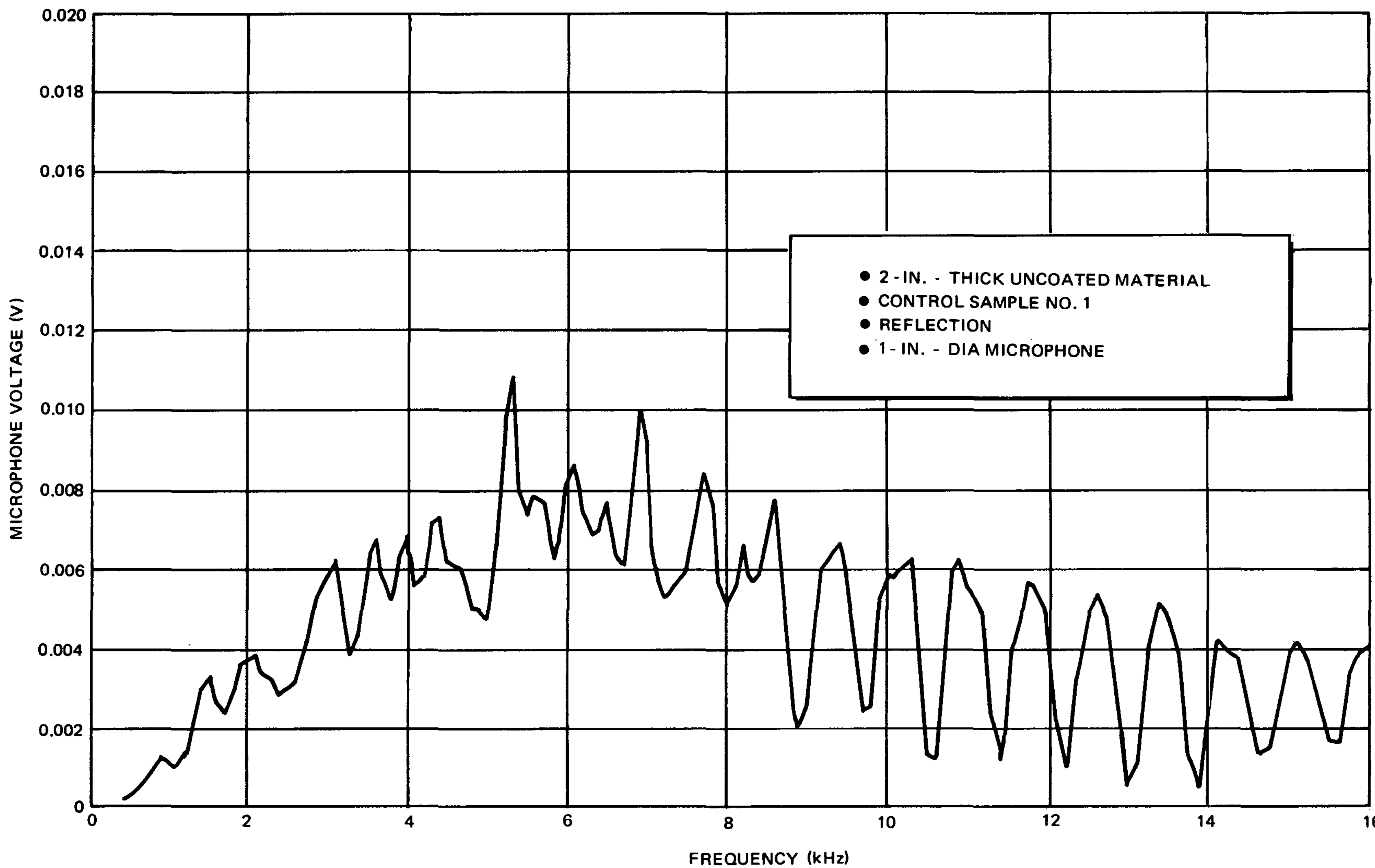

Figure 2-19. Air-Coupling Response for Sample No.1 (Reflection)

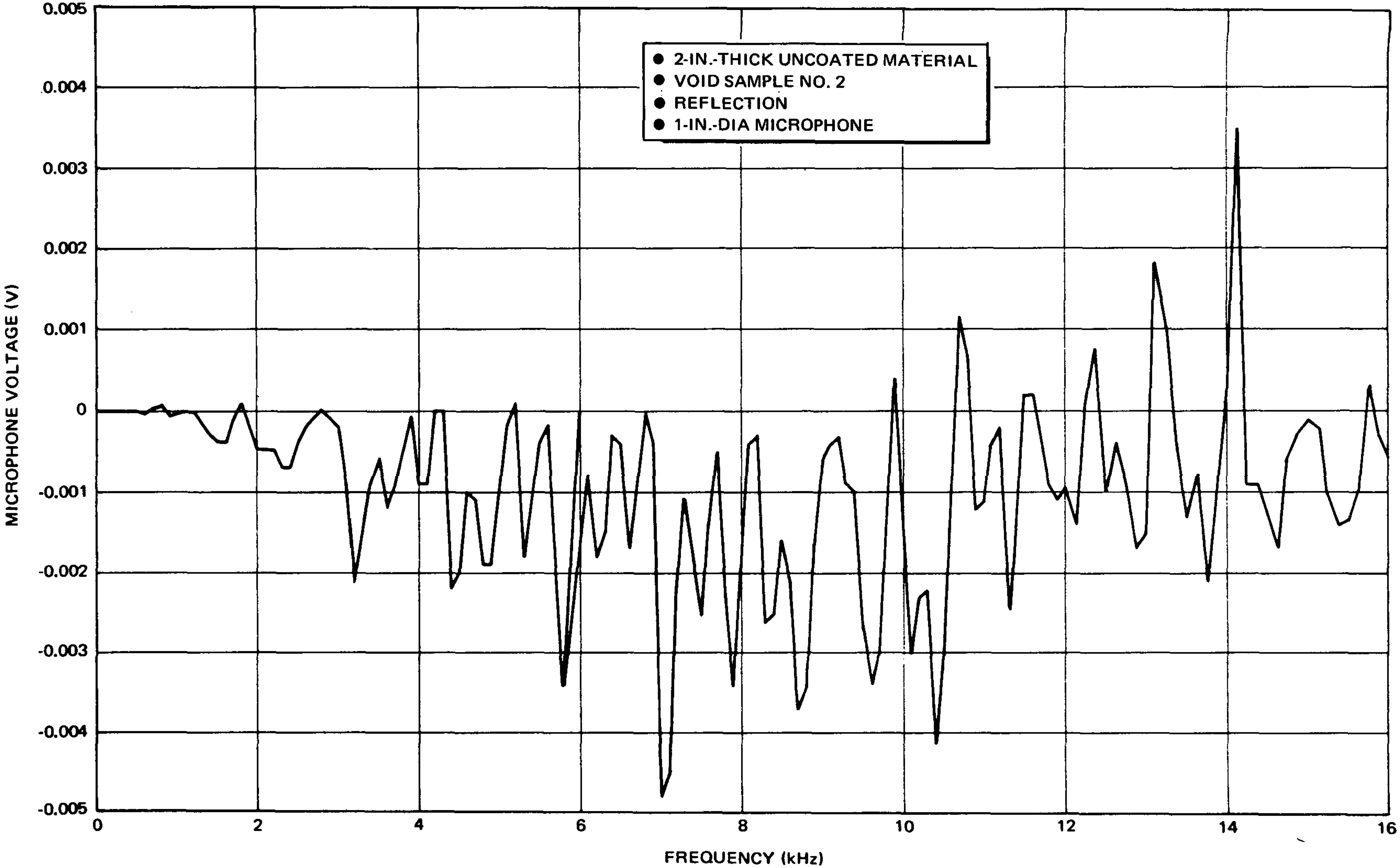

Figure 2-20. Difference in Air-Coupling Response for Sample No. 2 (Control Sample No. 1)

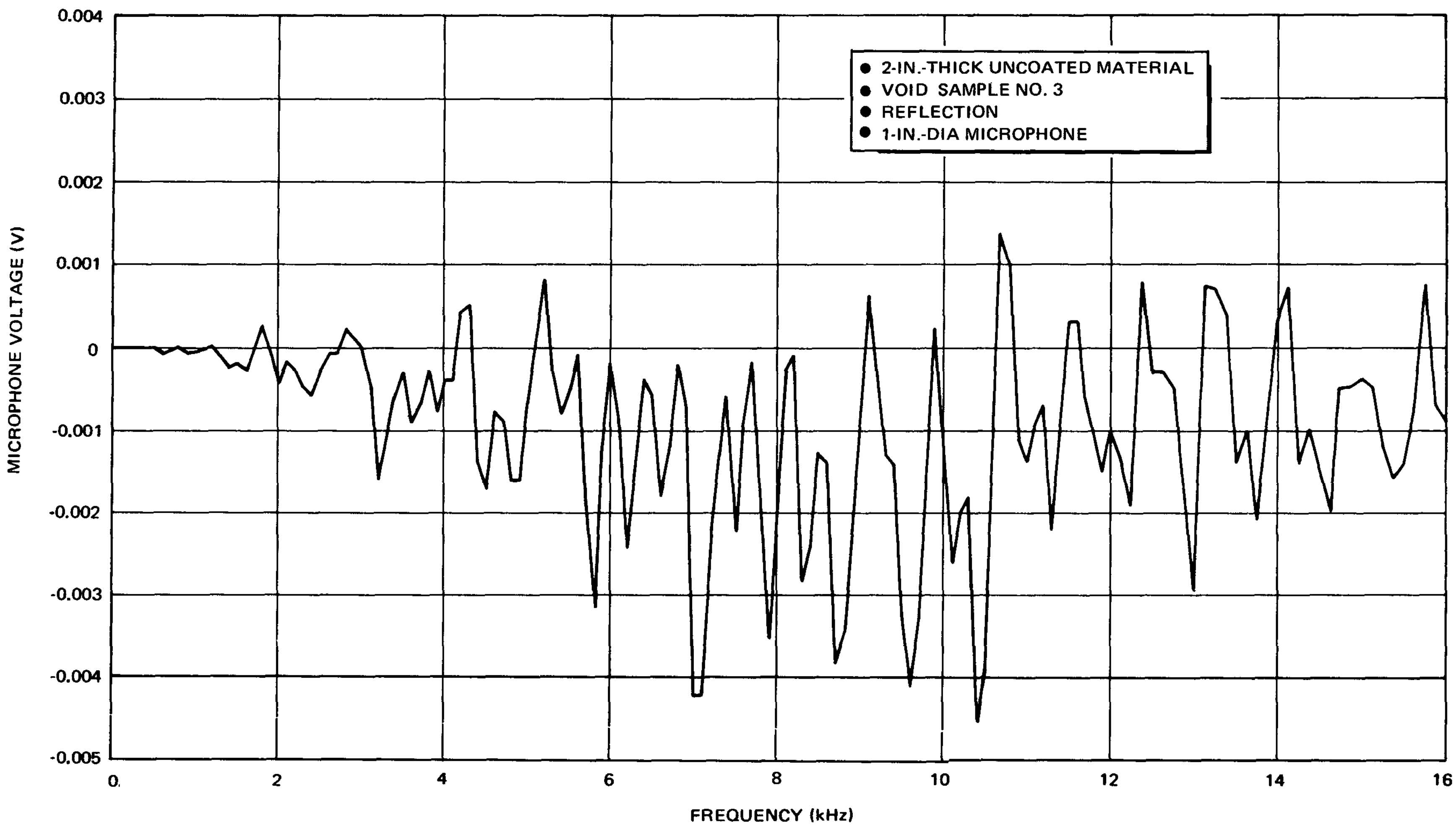

Figure 2-21. Difference in Air-Coupling Response for Sample No. 3 (Control Sample No. 1)

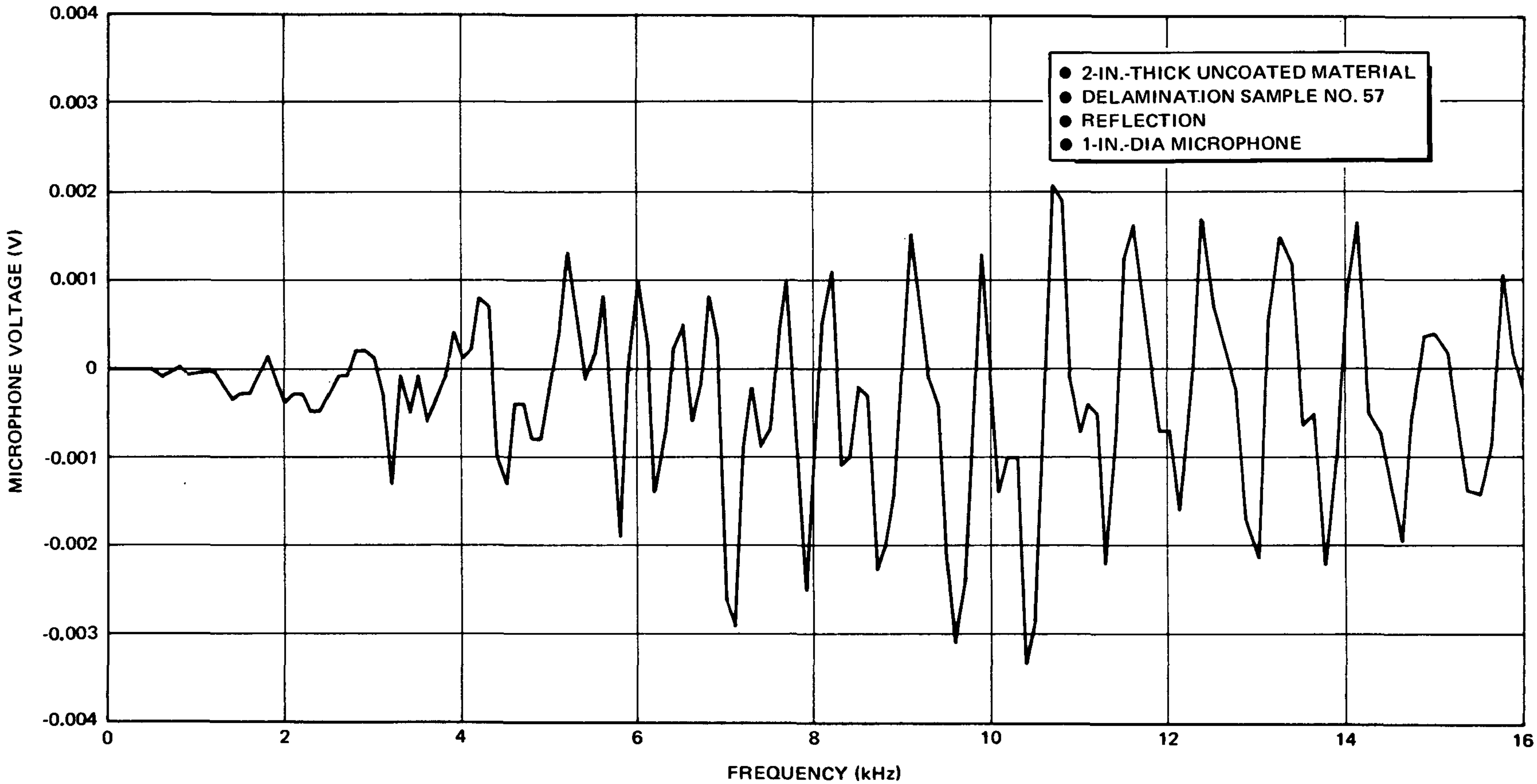

Figure 2-22. Difference in Air-Coupling Response for Sample No. 57 (Control Sample No. 1)

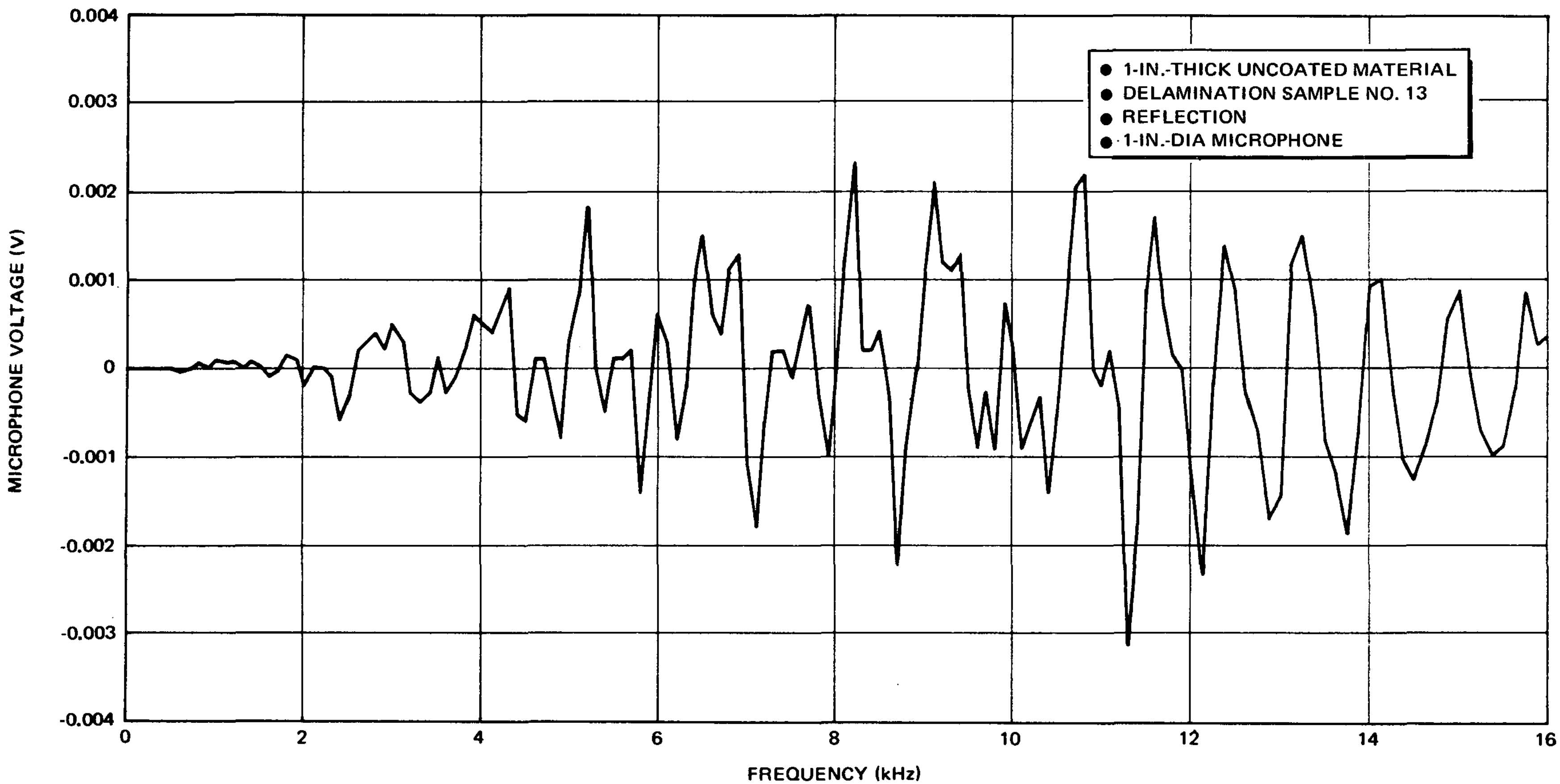

Figure 2-23. Difference in Air-Coupling Response for Sample No. 13 (Control Sample No. 58)

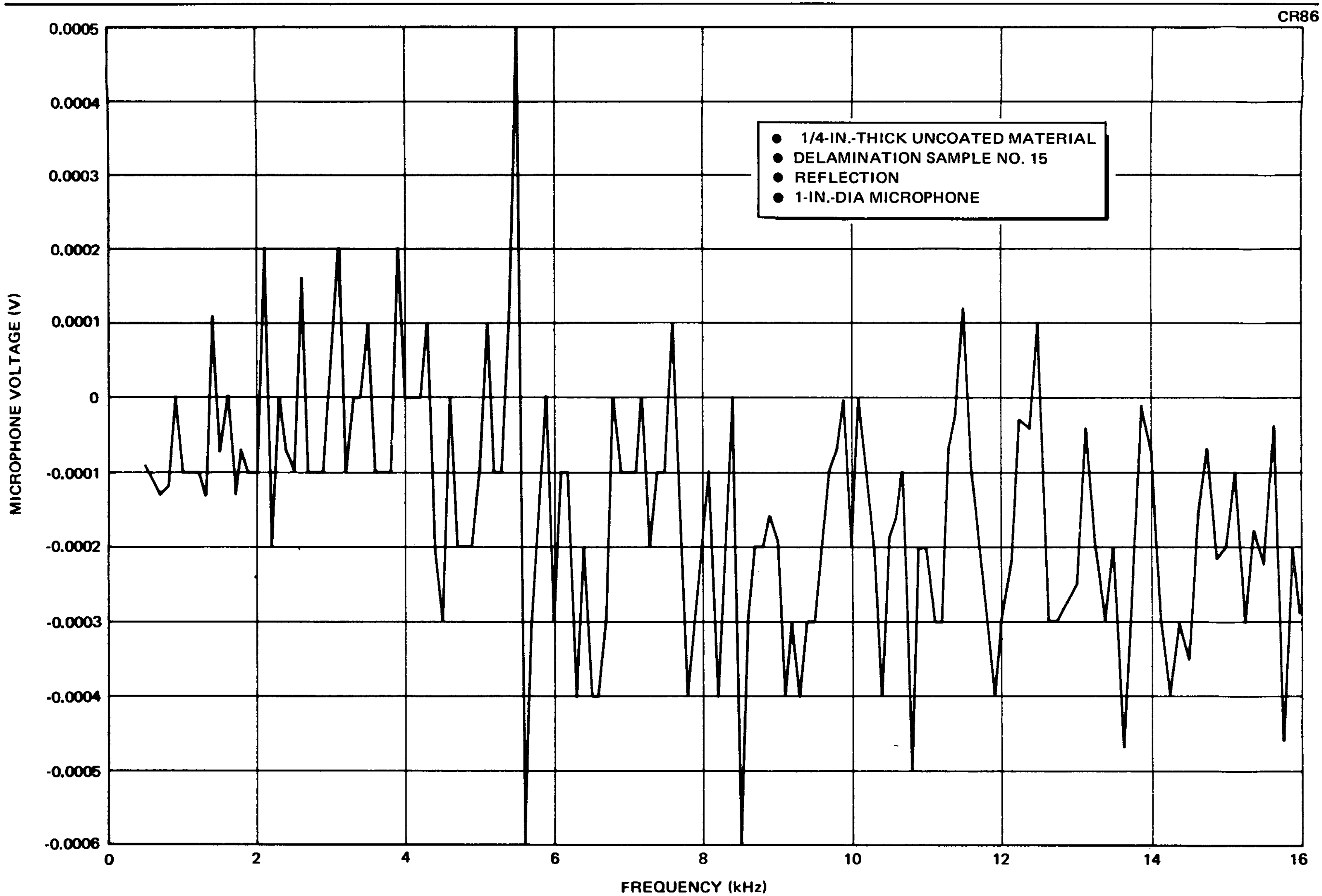

Figure 2-24. Difference in Air-Coupling Response for Sample No. 15 (Control Sample No. 14)

effects. Both these effects would be dependent upon the frequency. Assuming that the peaks were caused by standing waves for specific frequencies and working backward from the observed spacing of the peaks, the calculated distance between the sound source and the reflecting surface was approximately the same as that used. Nevertheless, it might be expected that such a response would cancel out when the results of one sample are compared to another. The results for the void, delamination, and density samples (Figures 2-20 through 2-24), however, still reveal the presence of these peaks. In particular, the difference in the responses for the 2-in.-thick control samples which differed in density (Figure 2-25) was on the order of the difference observed for the other samples as well. Thus, it would be difficult to say that the acoustic reflection method was capable of detecting voids or delaminations in 2-in.-thick uncoated material.

Better results were obtained for the 1- and the 1/4-in.-thick material. The effect of density variations for 1-in.-thick control samples is shown in Figure 2-26. The difference in response for the samples containing defects was larger than the difference due to density variations for this thickness.

2.4.2.5 Coating Samples

The results for the loss of adhesion defect samples are shown in Figures 2-27 through 2-30. These figures show an interesting change in behavior. The amplitude of the difference in response using the reflection method was much larger than the amplitude of the difference in response using the transmission method. It appears as though the coating does have some effect upon whether or not sound is transmitted or reflected. Thus, reflection measurements are potentially better suited for the detection of loss-of-adhesion defects. Whether the differences in response are significant or not, however, would depend upon how large a difference would have been observed between coated samples of different densities. This information was not available for these samples.

2.4.2.6 Coated Samples

The transmission and deflection results for the coated samples containing void and delamination defects are shown in Figures 2-31 through 2-34.

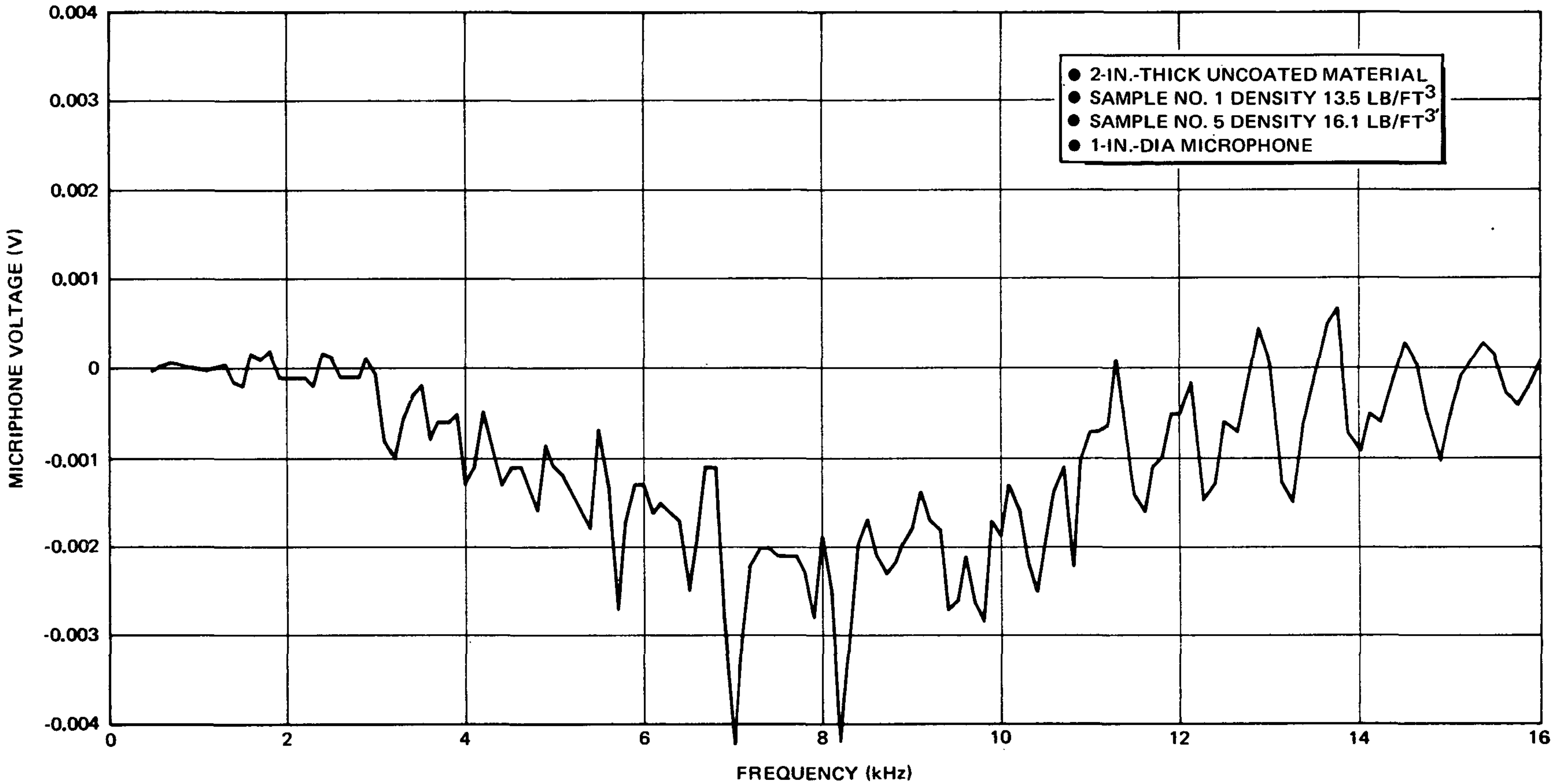

Figure 2-25. Difference in Response (Sample 1 - Sample 5)

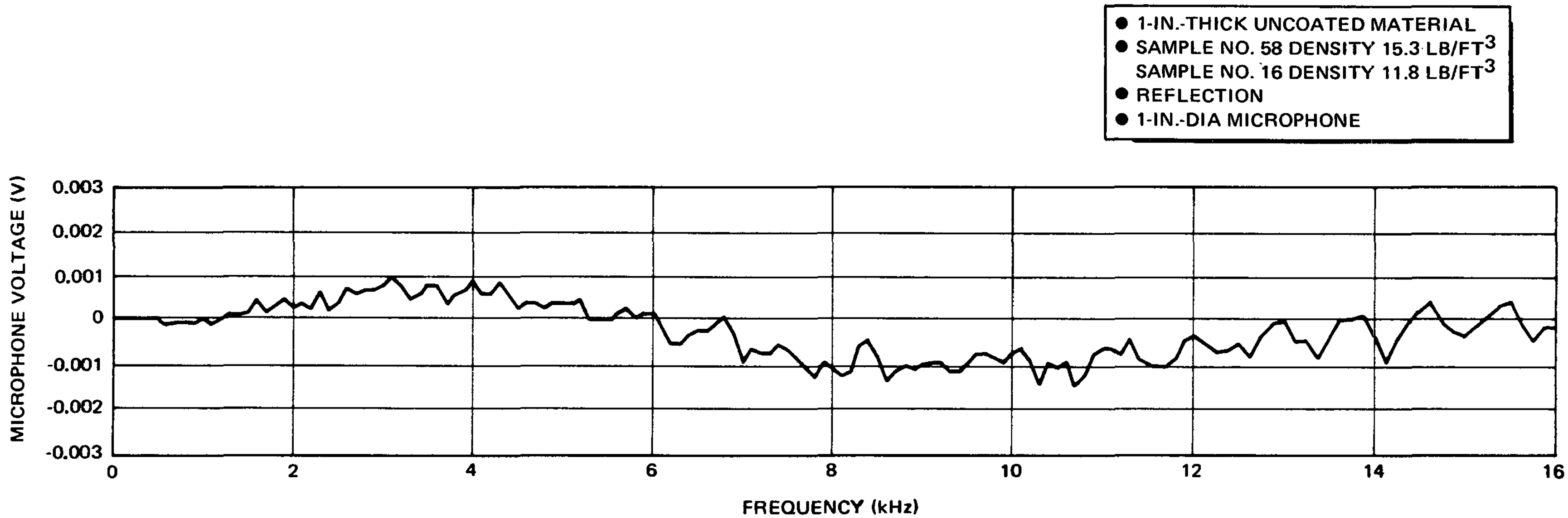

Figure 2-26. Difference in Response (Sample 58 - Sample 16)

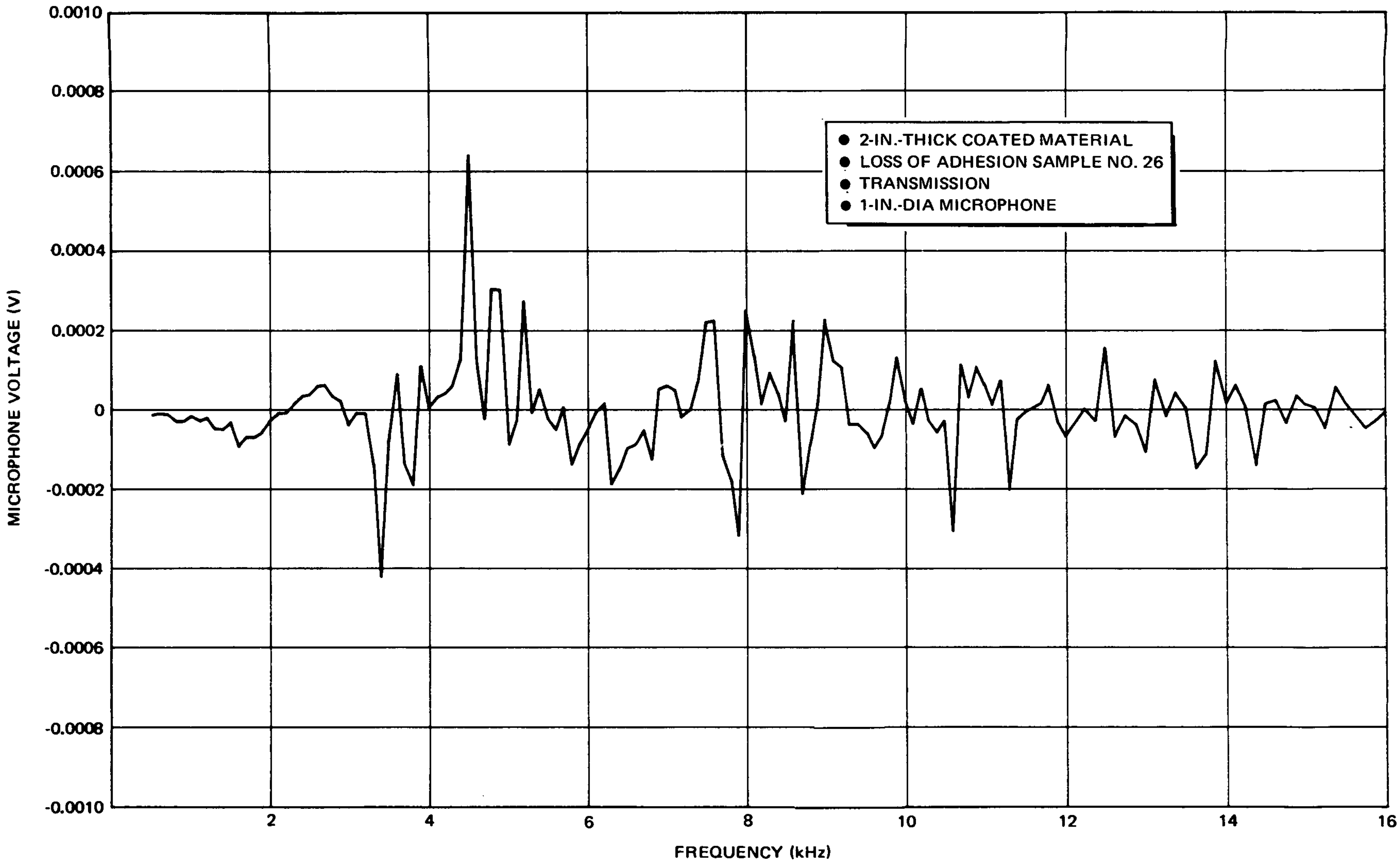

Figure 2-27. Difference in Air-Coupling Response for Sample No. 26 (Control Sample No. 37)

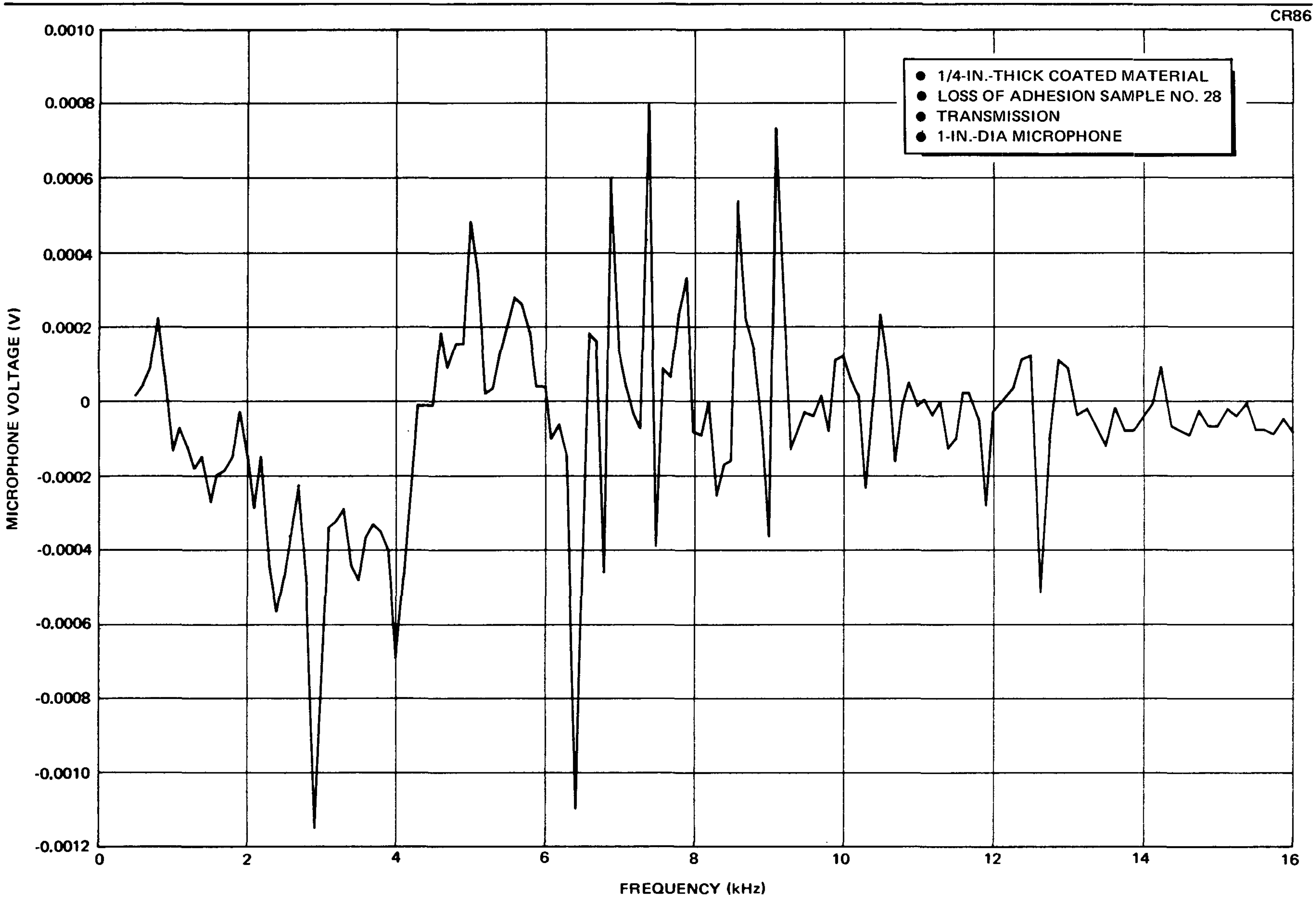

Figure 2-28. Difference in Air-Coupling Response for Sample No. 28 (Control Sample No. 27)

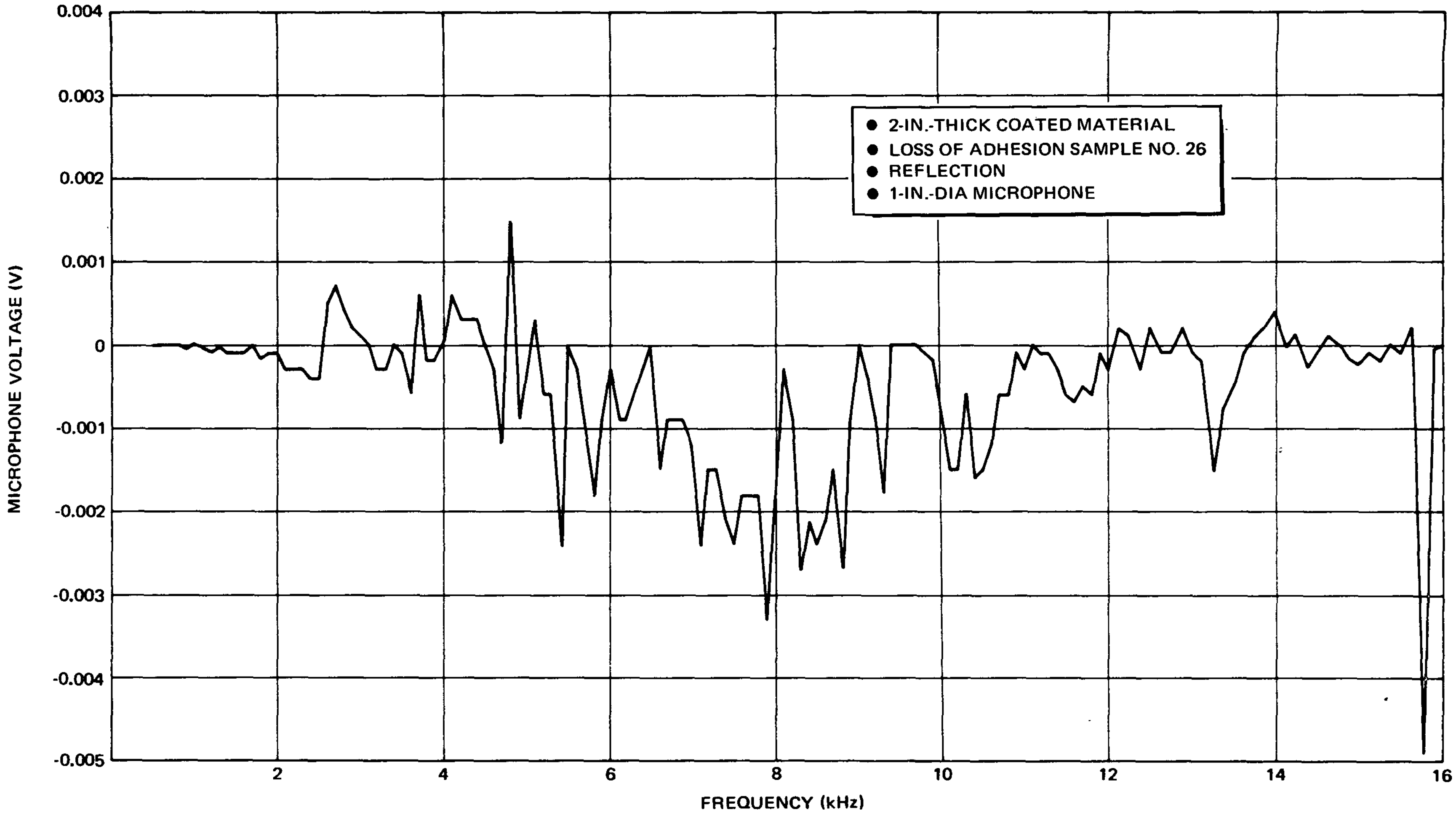

Figure 2-29. Difference in Air-Coupling Response for Sample No. 26 (Control Sample No. 37)

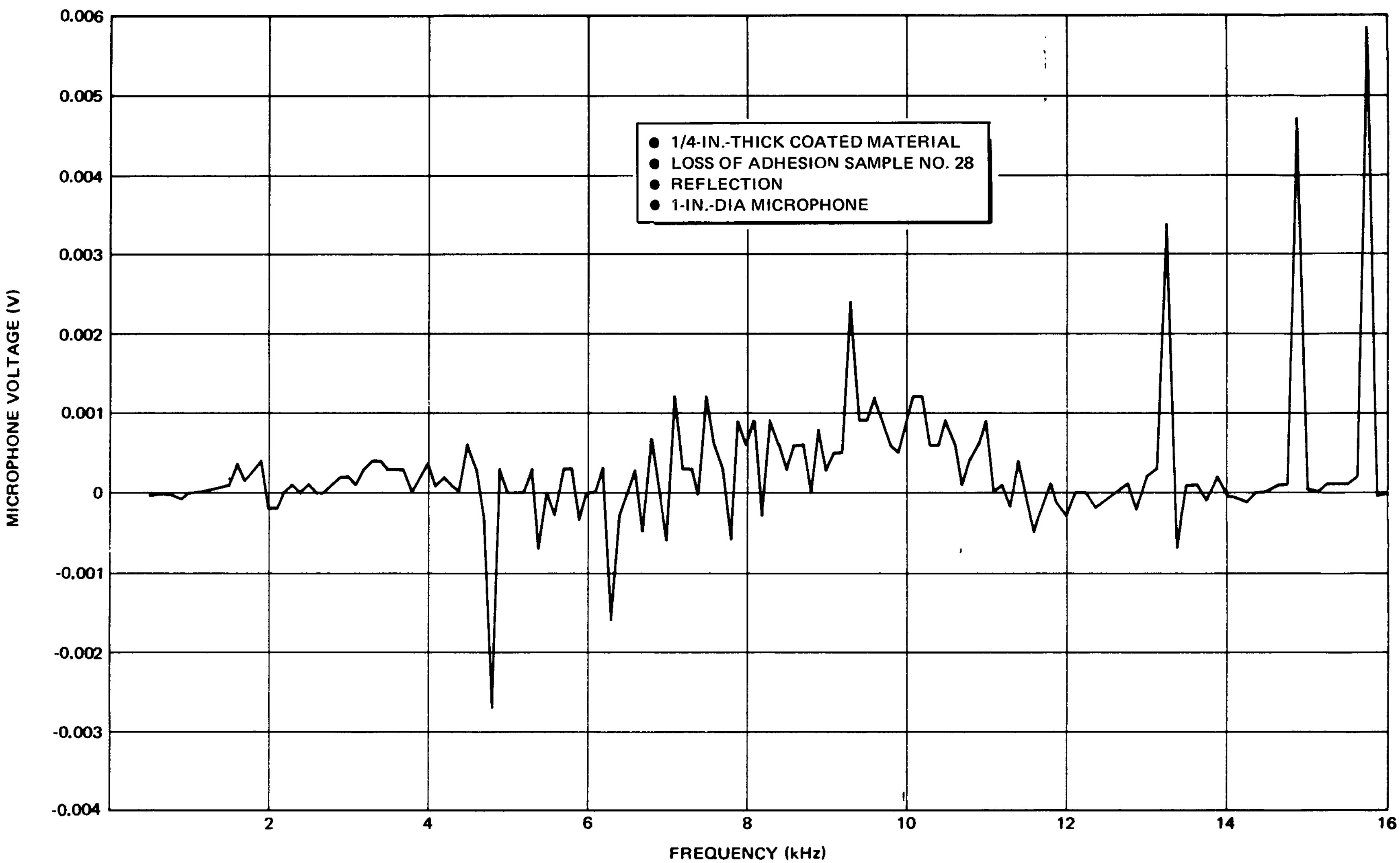

Figure 2-30. Difference in Air-Coupling Response for Sample No. 28 (Control Sample No. 27)

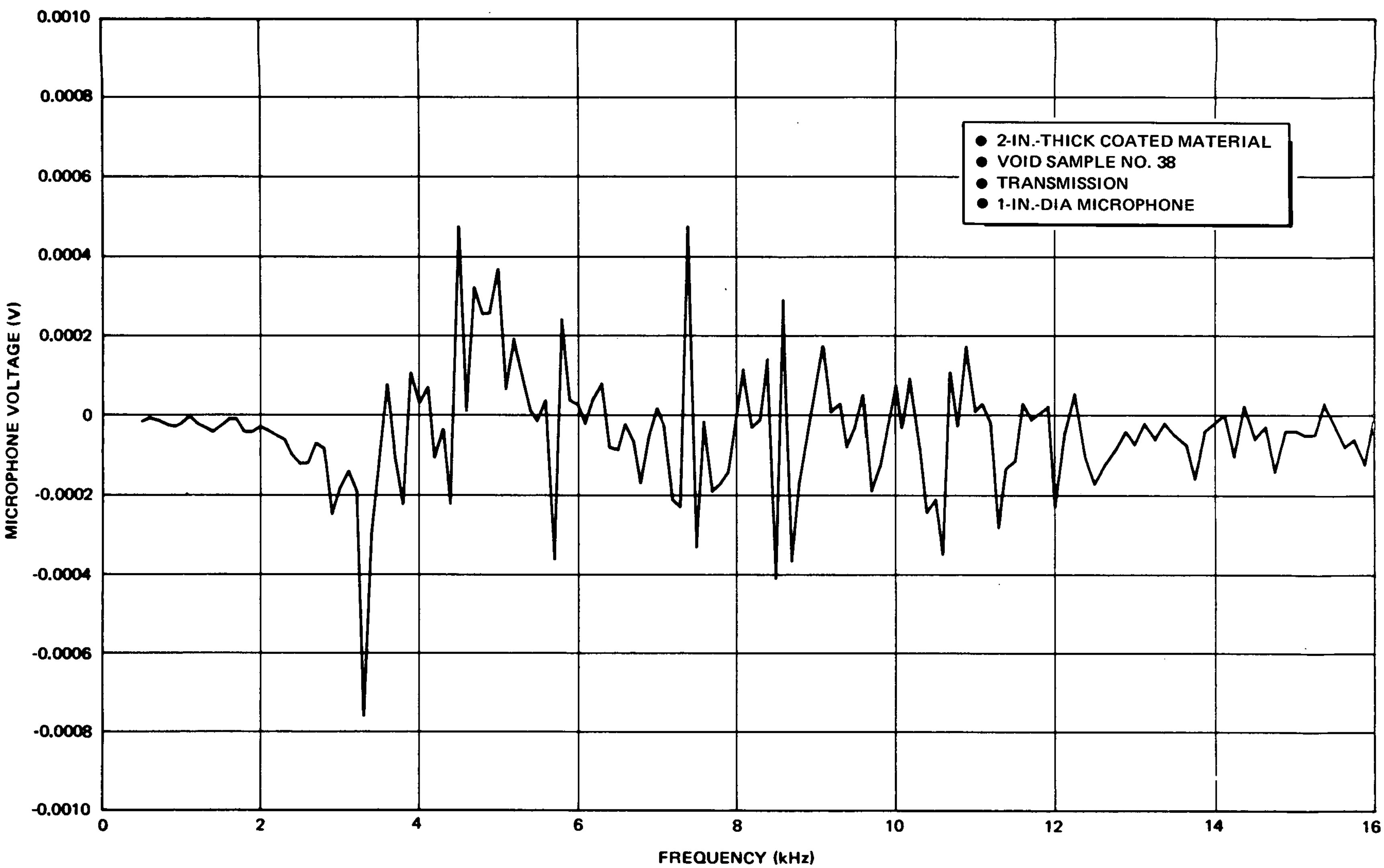

Figure 2-31. Difference in Air-Coupling Response for Sample No. 38 (Control Sample No. 37)

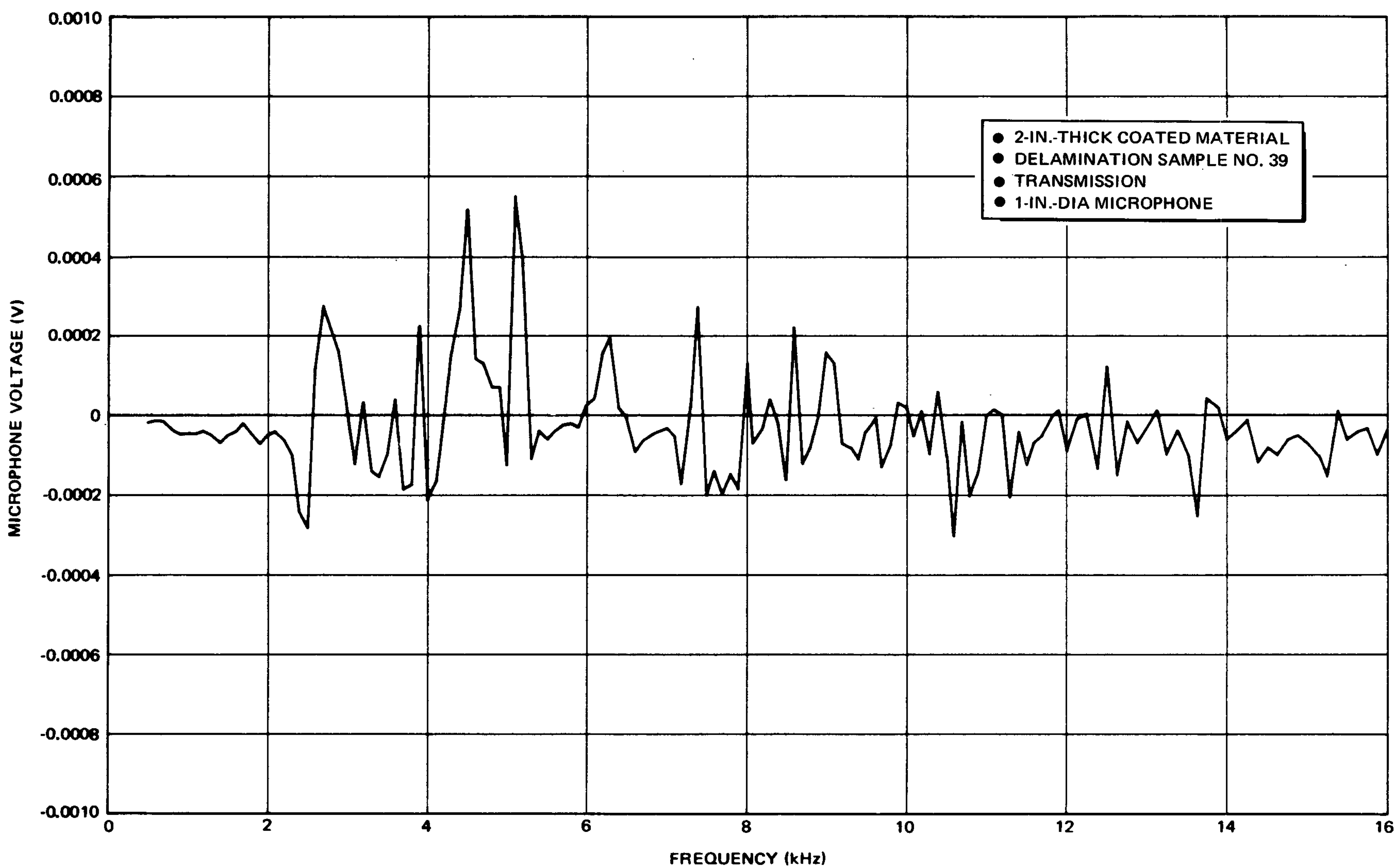

Figure 2-32. Difference in Air-Coupling Response for Sample No. 39 (Control Sample No. 37)

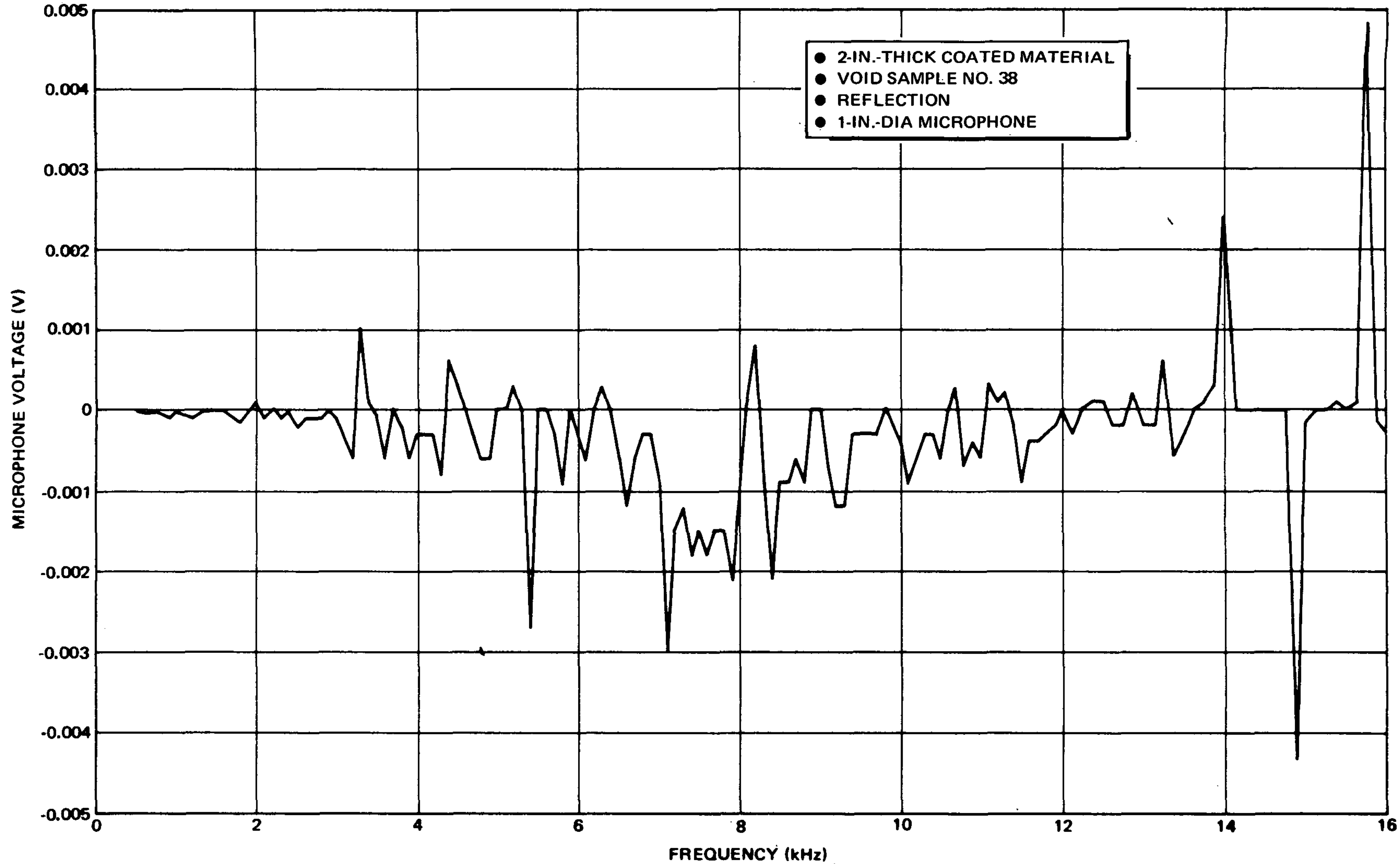

Figure 2-33. Difference in Air-Coupling Response for Sample No. 38 (Control Sample No. 37)

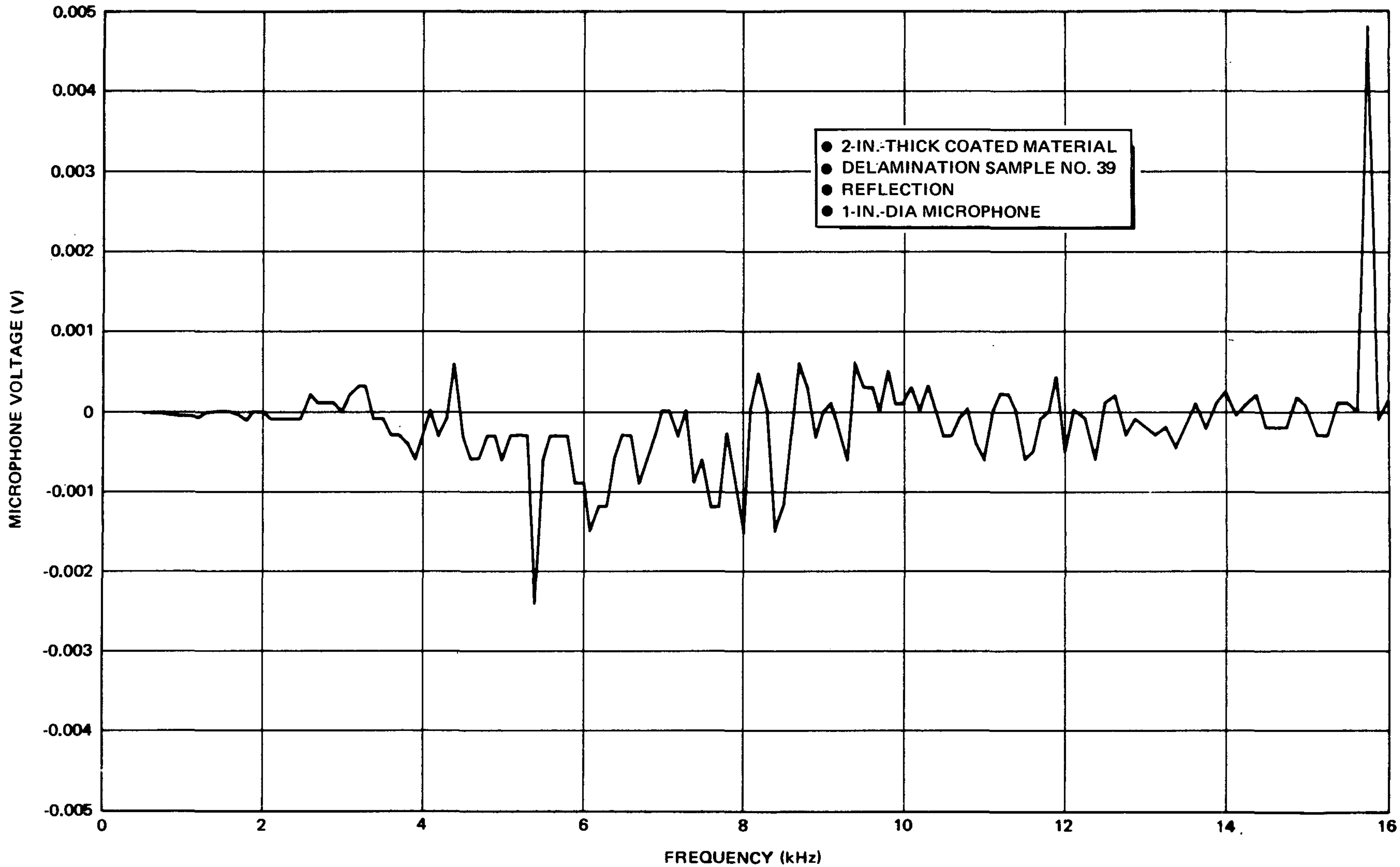

Figure 2-34. Difference in Air-Coupling Response for Sample No. 39 (Control Sample No. 37)

Again, the amplitude of the difference in transmission response was much smaller than the amplitude of the difference in reflection response. Further information on the range of differences expected for variations in material density would be needed in order to determine whether these defects were indeed detectable.

2.4.2.7 Bonded Samples

The results for bonded samples are shown in Figures 2-35 through 2-46. Greater differences were obtained for the reflection measurements than for the transmission measurements for these samples. There were considerable changes in the difference of response for some frequencies as compared to other frequencies. Generally, the greatest changes in response occurred for frequencies below 10,000 Hz. The strongest indication of the presence of any defects were provided in the case of reflection measurements made on the samples containing unbond defects in the bondline. The difference in response curves for these samples showed deviations either predominately below zero or above zero. The deviations below zero occurred for unbond defects in 2-in.-thick material and the deviations above zero occurred for unbond defects in 1/4-in.-thick material.

2.4.2.8 Electromagnetically Introduced Vibrations

A commercial instrument, the Shurtronics Harmonic Bond Tester, was evaluated for the introduction and detection of sound through the use of electromagnetically introduced vibration. The Harmonic Bond Tester is an eddy-sonic type of device which requires that at least one material in the bonded structure be metallic. A coil operating at 14 to 15 kHz introduces an eddy current field in the aluminum substrate. This field causes acoustic vibrations to be emitted and these are monitored by a receiving piezoelectric transducer operating over a narrow band, 28 to 30 kHz (second harmonic). Essentially, the instrument compares the relative rigidity of a well-bonded area to one having a void or unbond. The unbond or void area is expected to provide a larger amount of noise due to the greater freedom of movement.

The Harmonic Bond Tester was applied from both sides of the bonded samples. This technique does not require a couplant as the vibrations

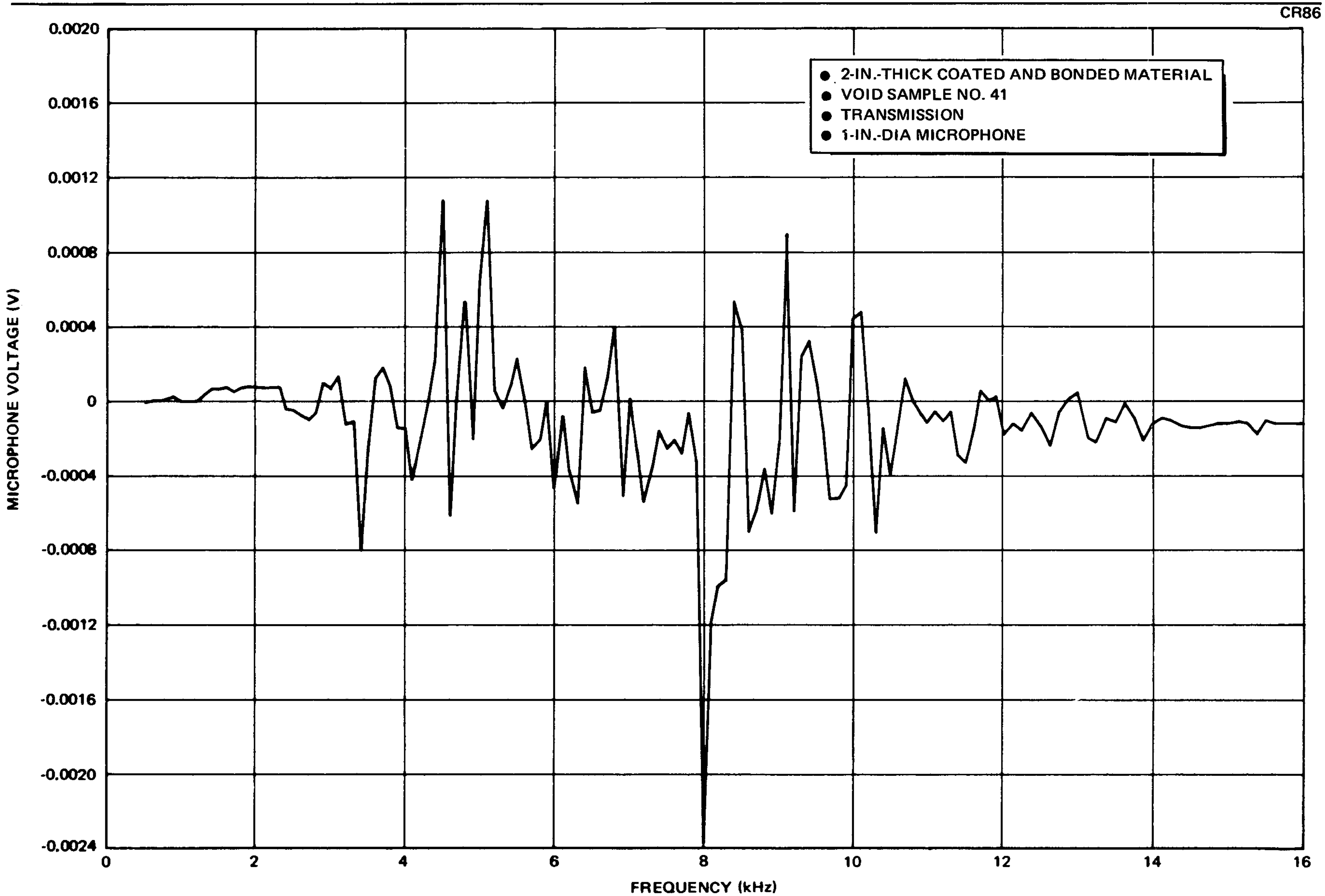

Figure 2-35. Difference in Air-Coupling Response for Sample No. 41 (Control Sample No. 42)

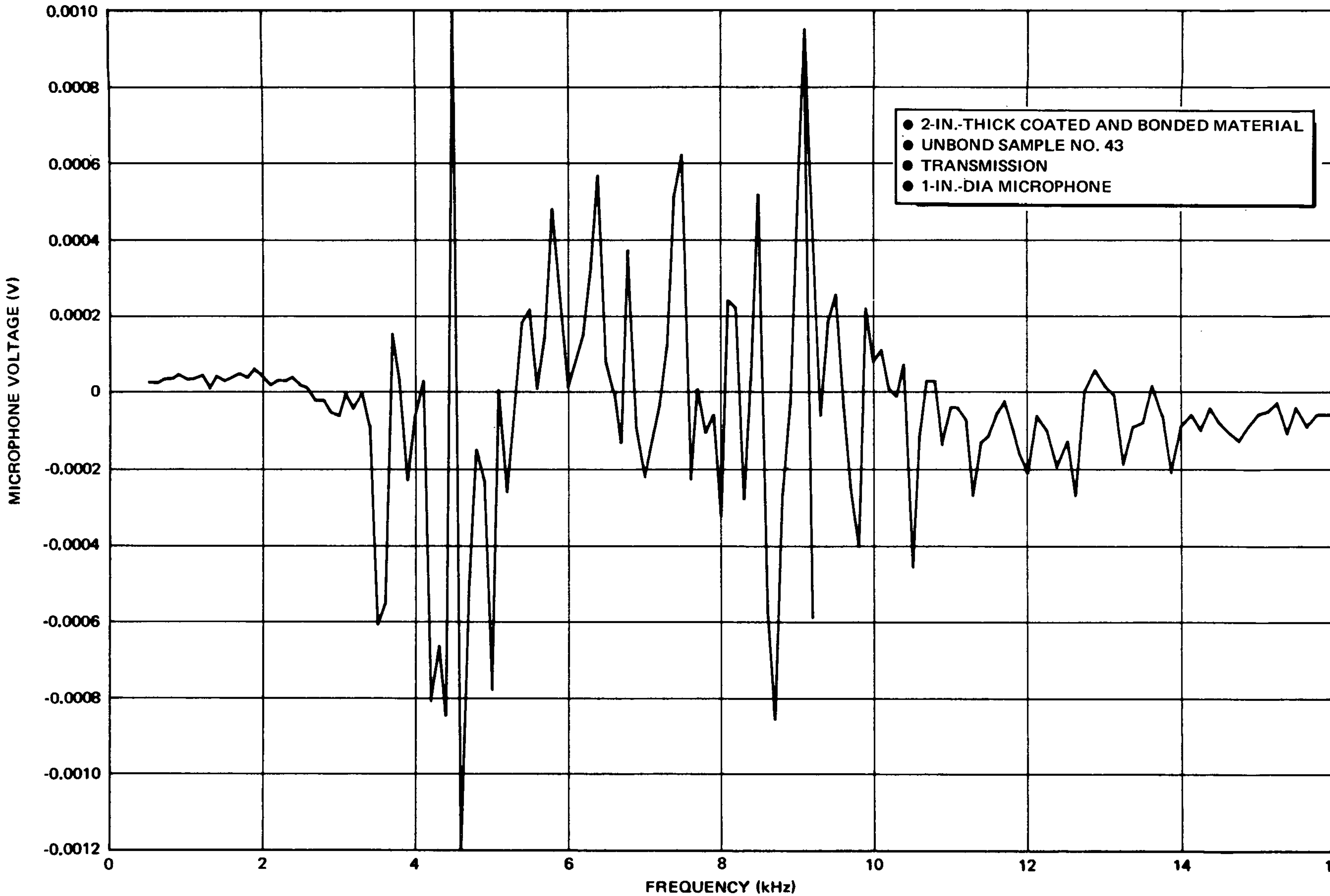

Figure 2-36. Difference in Air-Coupling Response for Sample No. 43 (Control Sample No. 42)

CR86

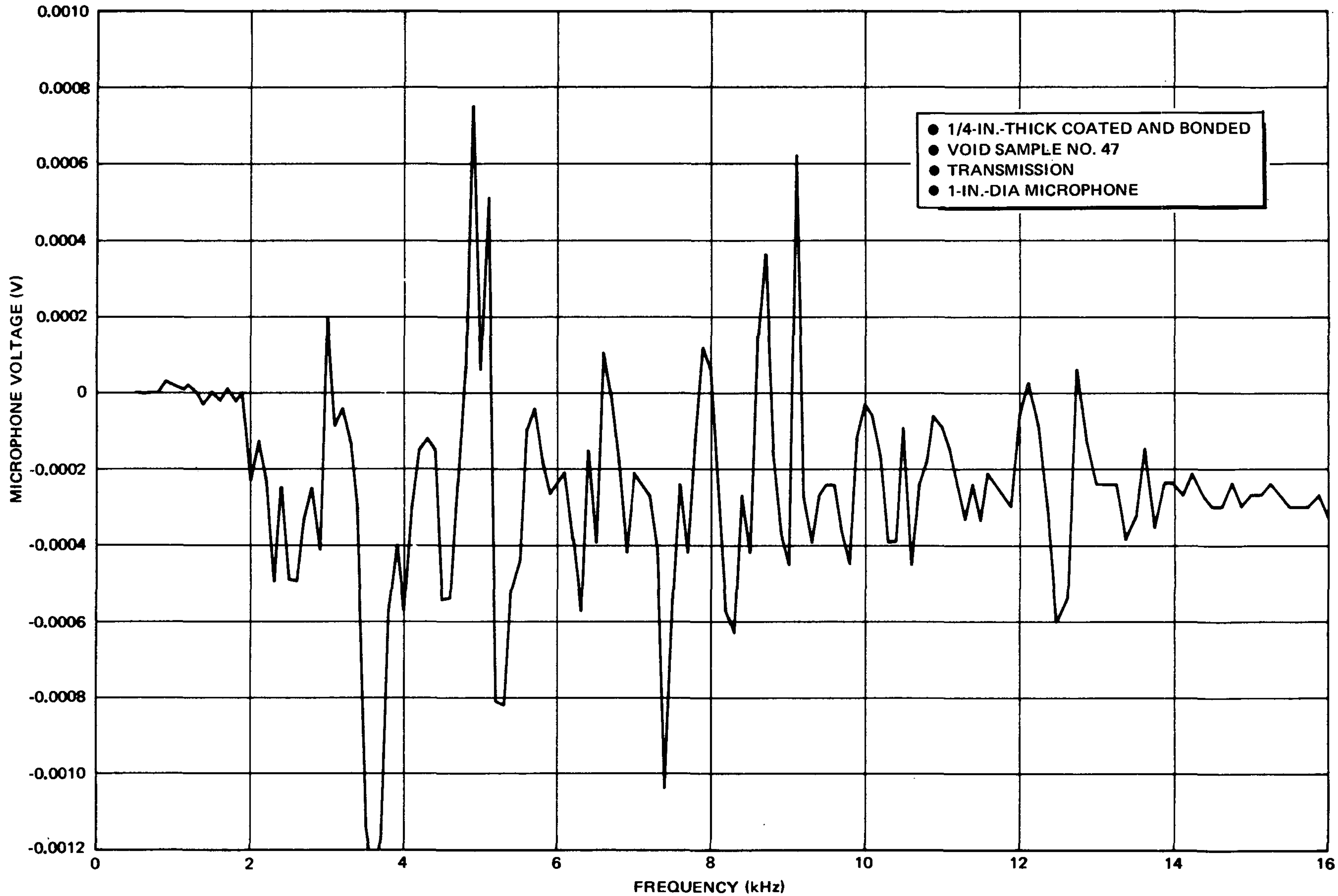

Figure 2-37. Difference in Air-Coupling Response for Sample No. 47 (Control Sample No. 46)

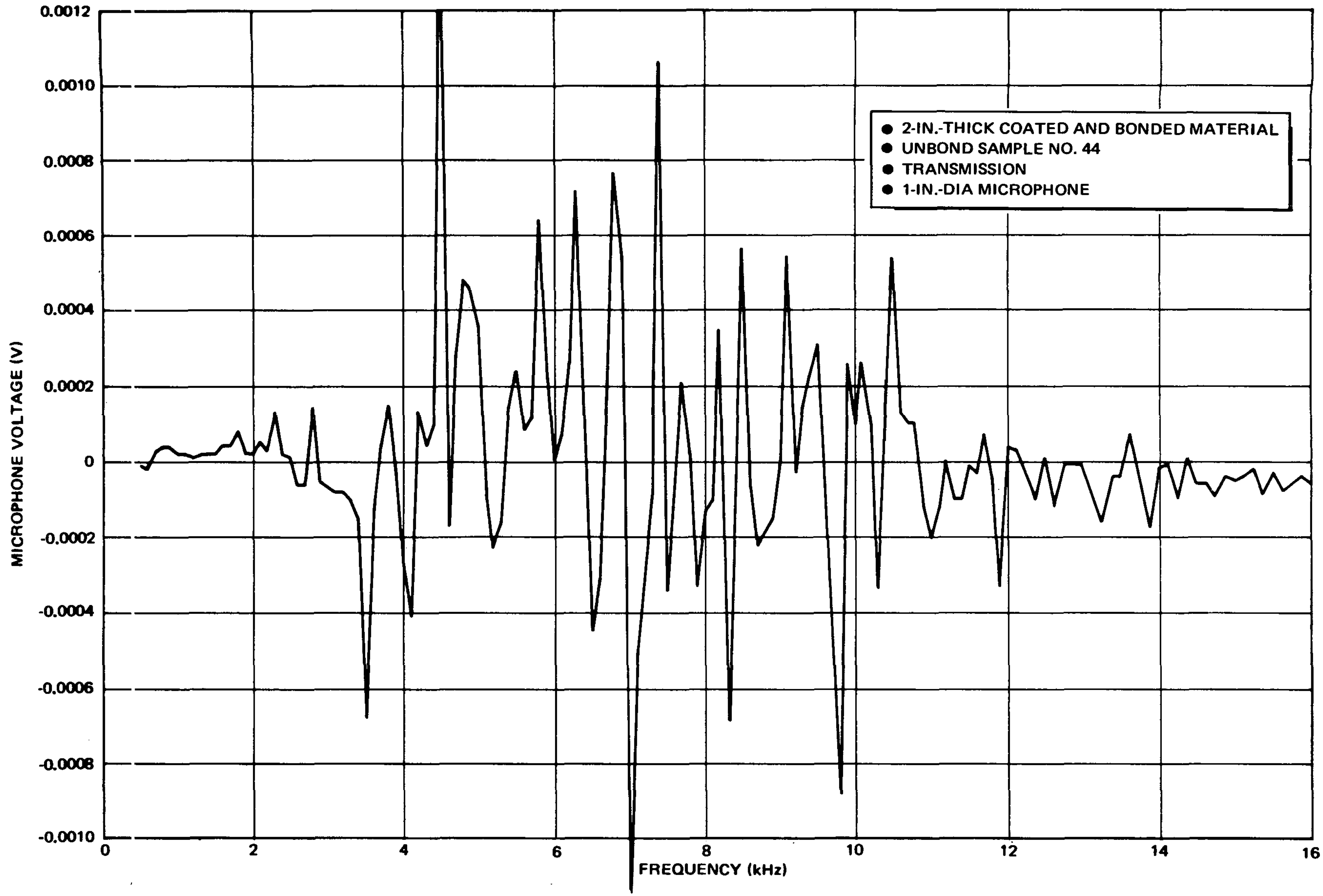

Figure 2-38. Difference in Air-Coupling Response for Sample No. 44 (Control Sample No. 42)

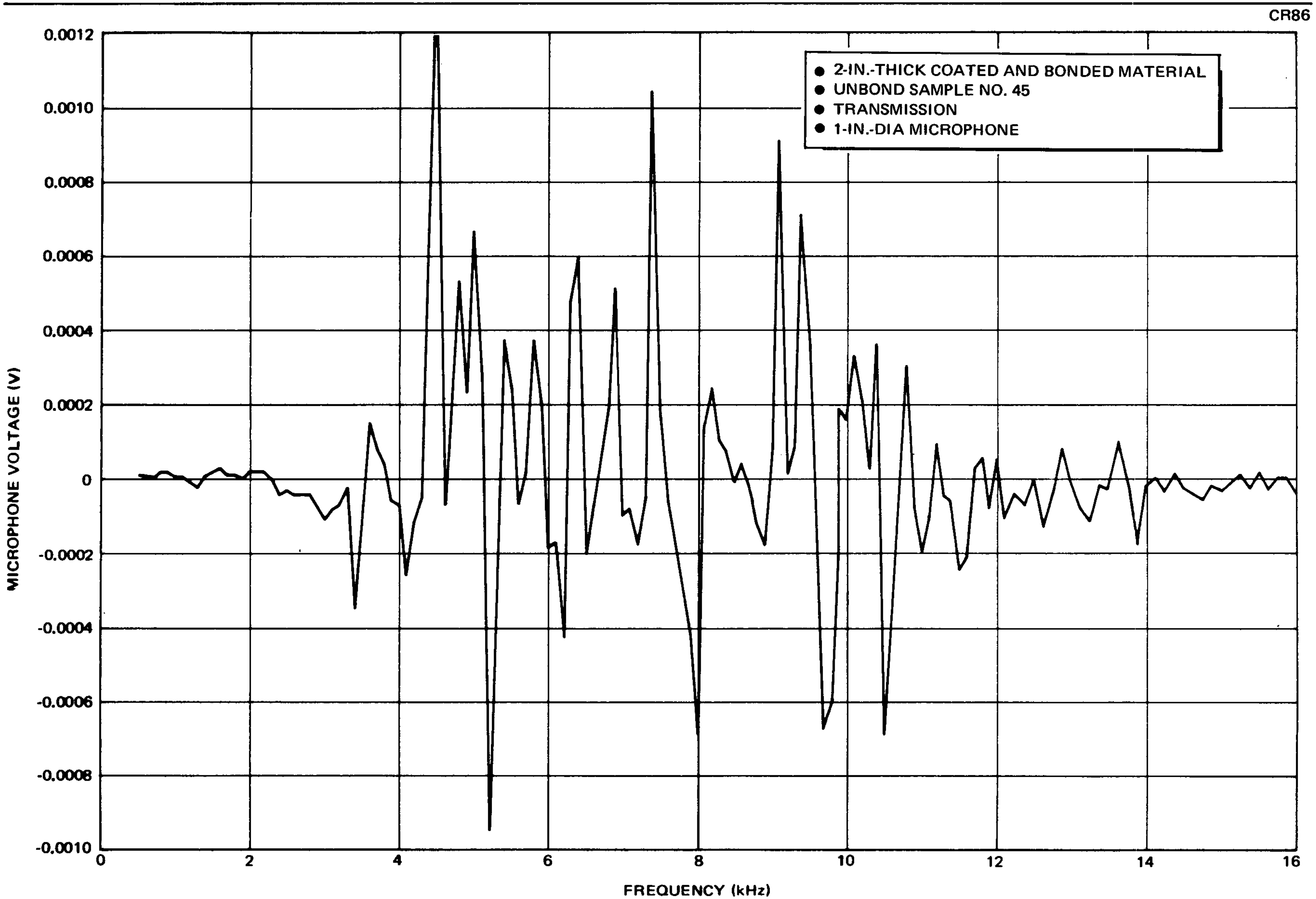

Figure 2-39. Difference in Air-Coupling Response for Sample No. 45 (Control Sample No. 42)

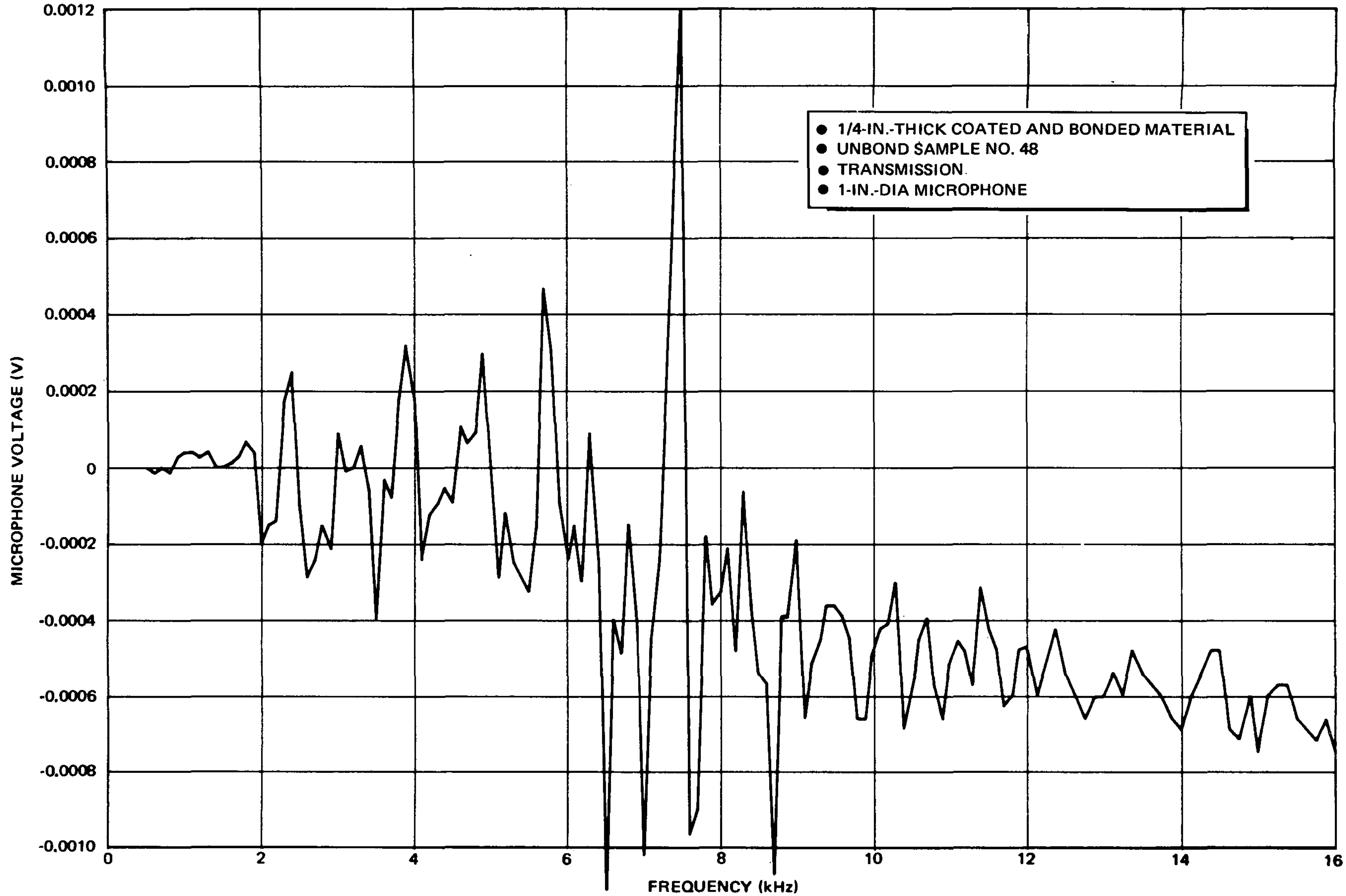

Figure 2-40. Difference in Air-Coupling Response for Sample No. 48 (Control Sample No. 46)

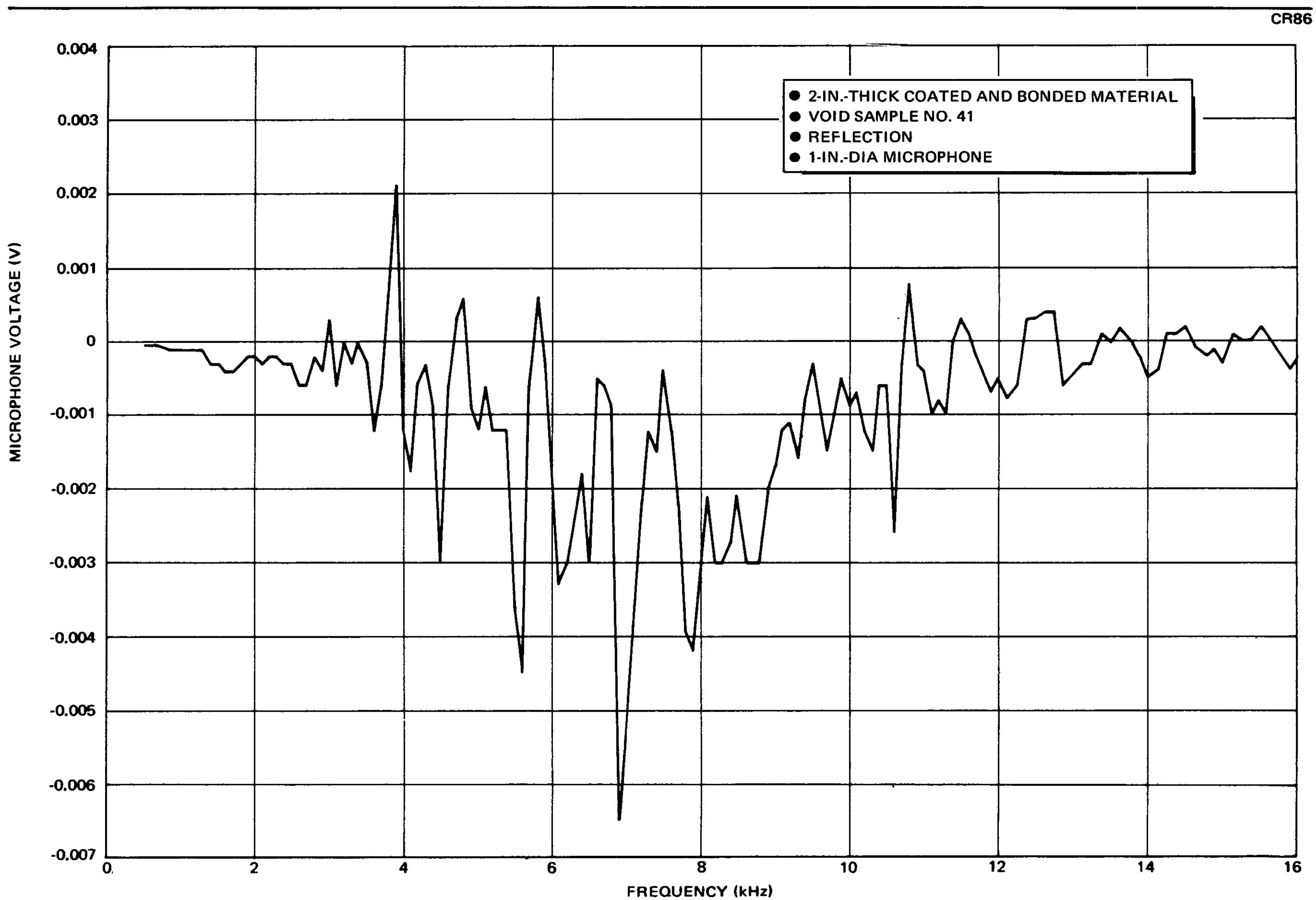

Figure 2-41. Difference in Air-Coupling Response for Sample No.41 (Control Sample No.42)

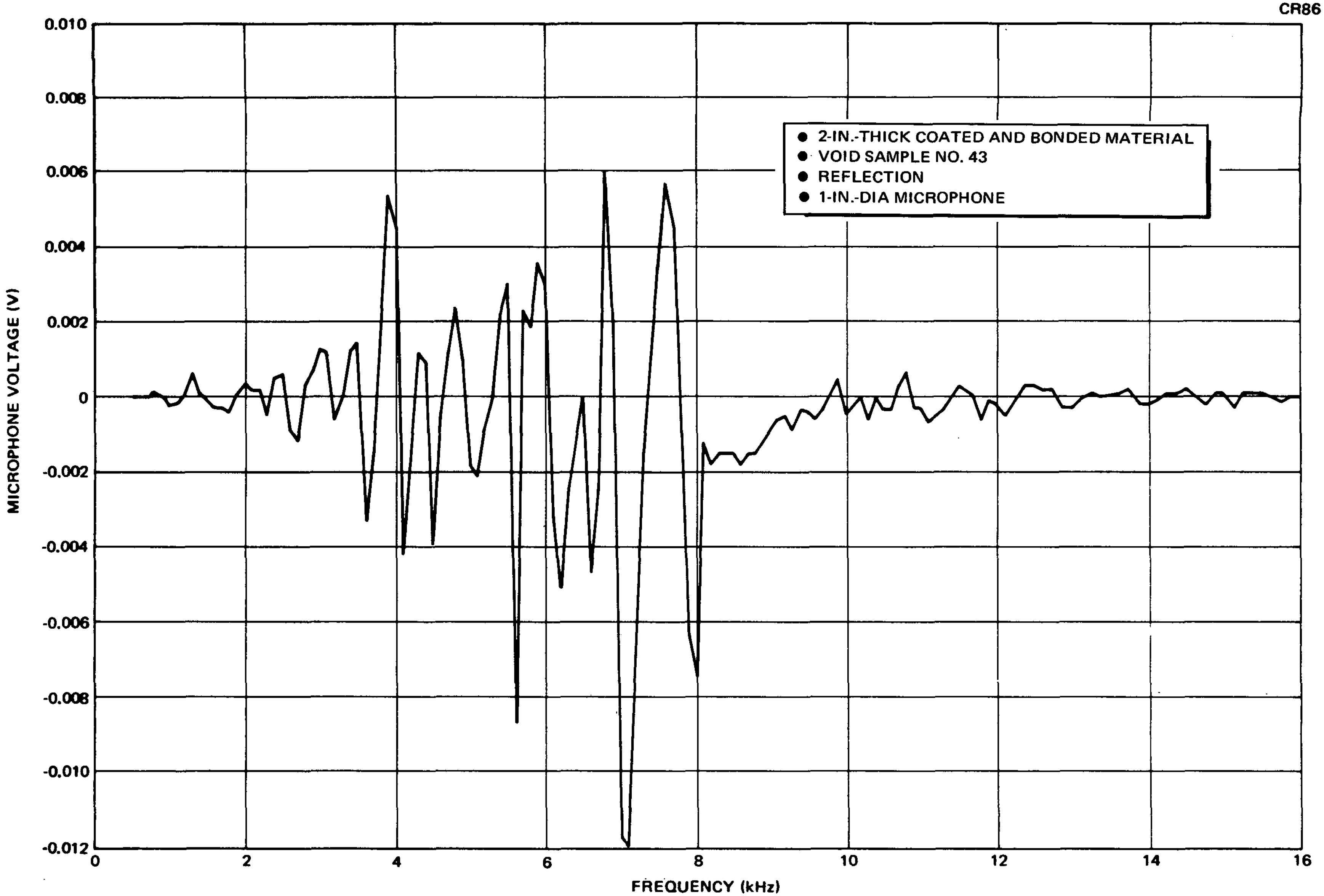

Figure 2-42. Difference in Air-Coupling Response for Sample No. 43 (Control Sample No. 42)

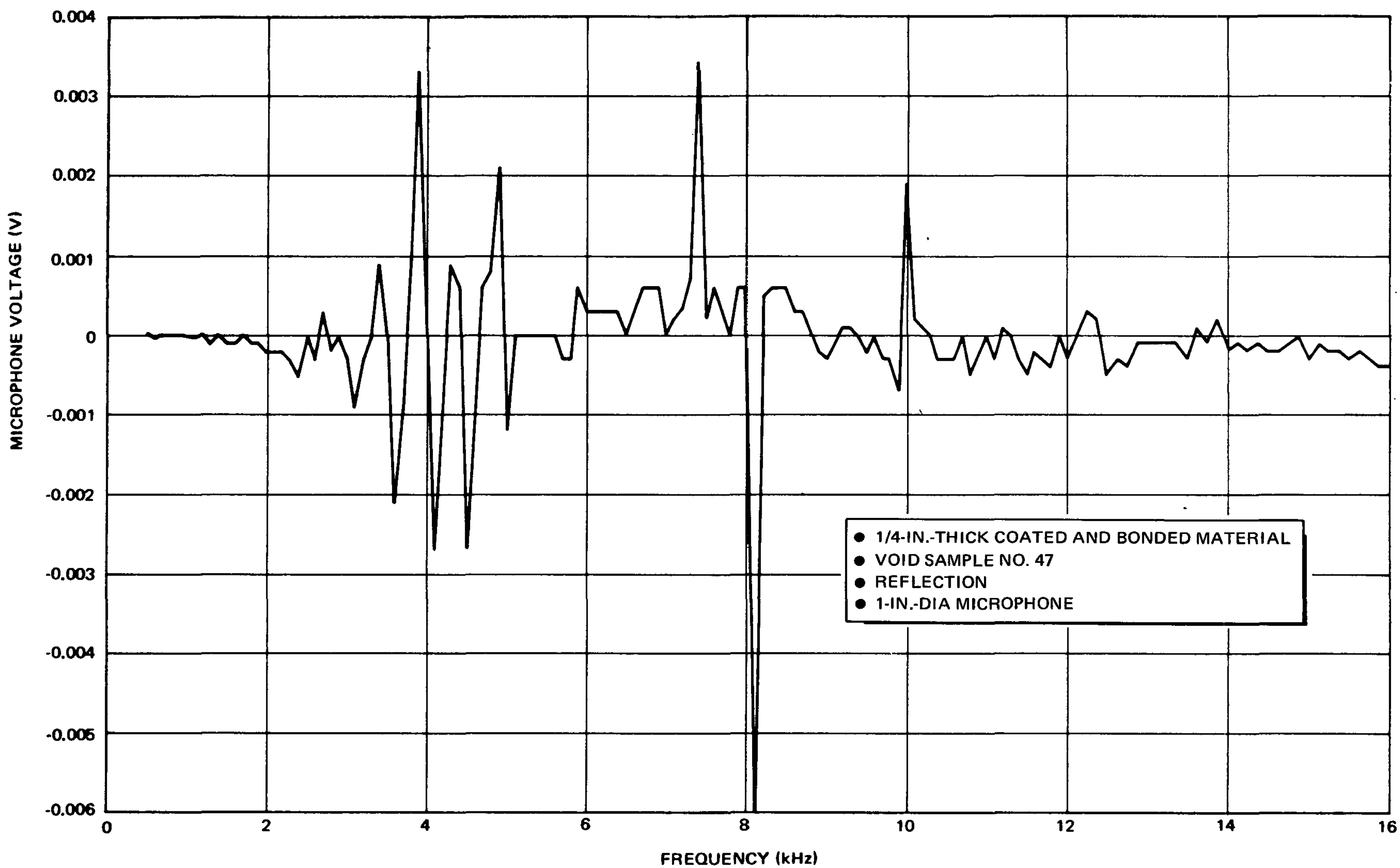

Figure 2-43. Difference in Air-Coupling Response for Sample No. 47 (Control Sample No. 46)

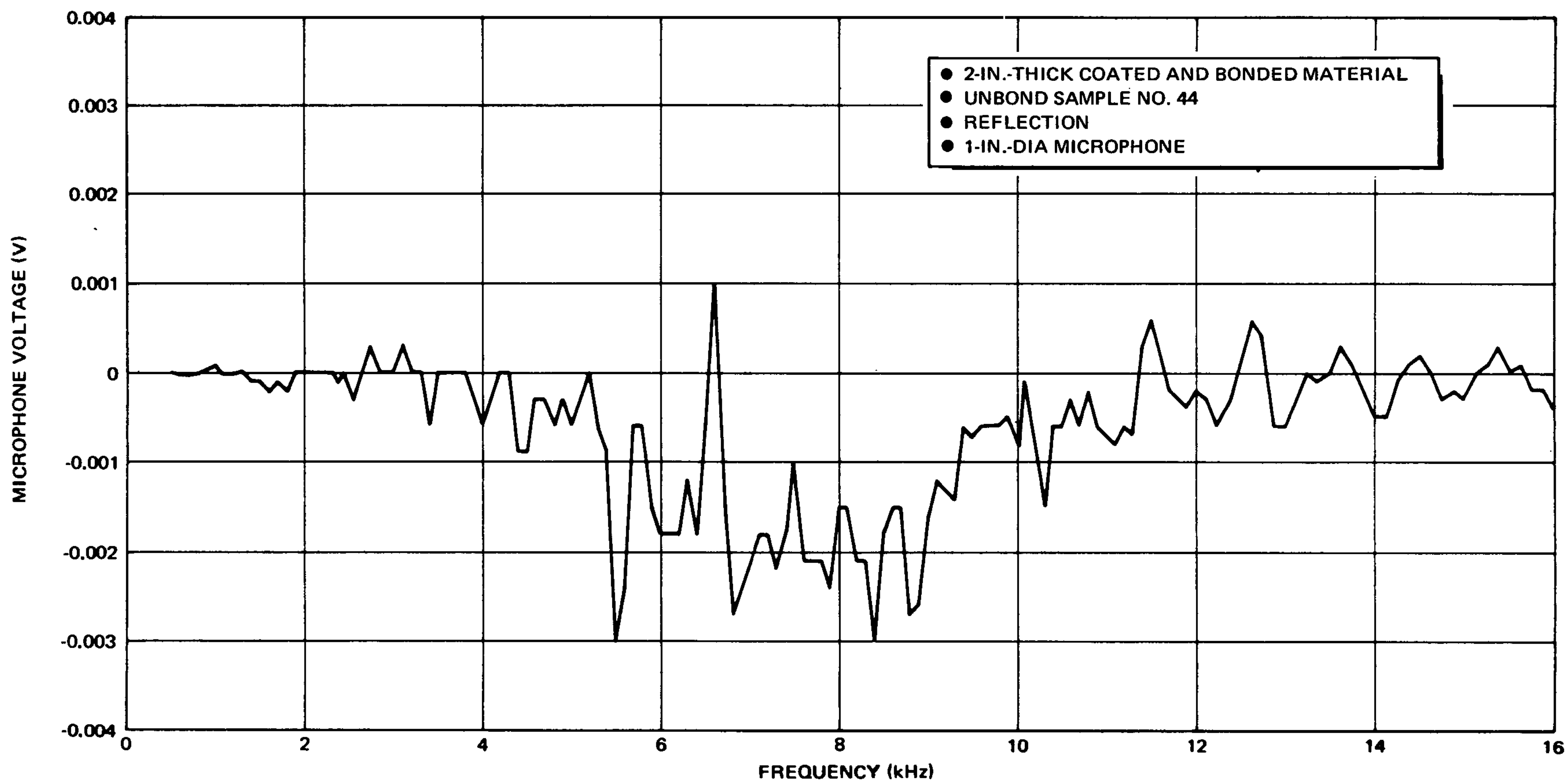

Figure 2-44. Difference in Air-Coupling Response for Sample No. 44 (Control Sample No. 42)

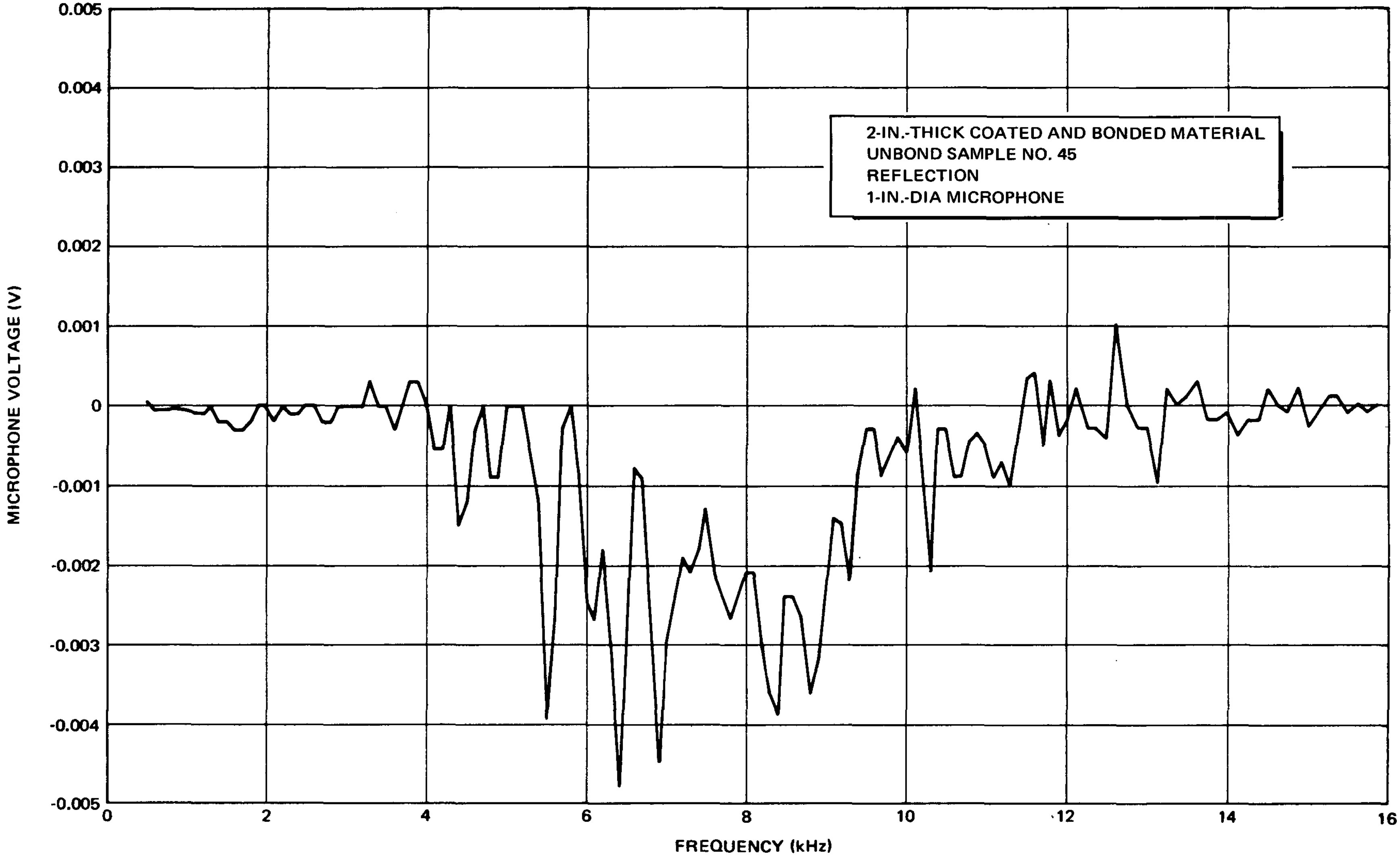

Figure 2-45. Difference in Air-Coupling Response for Sample No. 45 (Control Sample No. 42)

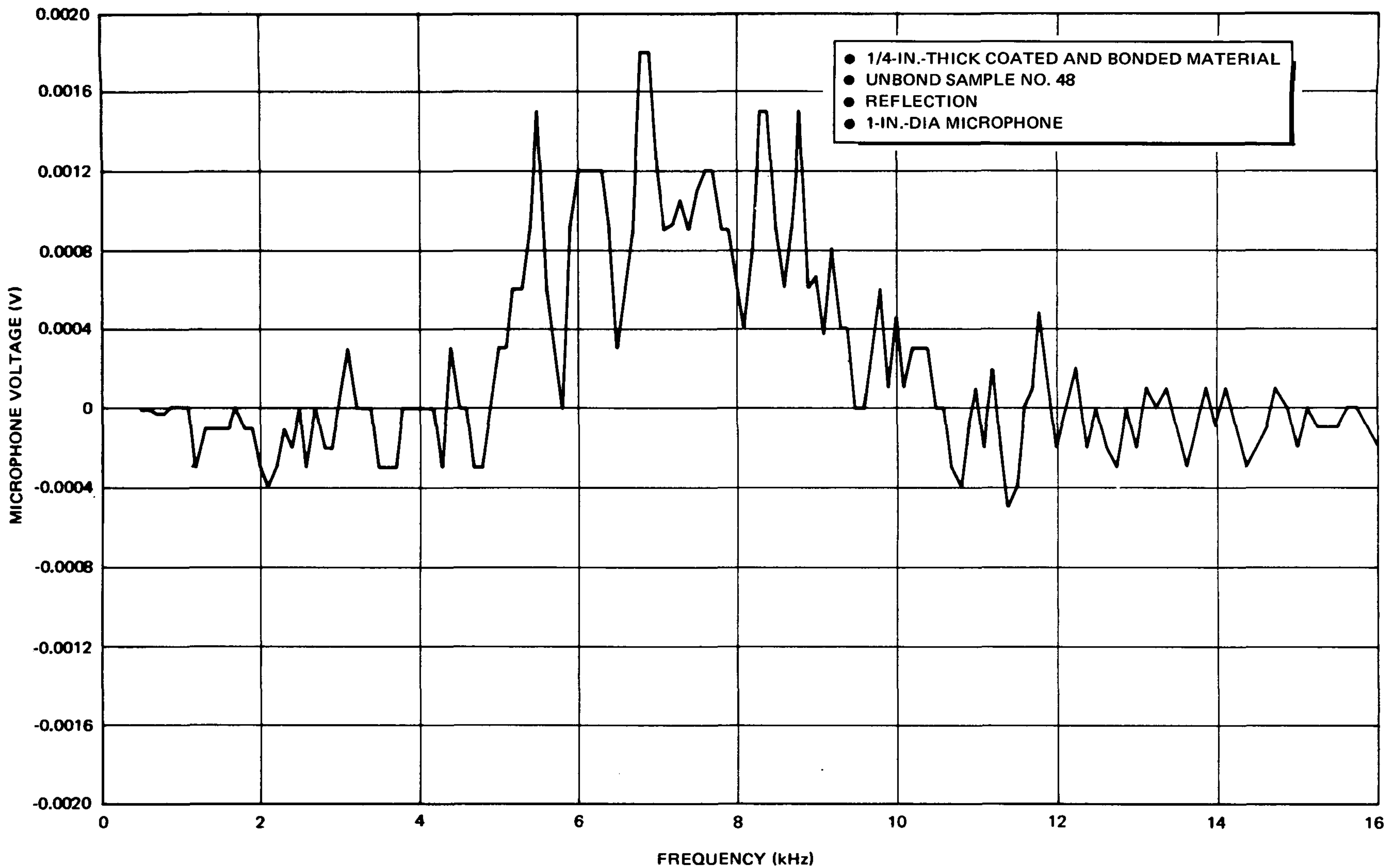

Figure 2-46. Difference in Air-Coupling Response for Sample No. 48 (Control Sample No. 46)

are introduced electromagnetically. Many different combinations of instrument dial settings appeared to yield essentially the same results. A representative setting was 8.85 for the Frequency and 9.3 for the Sensitivity with the Output on HI. The alarm level was adjusted for these settings until good and bad bond regions could be distinguished. This technique was successful when applied from the metallic side for the bondline void defects. The technique was not successful for the unbond defects nor for the void defects when applied from the RSI side of the samples. The probe would not properly excite the aluminum substrate through the separation of RSI.

2.4.3 Microwave

Microwaves are electromagnetic radiation with frequencies between those of radiowaves and infrared, roughly from 1 to 100 GHz. Microwaves travel in straight lines, reflect, refract, diffract, interfere and scatter according to the same laws as light. Unlike light, microwaves penetrate most nonmetallic materials, reflecting and scattering from internal discontinuities and boundaries, and interacting with the molecules of the material. These properties lead to numerous applications in nondestructive testing (Reference 7 through 9).

One of the primary applications of microwaves has been the measurement of moisture (References 10 and 11). Water has a dielectric constant of 35 or higher and high loss properties. Most nonmetallics have a dielectric constant ranging from 1.5 to 5 and very low loss properties. The RSI material evaluated in this program is a form of silica and mullite (predominately silica and alumina) and has a dielectric constant of approximately 9 and very low loss properties, as much as 1,000 times less than that of water. Thus, even a small amount of moisture in a specimen will cause an appreciable change in the overall electromagnetic impedance.

Other applications of microwaves have been their aid in the detection of cracks, delaminations, and voids in nonmetallics (Reference 12). Studies have also been conducted on the microwave detection of bondline defects (Reference 13).

Microwave transmission and reflection techniques are used for nondestructive testing in much the same way as ultrasonic techniques. The primary difference is that microwaves are sensitive to changes in electromagnetic impedance rather than acoustic impedance. Changes in the amplitude and phase of the received microwaves relative to the transmitted microwaves are related to changes in the electromagnetic impedance. The basic method consists of adjusting the analyzer for some arbitrary phase and amplitude reading. A sample of the material being evaluated is then placed on the horn (between the horns for transmission) and the resulting phase and amplitude of the reflection or transmission coefficient is determined. This method depends upon the sample being somewhat larger than the horn aperture in order to ensure adequate decoupling from reflection at the sample edges.

Since transmission and reflection techniques should have the same sensitivity for moisture detection and the transmission technique will not be applicable to the final, metal-backed, sample configuration, only the reflection technique was evaluated in this program. To determine the effect of frequency upon moisture, density, delamination, and void defects, two frequencies were selected. The lower frequency of 9 GHz was chosen based upon the size of the samples available. Lower frequencies would have re required larger samples. The higher frequency of 15 GHz was chosen for the upper limit because higher frequencies might provide too high a sensitivity to material nonuniformity.

2.4.3.1 Microwave Measurement Equipment

Two different microwave measurement systems were employed, one for each frequency. Hewlett-Packard equipment was used for the 9 and 15 GHz systems, as shown schematically in Figures 2-47 and 2-48, respectively. The 9-GHz horn aperture was 2-5/8 x 2 in. and the 15-GHz horn aperture was 1-9/16 x 1-1/8 in.

The microwave phase and amplitude reference levels for both frequencies were established as follows. The gain on the HP 8410A Network Analyzer was set at 21 db. A metal short was placed across the horn, reflecting

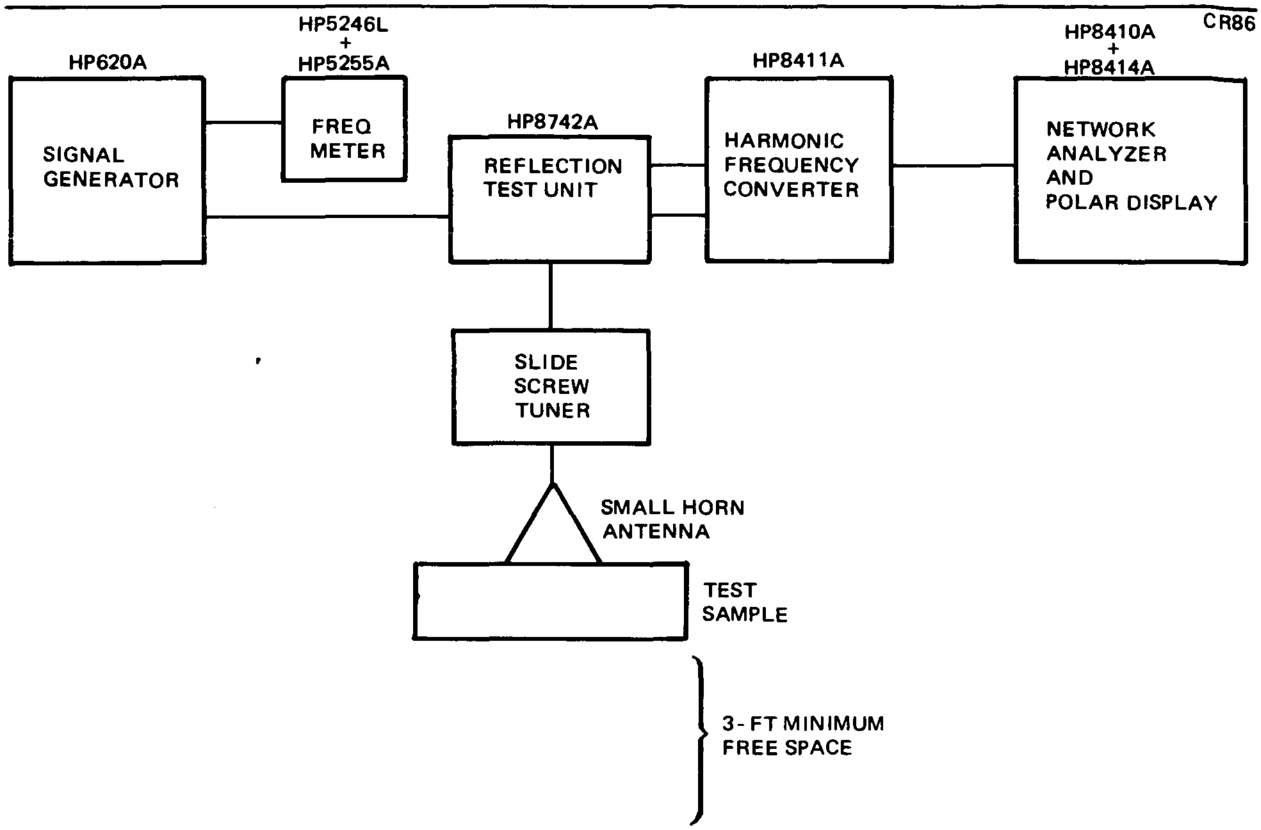

Figure 2-47. 9-GHz Microwave Measurement System.

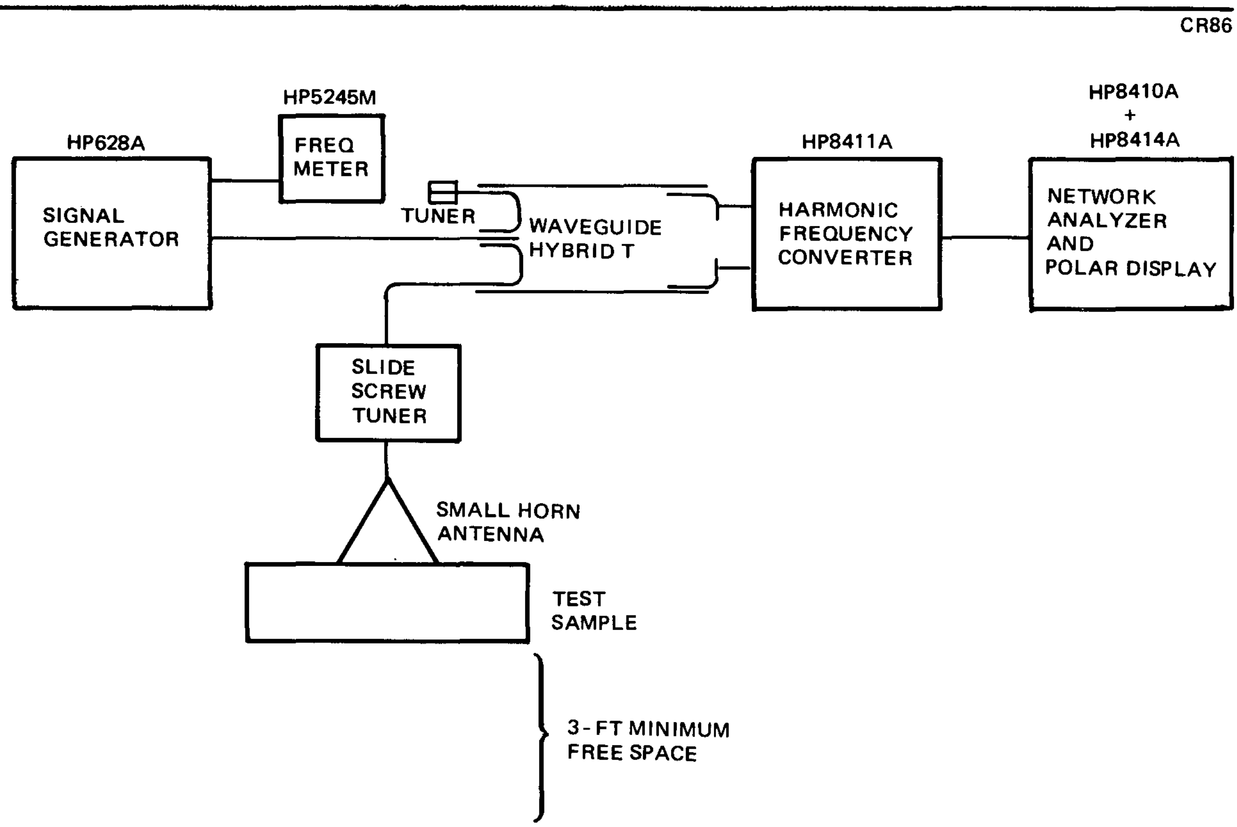

Figure 2-48. 15-GHz Microwave Measurement System

all the incident energy back into the horn. The amplitude gain was then adjusted for an amplitude of 1 on the polar display. With the metal short removed and the HP 8410A gain set at 35 db, the slide screw tuner was adjusted for zero phase and amplitude on the polar display. A change of gain from 21 to 35 db corresponds to an amplification of 5 times. With the metal short placed on the horn and the gain reduced to 21 db, the HP 8410A was readjusted for zero phase and an amplitude of 1. The reflected and transmitted microwaves are actually out of phase by 180 degrees. The analyzer was adjusted for a phase of 0 degree, solely for convenience.

2.4.3.2 Uncoated Samples

The uncoated samples were then centered on the horn and the resulting phase and amplitude measured. The results for the 2-in.-thick control, void, delamination, and density variation samples are shown in Figure 2-49 for 9 GHz and Figure 2-50 for 15 GHz. In these figures the phase is given by the polar angle and the amplitude is given by the radial distance. As the figures show, each type of sample has a different combination of phase and amplitude than every other sample. The void sample was placed on the horn both with the void up (away from the horn) and with the void down (toward the horn). The samples were chosen for uniformity by x-ray density, dimensional, and visual checks. The phase and amplitude for the void and delamination defects were different than for the control. The difference was greater for 15 GHz. The lower density sample also had a different phase and amplitude than the higher density control. These results suggest that it may be possible to distinguish between different types of defects through microwave measurements. For larger sample sizes, it should be possible to scan the sample and detect these defects as changes in the basic phase and amplitude of the nondefective sample.

The microwave moisture measurements were made as follows. First, the phase and amplitude reference levels for both systems were established as before — zero phase and amplitude of 1 for metal short, zero phase and amplitude for open horn. The samples were then weighed. Water was uniformly sprayed on one of the two large faces until the weight of the sample plus water was approximately 30 percent greater than the dry sample weight.

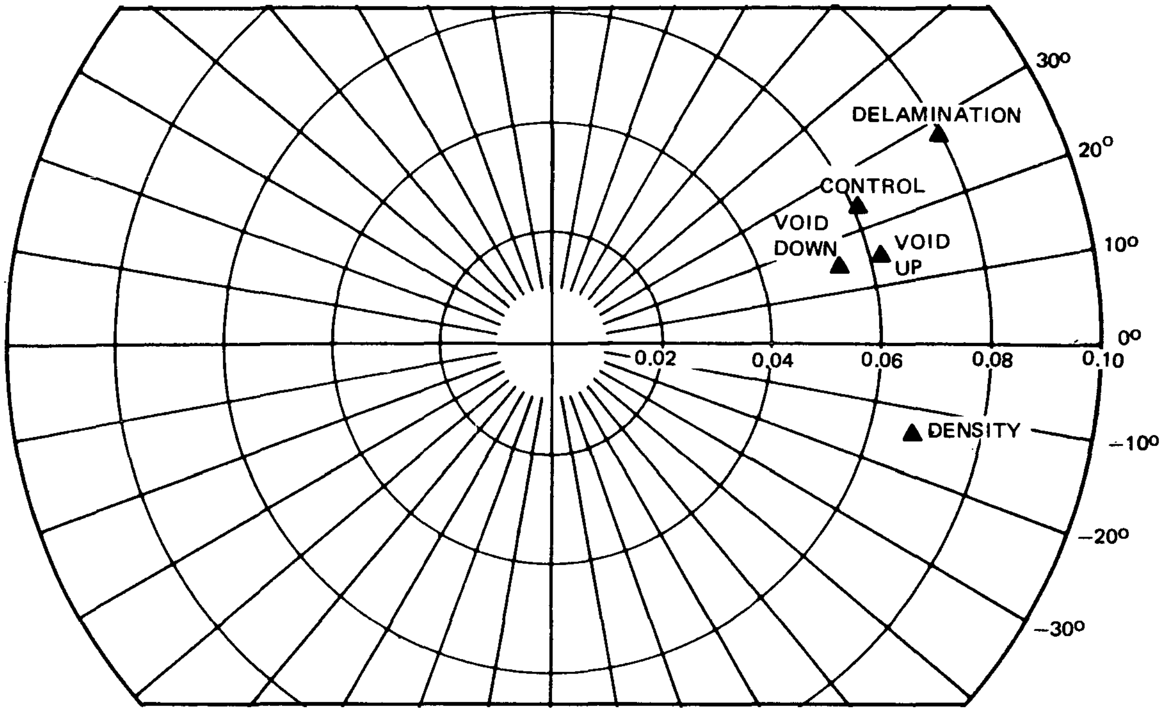

Figure 2-49. Microwave Results at 9 GHz for 2-In.-Thick Uncoated Material

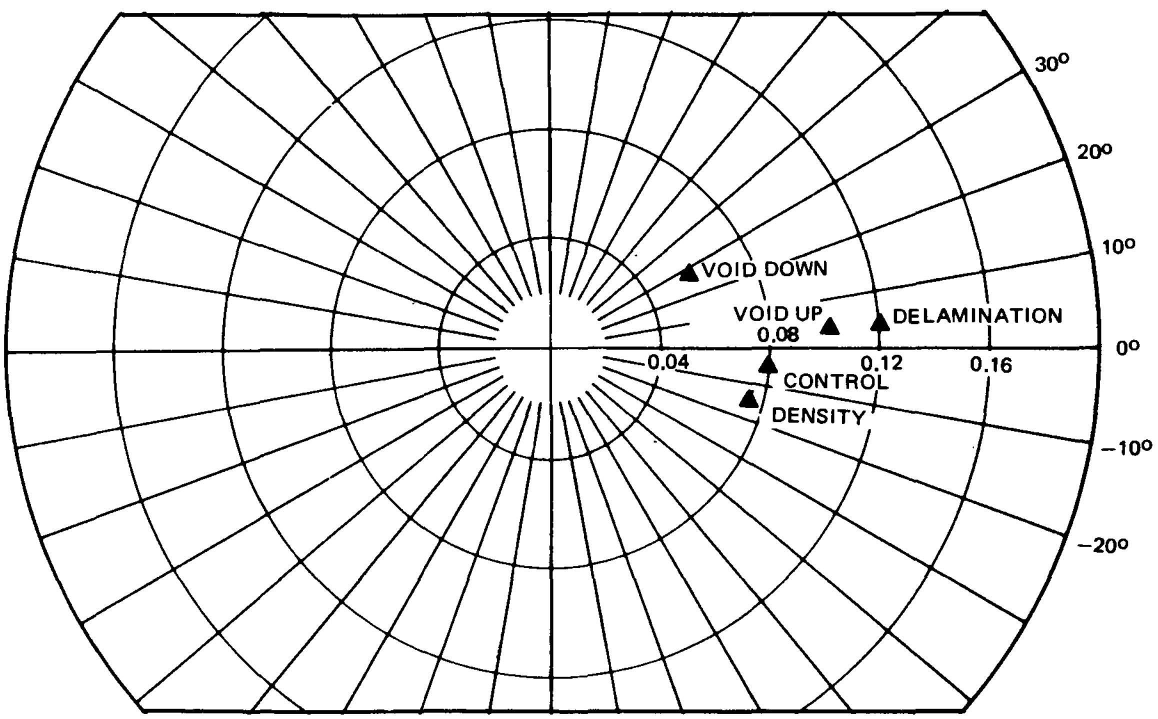

Figure 2-50. Microwave Results at 15 GHz for 2-In.-Thick Uncoated Material

The samples were kept at room temperature until the percentage of moisture had fallen to approximately 25 percent and the water had been allowed to disperse itself more uniformly throughout the samples. The samples were then placed with the drier face on the horn and phase and amplitude measurements were taken. This procedure was repeated several times, each time for a different percentage of moisture.

A check to determine if the dry sample readings were repeatable was made after the samples had been allowed to dry at room temperature for a weekend.

Measurements were then taken at several different locations on the dry control and density variation samples to determine the variability in the measurements. Finally, the moisture measurements were repeated for very low moisture contents.

The moisture measurement results are shown in Figures 2-51 through 2-56. Figure 2-51 shows the results at 9 GHz for the 2-, 1-, and 1/4-in. -thick control samples. This figure shows the locus of points (phase and amplitude) followed by the samples for various percentages of moisture content. Figure 2-52 shows the same results expressed as amplitude versus moisture content and Figure 2-53 shows the results expressed as phase versus moisture content. Similarly, the results at 15 GHz are shown in Figure 2-54 as a polar plot of phase and amplitude as a function of moisture content. Figure 2-55 shows the same results as amplitude versus moisture content, and Figure 2-56 shows the results as phase versus moisture content.

Generally, the amplitude of the reflected microwaves is proportional to the percentage of moisture present. For large moisture contents, the slope of the amplitude-versus-moisture-content curve becomes smaller. Thus, microwave amplitude measurements are most sensitive for small percentages of moisture present. As would be expected, the technique is more sensitive for thinner material. Furthermore, the results at 15 GHz are more sensitive and uniform than those at 9 GHz. In some cases, the amplitude for low moisture contents becomes less than the amplitude for zero moisture content. This phenomenon might be due to interference effects from front and back surface reflections.

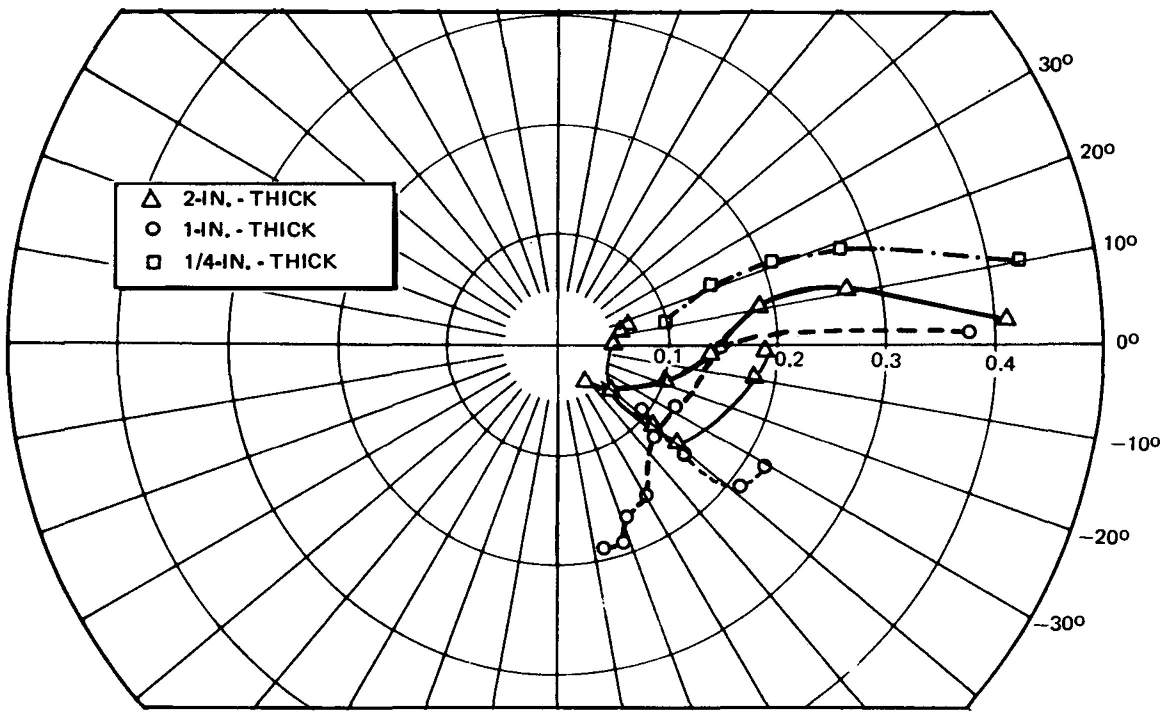

Figure 2-51. Microwave Moisture Detection at 9 GHz for Uncoated Material

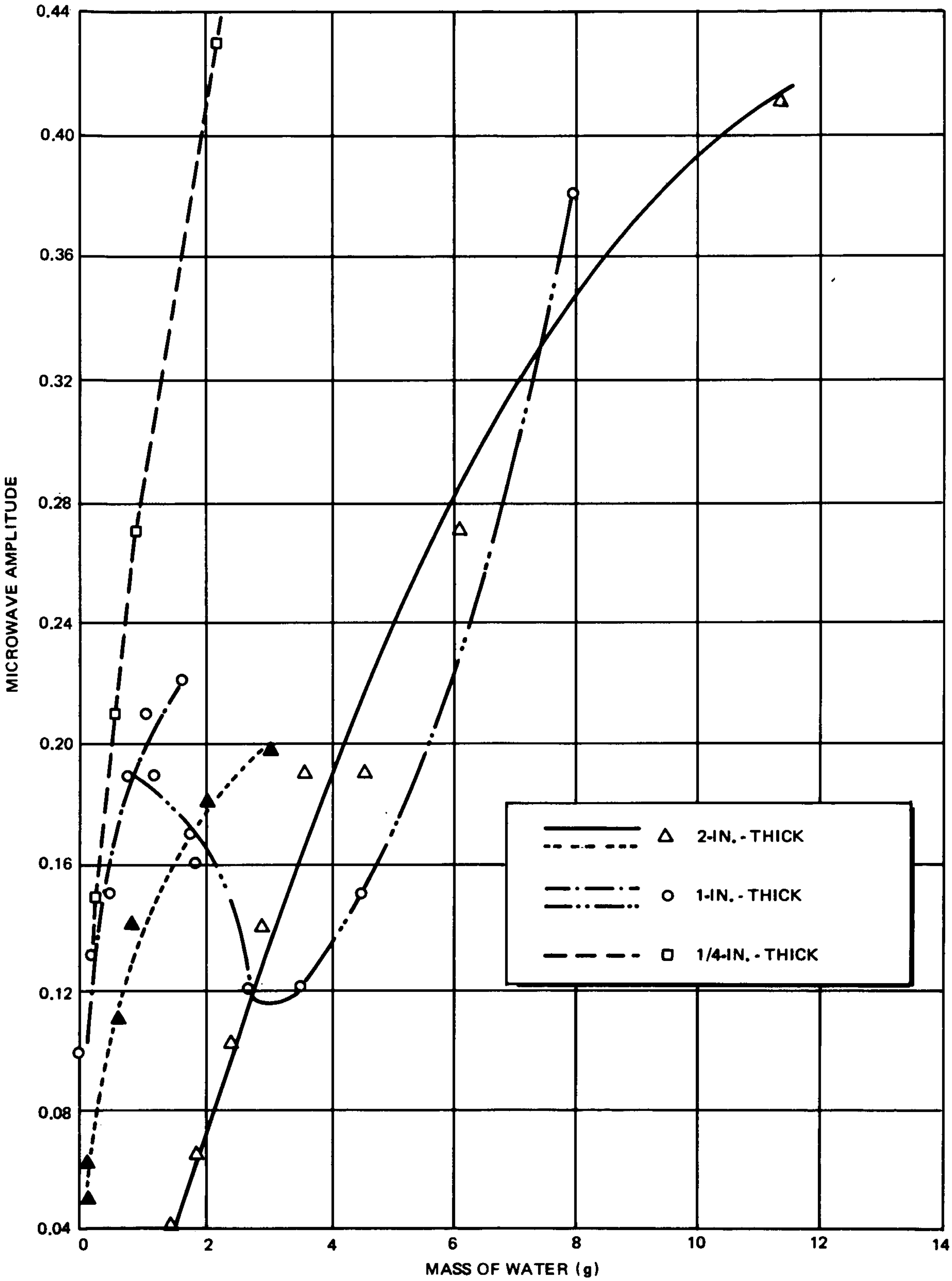

Figure 2-52. Microwave Amplitude Versus Mass of Water at 9 GHz for Uncoated Material

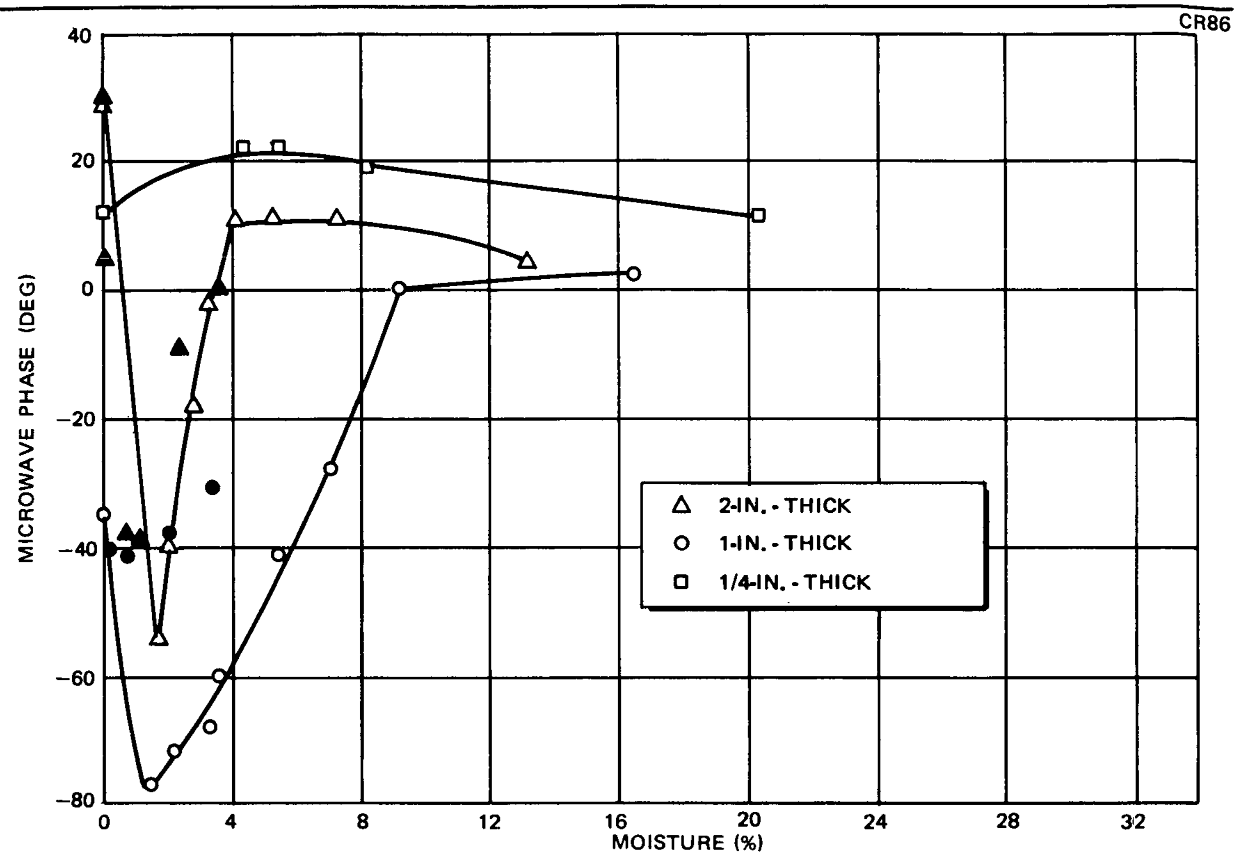

Figure 2-53. Microwave Phase Versus Moisture Percentage at 9 GHz for Uncoated Material

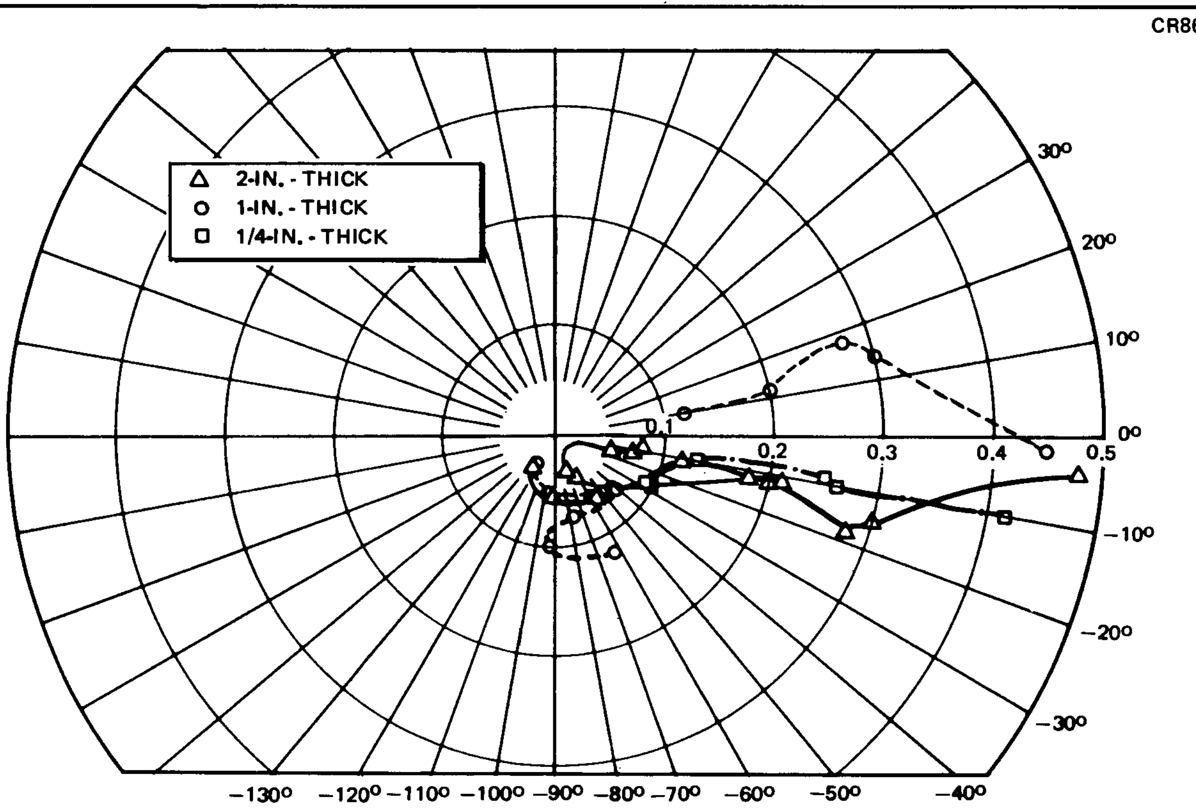

Figure 2-54. Microwave Moisture Detection at 15 GHz for Uncoated Material

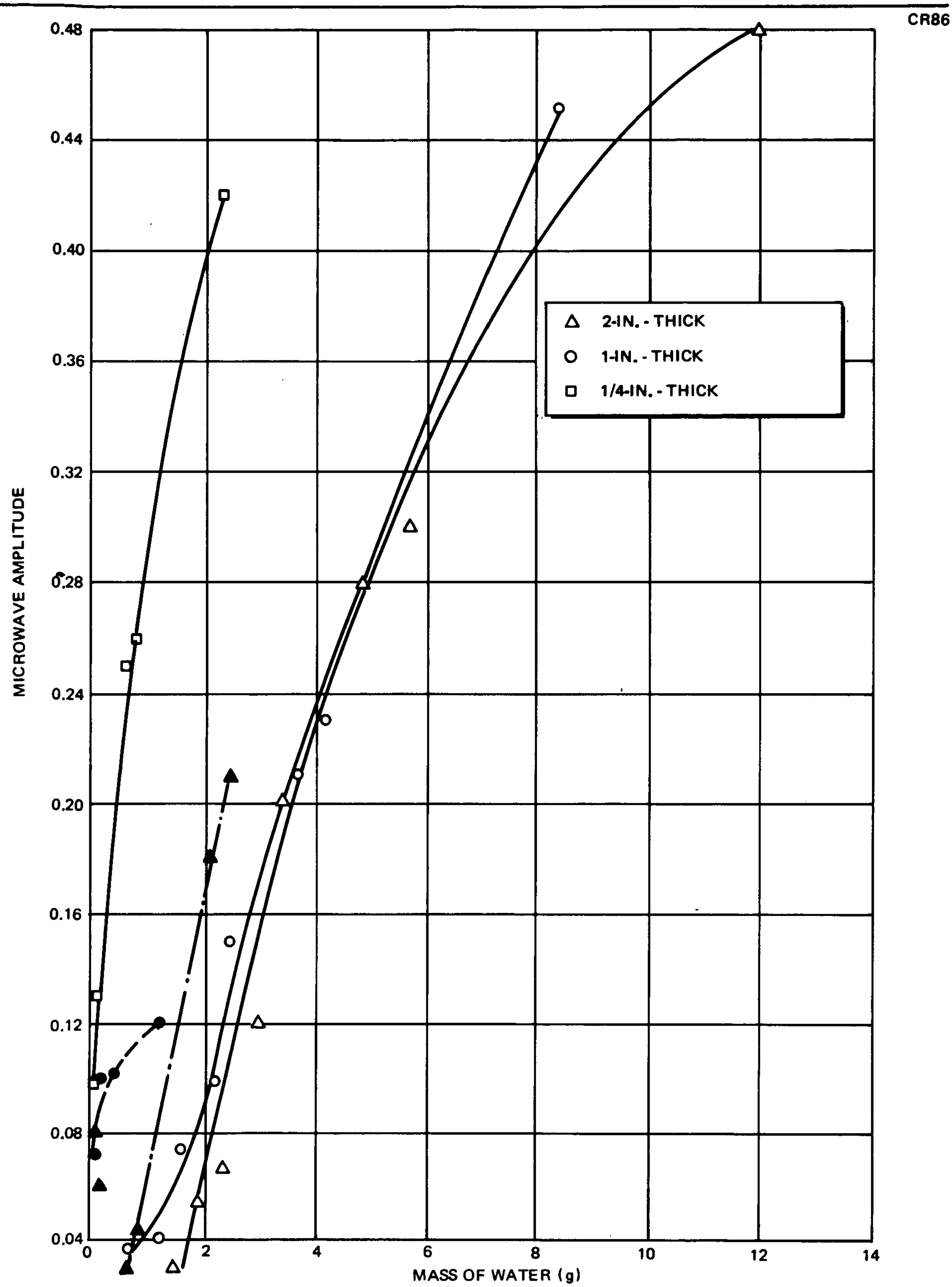

Figure 2-55. Microwave Amplitude Versus Mass of Water at 15 GHz for Uncoated Material

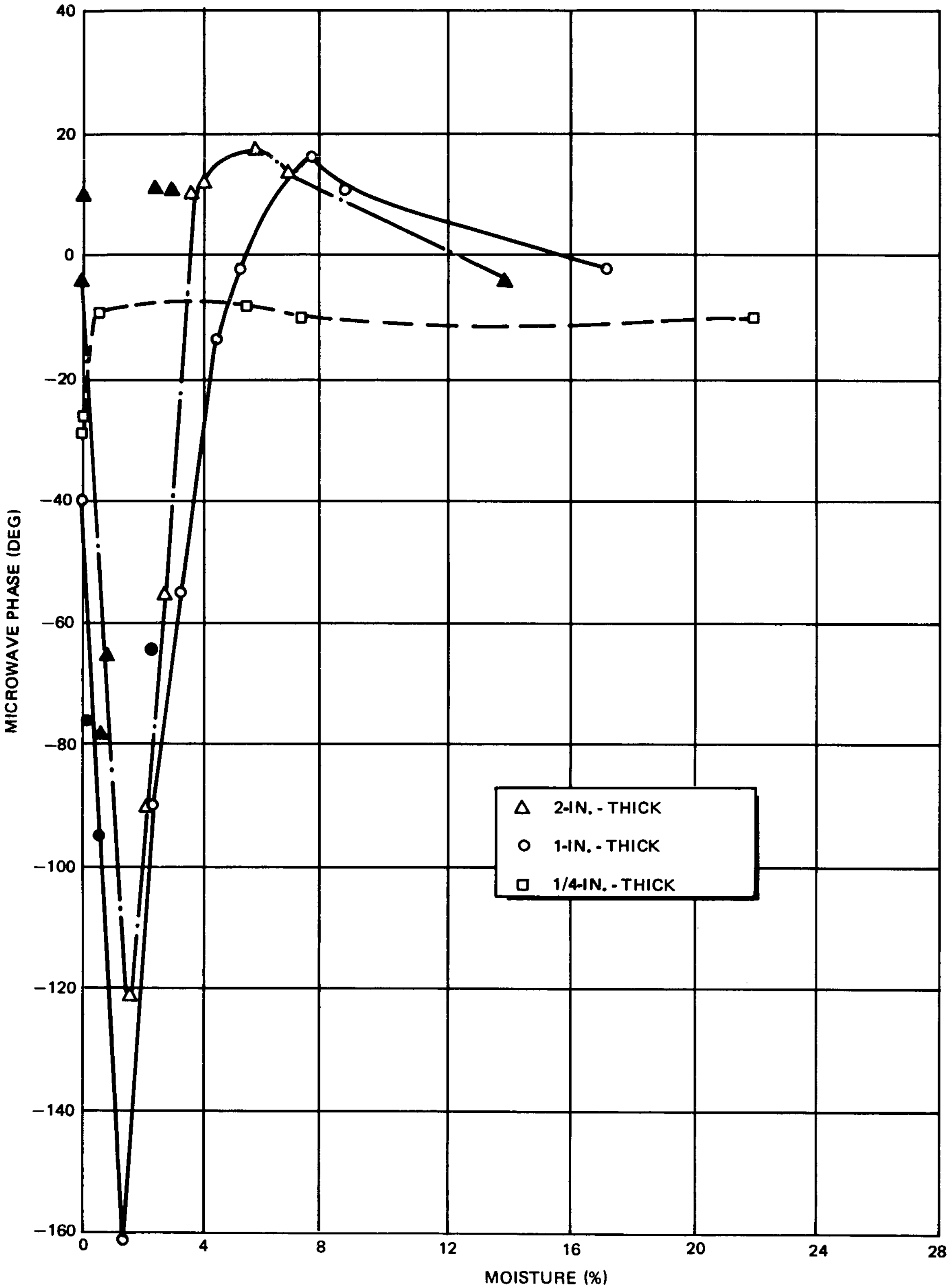

Figure 2-56. Microwave Phase Versus Moisture Percentage at 15 GHz for Uncoated Material

The phase-versus-moisture-content plots show a dip at approximately 2 percent moisture content. This is due to a bend in the polar plot of phase and amplitude versus moisture. The phase does not provide as useful a measure of the moisture content as does the reflection amplitude.

A recheck of the dry sample measurements showed that the sample mass returned to within less than 0.5 percent of the original mass, the reflection amplitudes returned to their original values, and the phases returned to within 20 percent (at most) of their original values

A check of sample variability showed that readings taken from various locations on the samples had less variability at 9 GHz than at 15 GHz. There was less variability in the amplitude than in the phase readings. The low density sample had the greatest variability, up to 9 percent variability in the amplitude readings and 57 percent variability in the phase readings at 15 GHz. For the control samples, the amplitude variability was less than 4.3 percent and the phase variability was less than 20 percent.

2.4.3.3 Coating Samples

The microwave measurement systems were adjusted as before. The coated surface of samples with different coating thicknesses was placed on the horn and phase and amplitude measurements taken at different locations for each sample. It was not possible to distinguish changes in coating thickness as the variability in both the phase and amplitude measurements resulted in overlapping values from sample to sample. Thus, coating thickness did not influence the readings obtained. Measurements taken on a sample with a loss of adhesion between the coating and the basic RSI material were the same as those for the coating thickness variation samples. Thus, it was not possible to detect a loss of adhesion defect.

2.4.3.4 Coated Samples

Two sets of moisture measurements were taken for 2- and 1/4-in.-thick coated samples as before. The results for 9 GHz are shown in Figure 2-57 as a polar plot and in Figure 2-58 as amplitude versus moisture content. The results for 15 GHz are shown in Figure 2-59 as a polar plot and in Figure 2-60 as amplitude versus moisture content. Water was sprayed on the noncoated surface and the coated surface was placed on the horn. The results for the coated specimens were not as conclusive as for the uncoated specimens. The results at both frequencies were acceptable

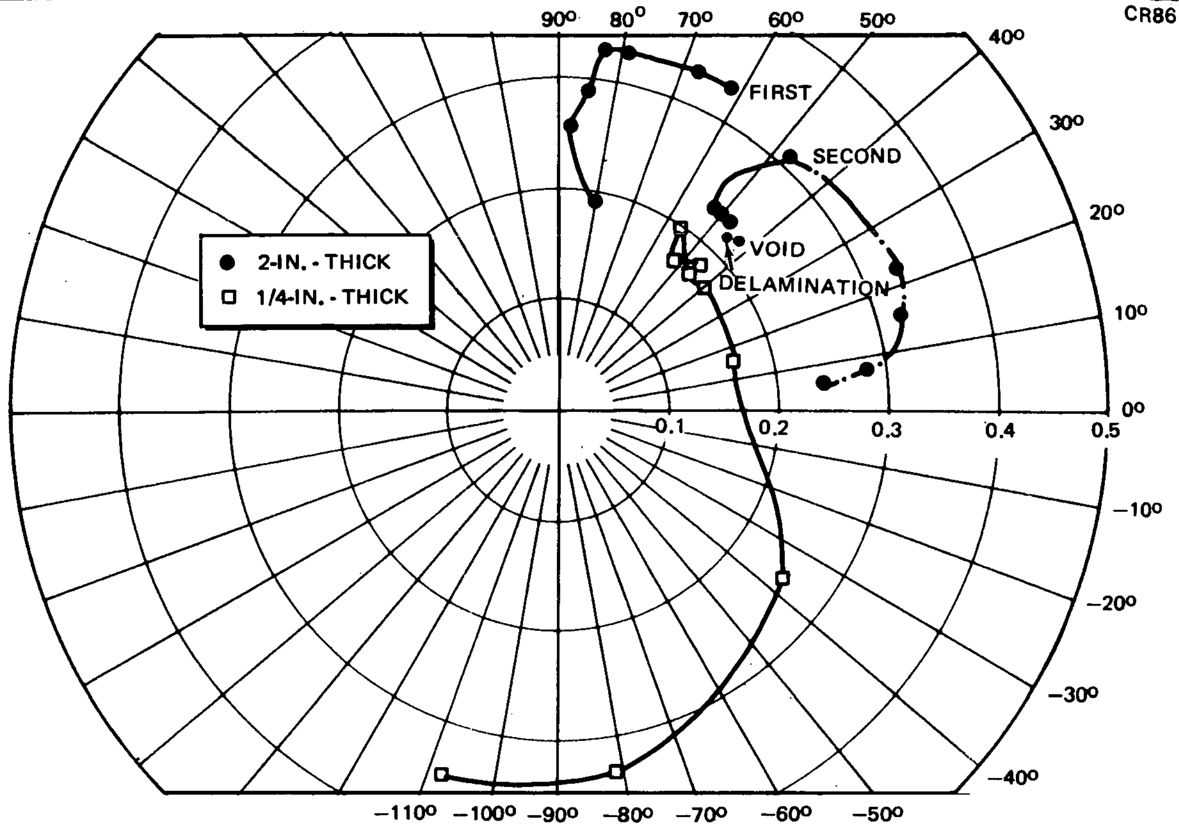

Figure 2-57. Microwave Moisture Detection at 9 GHz for Coated Material

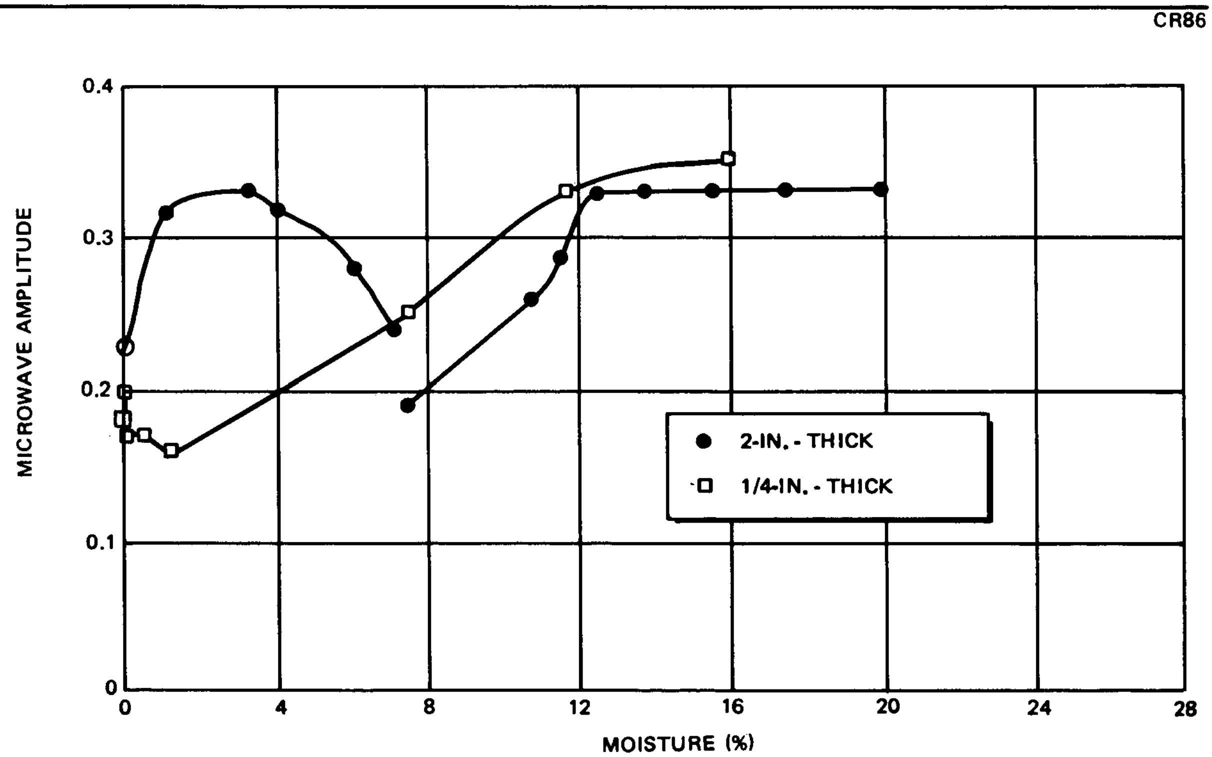

Figure 2-58. Microwave Amplitude Versus Moisture Percentage at 9 GHz for Coated Material

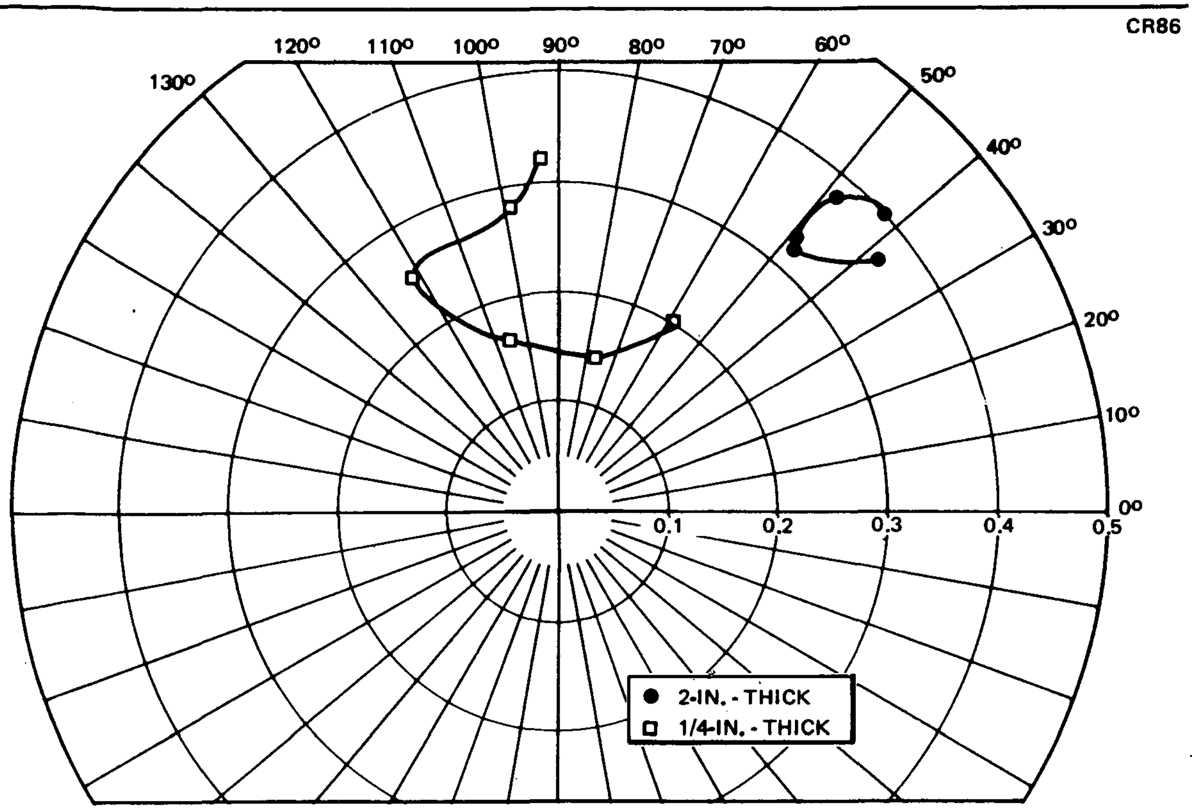

Figure 2-59. Microwave Moisture Detection at 15 GHz for Coated Material

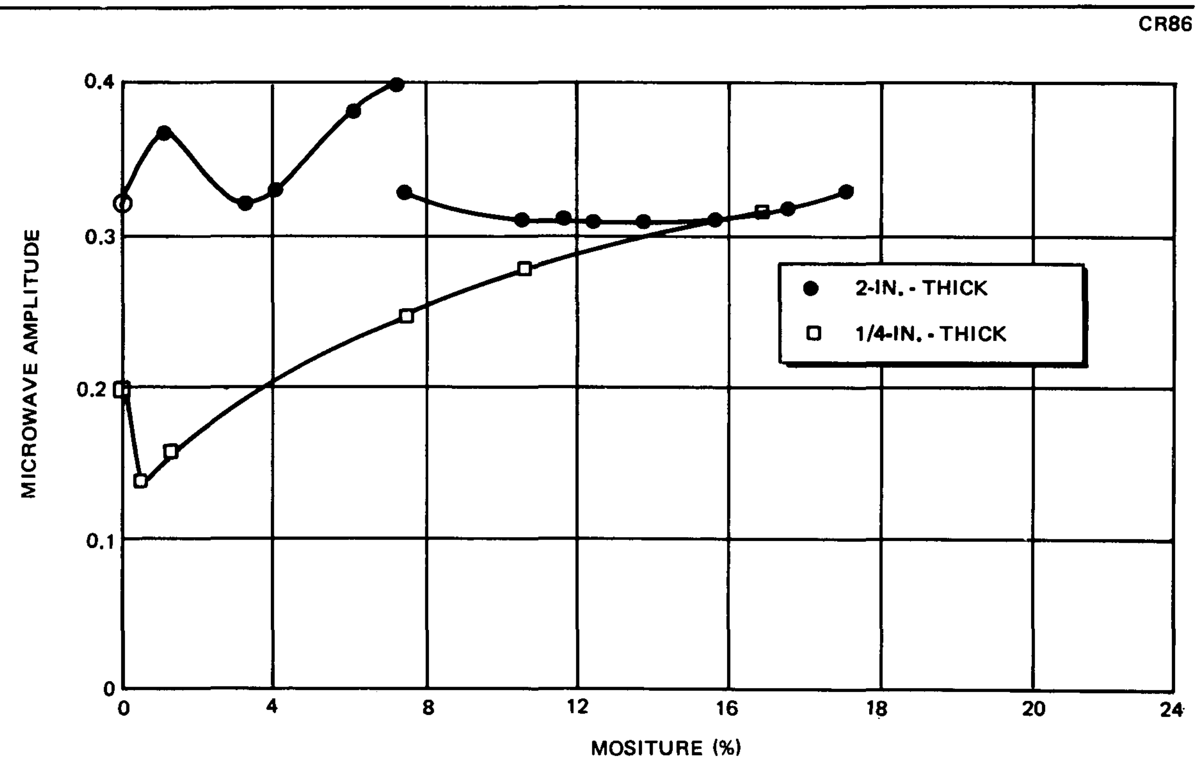

Figure 2-60. Microwave Amplitude Versus Moisture Percentage at 15 GHz for Coated Material

for the 1/4-in.-thick sample, but there were anomalies in the results for the 2-in.-thick sample. For the 2-in.-thick sample, the amplitude readings did not change much with changes in moisture content for the first set of readings. Furthermore, the second set of amplitude readings did not monotonically decrease with decreasing moisture content as expected. These results are unexplained at this time.

Measurements were also taken for dry, 2-in.-thick void and delamination samples. These points are also shown on Figure 2-57. As shown in the figure, the readings for the void and delamination samples were not significantly different than those for the dry control sample.

2.4.3.5 Bonded Samples

After adjusting the phase and amplitude as before, microwave measurements were taken for control, bondline void, and bondline unbond samples. The results for 9 GHz are shown in Figure 2-61 and the results for 15 GHz are shown in Figure 2-62. The amplitudes measured for these samples

CR86

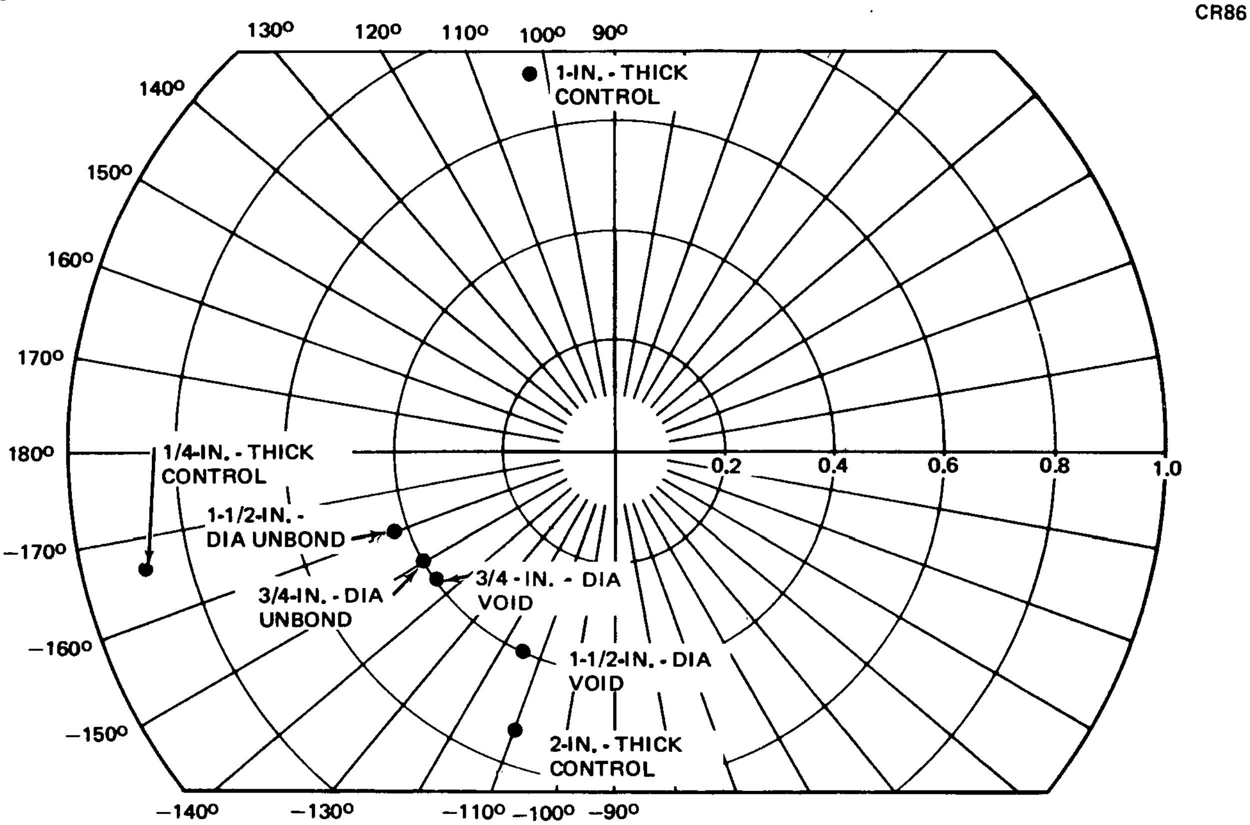

Figure 2-61. Microwave Bondline Defect Detection at 9 GHz

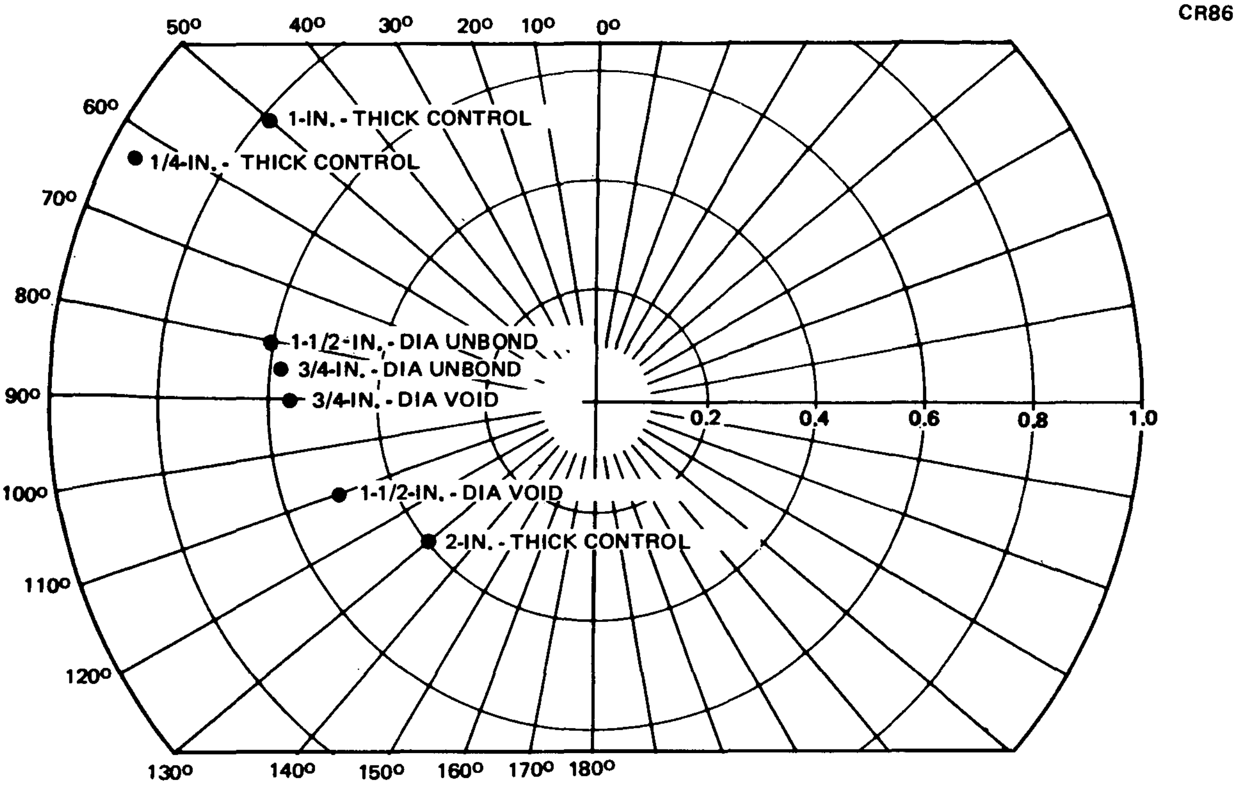

Figure 2-62. Microwave Bondline Defect Detection at 15 GHz

are much larger than for previous samples due to the presence of a metal backing. The results were very similar for both frequencies, except that the amplitude for the control sample changed its position relative to that of the other samples from one frequency to the other. While there was not too much difference in the amplitudes, there appears to be a difference in the phases. This shift in phase might be expected to be due to different sample thicknesses. Since the metal plate alone is displaced from the horn, the polar display traces a spiral, starting with a phase of zero and amplitude of 1, which proceeds clockwise to zero phase and amplitude.

The sample thicknesses were:

1-1/2-in. void	—	2.004 in.
Control	—	2.015 in.
3/4-in. unbond	—	2.071 in.
3/4-in. void	—	2.077 in.
1-1/2-in. unbond	—	2.078 in.

The total spread in thickness was 0.074 in. Based on actual measurements with a metal plate, such a difference in plate-to-horn distance would account for an angular displacement of approximately 50 degrees. This is the displacement actually observed in the results for the control of 1-1/2-in. unbond samples. The relative order of the samples based on thickness, however, does not correspond to the relative order obtained from the specimens. Thus, the results obtained here are not conclusive, but suggest that there may be an effect which could be detected by scanning techniques.

Microwave moisture measurements were made as before, except that water had to be sprayed on the edges only as the front surface was coated and the back surface was bonded. This procedure is less desirable than the procedure used for the uncoated samples because the moisture variation necessarily varies radially rather than through the thickness. This means that a microwave horn placed on the center of a sample may not be measuring the same moisture content as would be indicated by the overall weight percentages. It was not possible to obtain moisture measurements from the 1/4-in.-thick sample as the sample would not absorb any water, even when completely immersed for several hours. The edges of this sample were somewhat sealed off due to excess adhesive. The results for the 2- and the 1-in.-thick control samples are shown in Figure 2-63 for 9 GHz and in Figure 2-64 for 15 GHz.

The moisture measurements for the coated and bonded samples were quite different from those for the uncoated and coated samples. With the presence of the metal backing, the microwave response changes from primarily a change in amplitude to primarily a change in phase. The phase angle decreased with increasing moisture content. Thus, microwave measurements may be made for samples both with and without a metal backing, provided the correct type of measurement is used. The primary limitation to measurements for samples with a metal backing is that the response is sensitive to the distance of the metal from the horn. Additional work is required to suppress this variable in favor of more sensitive moisture measurement.

C.2

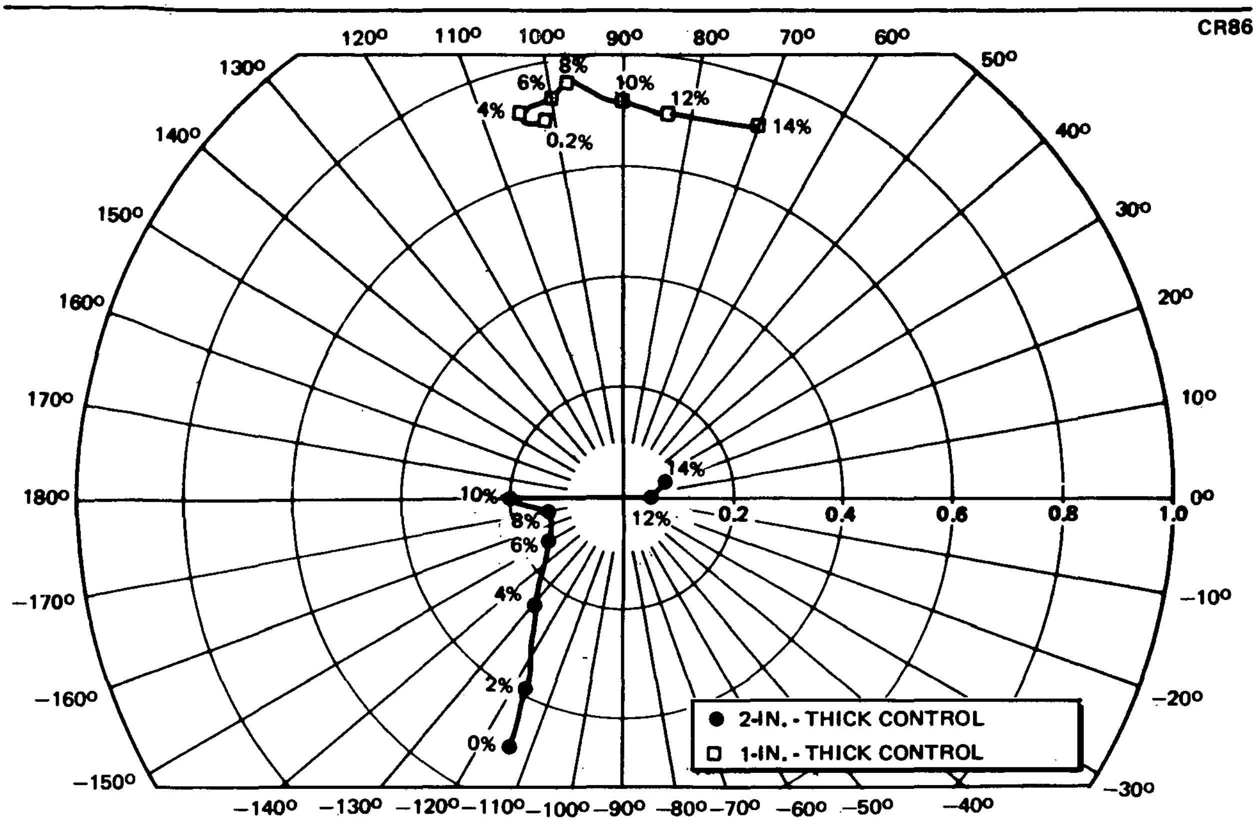

Figure 2-63. Microwave Moisture Detection at 9 GHz for Coated and Bonded Material

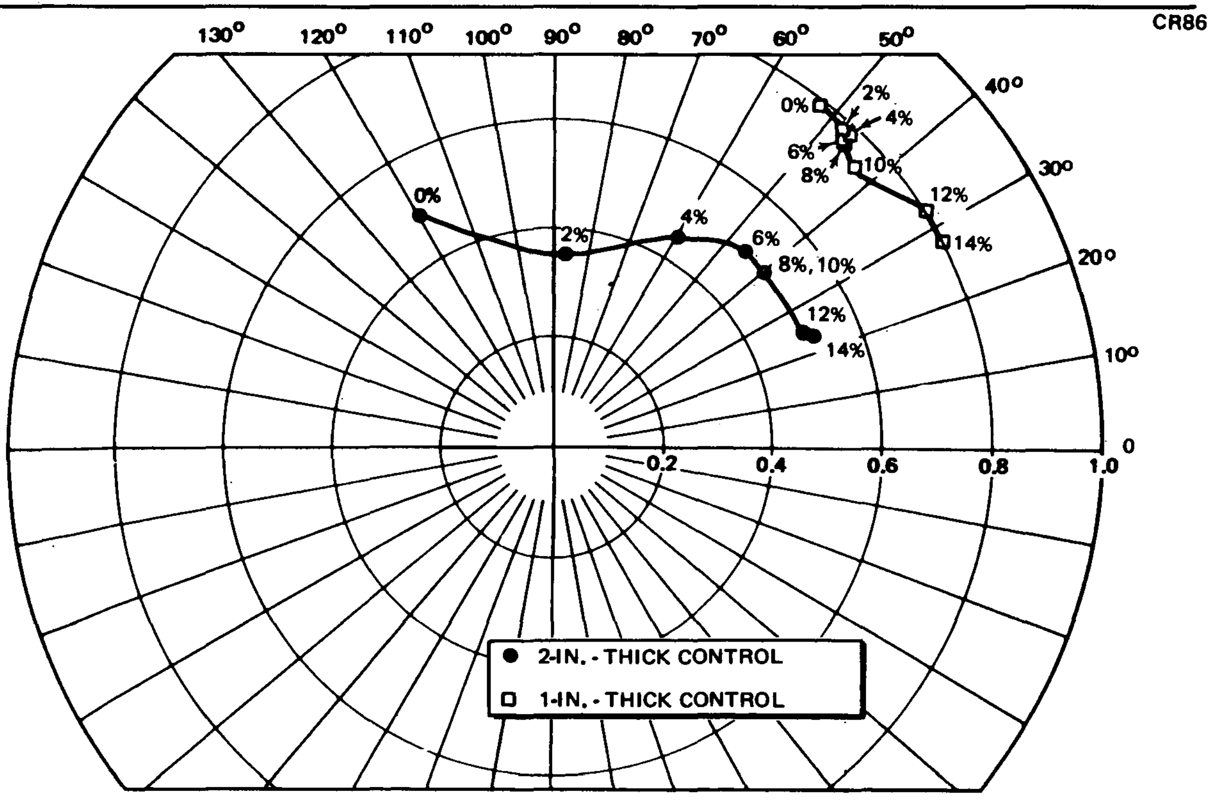

Figure 2-64. Microwave Moisture Detection at 15 GHz for Coated and Bonded Material

2.4.4 High-Frequency Ultrasonics

The detection of defects (voids and unbonds) in the bondline between RSI material and a metallic substrate presents certain difficulties. If the RSI material is bonded directly to primary structure, access to the metallic substrate will not be possible. Thus, inspection for bondline defects must be conducted from the RSI side. Techniques which may be applicable from the RSI side (low frequency acoustic and microwave reflection) are discussed elsewhere in this report.

If the RSI material is bonded to metallic substructure which in turn is later mechanically attached to primary structure, access to the metallic substrate will be possible. In this case, a variety of higher-frequency techniques are possible. Three commercial instruments were evaluated—the Fokker Bond Tester, Automation Industries Model UM700 Pulser-Receiver and 5 MHZ Transducer, and Automation Industries Sondicator Model S-2.

Fokker Bond Tester

The Fokker Bond Tester is a resonant-frequency device operating in the 80 kHz to 1 MHz frequency range. It might be expected that the high attenuation of low-density RSI would preclude the use of this instrument due to its high operating frequency. The use of an elastomeric adhesive, on the other hand, might provide the necessary response for the detection of bondline defects.

The Fokker Bond Tester was evaluated by trying all possible combinations of different probes and frequency ranges until a change in response could be observed from a sample with a bondline defect as compared with a sample without a bondline defect. The probes were coupled to the metallic surface using BTF 427 Fokker Bond Tester Couplant. A change in response was obtained using a No. 1218-0416 probe 1/2-in. in diameter and dial settings of 3.5 for the Sweep, 7.5 for the Tuning, 4 for the Band, and 9.5 for the Sensitivity. The response for a defect in the bond was a change in amplitude from 65 (for a good bond) to 145. The presence of a defect is revealed by the occurrence of a resonance in the vibrating system. All but the 3/4-in.-dia unbond defect in 2-in.-thick material were detected. An attempt was made to map the extent of the defects by repeatedly applying the probe in a regular pattern, overlapping successive positions, and marking the outer dimensions of the probe whenever a defect was indicated. The Fokker results generally overestimated the size of the defect, as shown by x-ray radiography. This is due somewhat to the relatively large diameter of the probe.

Ultrasonic Pulse-Echo

An Automation Industries Model UM700 pulser-receiver and Automation Industries Model SFZ 57A2214, 5 MHz, 1/4-in. dia, longitudinally cut piezoelectric transducer were evaluated in the same way. The same couplant was used as before. The presence of a defect was revealed on an A-scan oscilloscope presentation by the presence of multiple internal reflection within the metallic substrate. This technique was successful only for samples containing voids, not for samples containing unbonds. Apparently, the presence of a good bond transmitted the ultrasonic energy across the metal-adhesive interface and then rapidly attenuated the energy within the elastomeric adhesive. The presence of a void, on the other hand, presented a region of very low acoustic impedance which resulted in reflection of most of the energy between the metallic surfaces. An attempt was made to map the extent of the defects as before. The sizes indicated by this technique corresponded much better to those indicated by the radiographs due to the higher frequency and small transducer size employed.

Sondicator

The Sondicator is a low-frequency instrument operating at 25 kHz which monitors the amplitude and phase of an acoustic wave. The acoustic energy is introduced into the specimen by direct contact from a transducer and a second transducer is used to receive the acoustic energy. This instrument detects defects in the adhesive bond by monitoring changes in the amplitude and relative phase of the acoustic wave.

The Sondicator was applied from both surfaces of the bonded samples. A couplant is not needed for this technique. Dial settings of 4. 6 for the amplitude and 5. 0 for the phase provided the best defect detection for the 1/4-in.-thick samples from the metallic surface. Amplitude readings from 0. 4 to 0. 6 and phase readings of 1. 0 were representative of well-bonded regions. Voids and unbonds resulted in amplitudes of 0. 8 to 1. 0 and phases of 0. 5. The main criterion for defect detection was a change in phase.

Similarly, for the 2-in.-thick samples, dial settings of 4.6 for the amplitude and 5.32 for the phase resulted in the best response. The response for good and bad regions of bond were the same. All but the 3/4-in. unbond defects were detected.

Attempts to detect the defects from the RSI side of the specimen were not successful. Some indications were obtained for the 1/4-in.-thick samples, but the response was too weak to be reliable.

The Sondicator probe employs three small Teflon prongs in a triangular array. One prong is attached to a transmitting transducer, one is attached to a receiving transducer, and one is merely used to stabilize the other two prongs when in contact with a sample. A map of the defect size was made using the two active prongs. A defect indication was generated with both prongs within the defective area or with one within and one out. The size of the defects corresponded to the sizes found by the pulse-echo method.

The high-frequency ultrasonic techniques were applicable only from the metallic side. These techniques were evaluated in this program because the Shuttle configuration at the start of this program was such as to allow access to the metallic side. The latest change in configuration now has the RSI material being bonded directly to primary structure such that access to the metallic side is not possible. It was not possible to change the direction of this program in time to emphasize only those techniques applicable from the RSI side. Much further work will need to be done for the inspection of the bondline and will depend upon the final type of bonding scheme employed.

2.4.5 Beta Backscatter

Beta backscatter (back-emission electron radiography) was used to evaluate the waterproof coating for defects in the coating surface. This technique has been used to assess the integrity of the surface or near-surface material (Reference 14).

The beta backscatter technique differs from normal radiographic methods in that the film is placed between the x-ray source and the object (normal radiographic process places the film under the object). The technique relies on high-energy x-rays to excite electrons from the surface of the material whose emission is detected on film. A schematic of the beta backscatter technique is shown in Figure 2-65.

X-ray energies of at least 250 kV must be utilized since electron emission increases with increasing energy of radiation up to several hundred kilovolts. In the backscatter technique, the useful image is formed only by electron action and the direct x-rays act only to produce a uniform overall exposure. By utilizing high-energy x-rays, the ratio between electron exposure, which produces the image, and the overall exposure produced by the direct x-rays can be maximized (Reference 4).

The slowest or finer-grain, single-emulsion industrial x-ray films are most suitable for electron radiographic techniques. These fine-grain film

CR86

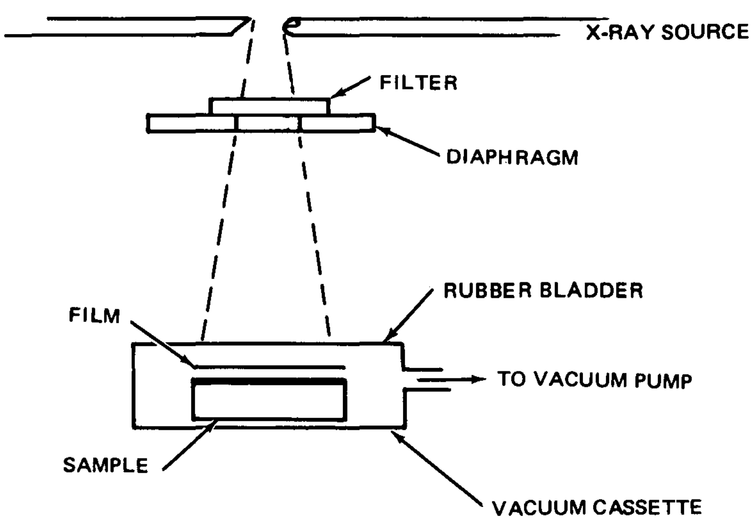

Figure 2-65. Schematic of Beta Backscatter Setup

emulsions are more sensitive to electrons than x-rays. In addition, the x-ray absorption coefficient of the emulsion decreases with increasing x-ray energy (making it less sensitive to high-energy x-rays). Therefore, ultrafine-grain, single-emulsion Kodak Type R film was used throughout this evaluation.

When operating an x-ray source at high voltages, the intensity of the lower voltage portion of the x-ray spectrum also increases. This portion will cause a uniform overall increase in film density, thereby reducing sensitivity. A copper screen was employed to filter the lower-energy x-ray spectrum.

Since the emitted electrons are absorbed very quickly, it is extremely important that the emulsion side of the film be in intimate contact with the sample. Otherwise, the electronics would be absorbed by the transparent cellulose film before reaching the emulsion. The single emulsion is used to avoid the presence of a second uniform background. A vacuum cassette was employed to provide contact between the film and the sample.

The x-ray source, filter, diaphragm, vacuum cassette, film, and RSI sample were arranged as shown in Figure 2-65. A 2-in.-thick sample with coating defects was used. The source focal spot size was 1.5 mm. A 0.120-in.-thick copper filter was used. A 0.5 in. wide by 1.6 in. long slot was machined in a piece of lead for use as a diaphragm. The x-ray source was placed 12 in. from the top of the diaphragm and the film was placed 38 in. beneath the top of the diaphragm. Thus, the source-to-film distance was 50 in. This combination of diaphragm size and spacing resulted in an exposure area 2.5 in. wide by 7.5 in. long. This area was larger than the area of the sample but was less than the area of the vacuum cassette. This arrangement minimizes any scattering effects.

Type R x-ray film was placed with the emulsion side next to the sample coating and a vacuum was created within the vacuum cassette. This procedure was repeated for a series of exposures as given in Table 2-8.

Table 2-8

BETA BACKSCATTER EXPOSURE PARAMETERS

Exposure No.	kV	ma	Time (min)	Density
1	250	10	1	0.74
2	250	5	3	1.10
3	250	5	7	2.50
4	250	5	8	2.70
5	250	5	9	3.00

None of the defects were detected for any of the different film densities due to the uneven surface texture of the coating. Back-emission electrons are only detected from those portions of the surface that are very close to the film. Since the coating surface had high and low spots whose size was on the order of the size of the defects, any indications which might be present were completely masked. Since the technique was not successful for exposures at 250 kV, nothing would be gained from lower energy exposures. Additional exposures were taken using a fine grain positive film and developed by hand also without success. This technique might be more successful with smoother coatings.

2.4.6 Thermal Techniques

Material integrity may be monitored by observing the heat flow patterns in a sample which has been disturbed from an equilibrium temperature condition. Anomalies which occur are expected to alter the internal heat flow patterns and thereby affect the specimen temperature distribution. This distribution will affect the surface temperature and provide a means of detecting anomalous areas. Thermal mapping techniques have been successfully applied to other insulation systems for the detection of defects (Reference 15).

Changes in the surface temperature of a specimen can be monitored by a number of thermal sensing techniques such as radiometers, liquid crystals, or infrared film. For the temperature ranges of interest to this program, only radiometers and liquid crystals appear applicable because infrared film is not sensitive to temperatures below 500° F. Commercial radiometer systems (sensing head with display console) typically have a temperature range of 0 to 300° F with a minimum detectable temperature difference of 0.4° F at approximately a 90° F target temperature. Liquid crystals are cholesteric chemicals which scatter various colors of light at various temperatures over a specific temperature range (Reference 16). A sensitivity of 0.2° to 0.9°F is available over an overall range of 0° to 500°F. For the purpose of this program, liquid crystals and radiometers appear to offer approximately equivalent sensitivity.

Liquid crystal sensing techniques were used for this program. Liquid crystals offer a sensitive, inexpensive means of evaluating the general feasibility of thermal techniques. Since the RSI material has a very low thermal conductivity, it is not expected that the thermal technique will be applicable to detecting defects in the RSI material or in the adhesive bond area. Liquid crystals were evaluated in this program primarily for detection of coating defects

The liquid crystal method of monitoring surface temperature requires direct contact of the liquid crystal system with the test article. This may be accomplished by either spraying a liquid crystal solution on the RSI coating or by placing a thin sheet of material to which the liquid crystal has been applied on the RSI. The latter method was selected for this study to avoid any contamination problems.

The thermal sensing technique requires that a uniform thermal input be provided to the test part for sensitive and repeatable results. The thermal input can either be a cooling or heating of the test object to obtain the desired temperature differential. A number of methods exist (oven, hot-gas gun, and radiant lamps) for introducing the thermal differential between the specimen and the ambient laboratory environment. For this program, an oven was used to introduce the thermal gradient in order to provide the most uniform thermal input.

Four different liquid crystal formulations made by the Roche Chemical Division were evaluated. These formulations were attached to 0.001-in. thick, black Mylar tape. Each formulation changed color from black to blue over a specific temperature range. The temperature ranges evaluated were: 23.0° to 27.0°C (73.4° to 80.6°F), 29.0° to 34.0°C (84.2° to 93.2°F), 35.0° to 39.0°C (95.0° to 102.2°F), and 47.0° to 48.0°C (116.6° to 118.4°F).

The procedure was the same for each temperature range. The tape was placed in contact with the coated surface of the sample and the sample was then placed in an oven at 170°F for 10 min. The sample was then removed from the oven and the liquid crystal tape observed until the sample returned to room temperature. The technique was generally unsuccessful. On occasion, a very slight indication could be obtained for the largest hole in the coating (0.064 in. in diameter). This indication could only be obtained through rapid cooling of the sample using the 29.0° to 34.0°C (84.2° to 93.2°F) tape when the sample temperature was near the transition temperature of the liquid crystals. Repeatedly blowing across the sample to lower the surface temperature below the transition and then letting the heat from the sample raise the temperature above the transition would sometimes result in an indication of the 0.064-in.-dia hole. The primary difficulty is the coating surface is so rough that the liquid crystal display presents a mottled appearance which masks the indications from any defects present. The technique may be more successful with a smoother coating.

In view of this difficulty, variations of the basic approach were examined. First, the liquid crystal display was observed while the sample was heated rather than while the sample was cooled. Again, the results were negative. Finally, water was applied to the coated surface just long enough for some water to be absorbed through the defects into the basic RSI. The excess water was removed, and the observations repeated as before with negative results.

Although liquid crystals and radiometers have approximately the same sensitivities, the radiometer may actually be the better approach due to the rough surface texture. Further work would be needed to examine this possibility.

Additional experiments were performed on the bonded specimens with bond line defects by placing the liquid crystals in contact with the metallic surface and heating as before. Again, the results were negative.

2.4.7 Holography

Holography is an optical process in which information about both the phase and amplitude of coherent light reflected from an object can be recorded on film by interference with another reference beam of coherent light. A laser is used as a source of coherent light. The information contained in this record, or hologram, may be reconstructed into a truly three-dimensional image by illuminating the hologram with a beam of coherent light. Interferometric holography is an application of holographic techniques in which the surface displacements of an object placed under stress can be determined through the generation of interference fringes. One method of generating such fringes is to expose the hologram with the object in one state of stress and then reexpose the hologram (double exposure method) with the object in another state of stress. Such a hologram will then contain two separate, three-dimensional images of the same object slightly deformed due to the different states of stress. Since displacements on the order of one fourth the wavelength of the illuminating light results in interference between the two images, extremely sensitive measurements of surface deformation can be made (on the order of 12 μin.). Other variations on this basic approach include real-time comparison of the object with its three-dimensional image and double-exposure holograms using a pulsed rather than continuous-wave laser. The real-time technique allows continuous observation whereas double-exposure holograms permit observation of only one change in stress state. Pulsed techniques allow rapid exposures which are useful for "freezing" rapidly changing surface deformations or when necessary to reduce the effect of external vibrations (a vibration isolation system is used for this purpose for a continuous wave system). Another approach is to expose a hologram over a relatively long time period while the object is stressed using vibration techniques.

Basically, defects in the object respond differently to the applied stresses than do other parts of the object. This results in distortions in the fringe pattern revealing the presence of the defect. Bondline defects (References 17 and 18) and cracks in metals may often be detected in this way.

Experimentally, the most difficult problem is to generate the correct type and magnitude of applied stress necessary to produce an indication of the presence of a defect. Two of the techniques most often employed are the use of thermal stressing and mechanical stressing. Both these techniques were evaluated for this program.

A 50-mW He-Ne continuous-wave gas laser (Spectra Physics Model 125) was used for all the testing.

2.4.7.1 Coating Samples

Several initial holograms were made using the control sample to determine if the light reflected from a coated sample was sufficient to expose a hologram, to determine the correct exposure parameters, to determine the stability of the holding fixture, and to determine the background fringe pattern from a defect free sample for both thermal and mechanical stressing. It was found that the sample reflectivity permitted excellent holograms to be made for reasonable exposures (less than 4 sec) and that the holding fixture was sufficiently stable. Three 1/4-in.-wide by 4-in.-long loss-of-coating adhesion defects were then introduced by inserting a piece of 0.005-in.thick steel shim stock just beneath the coating as shown in Figure 2-66. A series of holograms were then made using a variety of applied

CR86

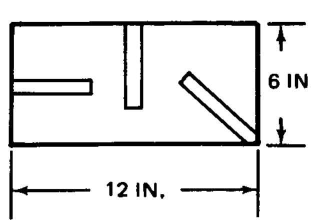

Figure 2-66. Location of Loss of Adhesion Defects

stress combinations in an attempt to find the best method for revealing this defect. The following stressing techniques were applied:

A. Mechanical stressing through pressurization of a rubber tube placed between the back of the specimen and the holding fixture.

B. Mechanical stressing through the use of a spring-loaded probe placed in contact with the front surface.

C. Thermal stressing using a 375-W heat lamp placed approximately 1 ft from the panel for less than 10 sec.

D. Thermal stressing using a hot-air blower applied for a few seconds.

E. Thermal stressing achieved by placing the panel on a hotplate.

The loss-of-adhesion defects were detectable in real time using thermal stressing but were not detectable using mechanical stressing. The results using thermal stressing were difficult to record photographically due to rapid motion of the fringe pattern. The relatively mild heat output of the hot-air blower was more useful than the high heat output of the heat lamp. Application of too much heat resulted in loss of the fringe pattern due to excessive surface deformations. A photograph taken through a real-time hologram using thermal stressing is shown in Figure 2-67. This photograph shows the presence of a crack and the lower right-hand loss-of-adhesion defect. The fringe contrast is relatively poor due to movement of the fringes during the exposure.

Two small cracks, not associated with the loss of adhesion defect, were detected early in the testing using either mechanical or thermal stressing. The cracks were most easily detected using mechanical stressing since this method would frequently display all the cracks present, whereas thermal stressing usually would not display all the cracks present. Later in the testing, while heating the surface of the sample on a hotplate, cracking sounds were heard. This was followed by larger indications for the cracks which had already been detected. Thus, apparently the existing cracks grew further during thermal stressing using the hotplate. An example of the results obtained using mechanical stressing is shown in Figure 2-68. This figure clearly shows the presence of two long cracks. The photograph was taken through a real-time hologram.

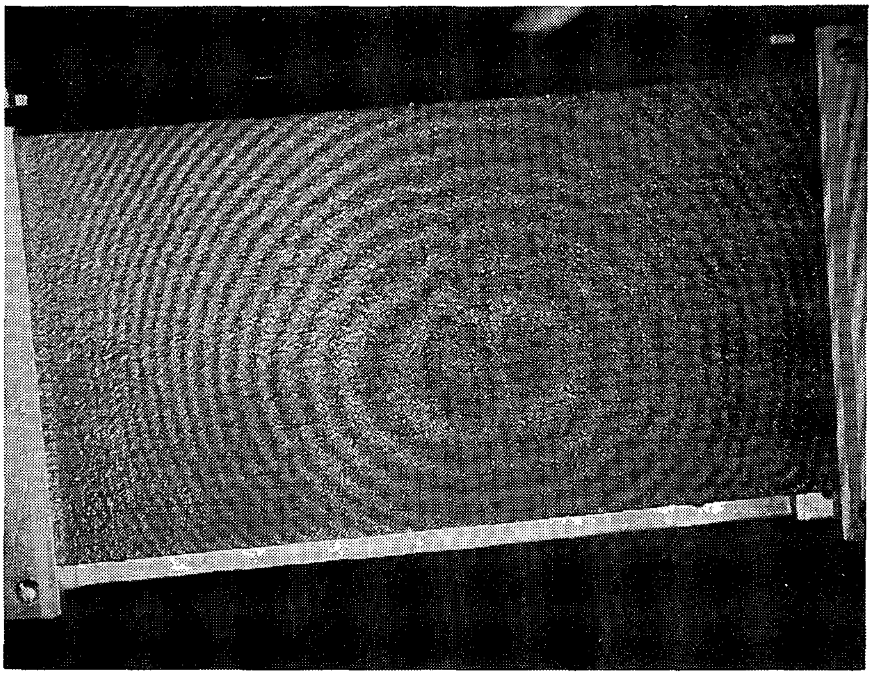

Figure 2-67. Real-Time Interferometric Hologram of Crack and Delamination Using Thermal Stressing

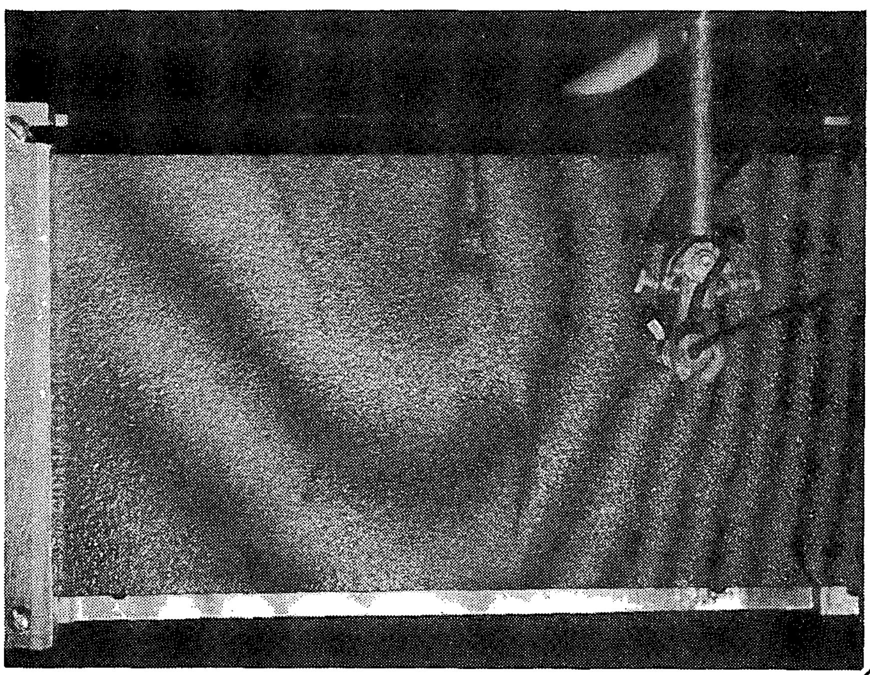

Figure 2-68. Real-Time Interferometric Hologram of Cracks Using Mechanical Stressing

2.4.7.2 Bonded Samples

Real-time interferometric holography techniques were employed for these samples using the same stressing techniques as for the coated samples. No evidence of bondline defects were obtained through observation from the RSI side of the samples. To complete the evaluation, these samples were also examined from the metallic side as well. The 3/4-in.-dia void, 3/4-in.-dia unbond, and 1-1/2-in.-dia unbond samples provided no indication of the presence of defects using both thermal and mechanical stressing of the metallic surface. Examination of the 1-1/2-in.-dia void sample, however, revealed the presence of a rather large bondline defect. A photograph of this sample taken through a real time hologram is shown in Figure 2-69. This figure shows the distortion around a spring-loaded probe due to the bondline defect. By moving this probe from point to point, it was possible to map the outside dimensions of the defect, as shown in Figure 2-70. This corresponded very well with the defect outline provided by x-ray radiography. Holographic inspection from the coated surface, however, did not reveal the presence of either the bondline defect or an internal crack revealed by the radiograph.

CR86

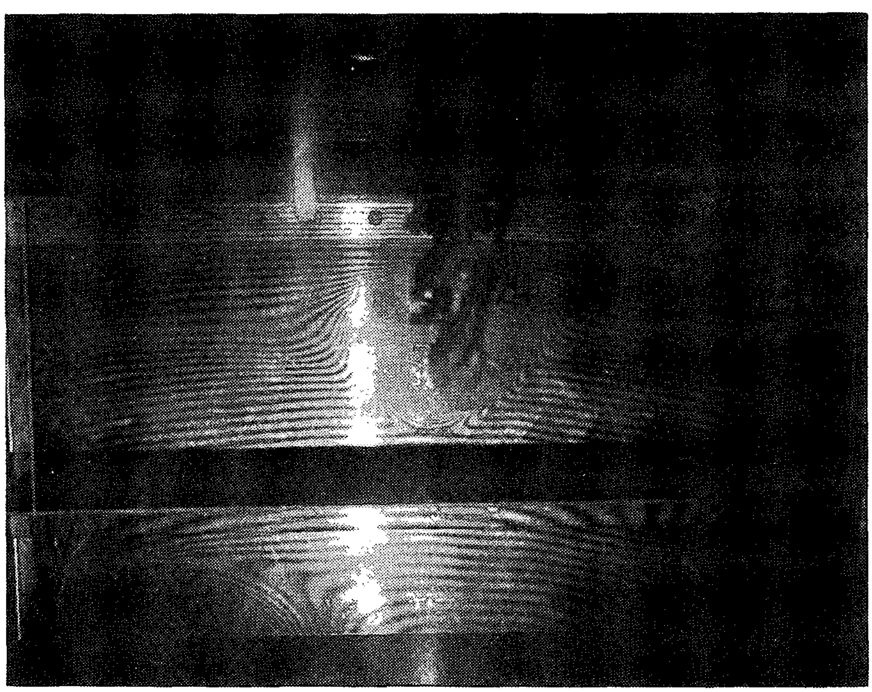

Figure 2-69. Real-Time Interferometric Hologram of Bondline Defect Using Mechanical Stressing

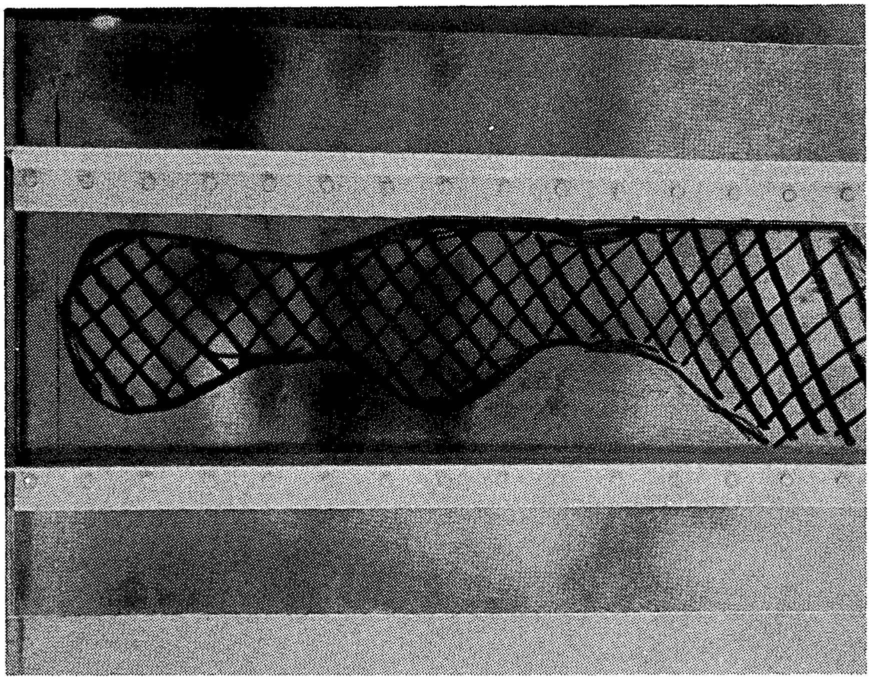

Figure 2-70. Extent of Bondline Defect Detected by Interferometric Holography

The results obtained here were for a limited number of samples and only a few types of stressing. The results were successful enough to warrant further study. The use of a pulsed-laser system would provide several advantages and perhaps reveal better the presence of defects. Acoustic vibration and other types of stressing should be investigated as well.

2.4.8 Visual

Visual techniques were used to evaluate uncoated RSI and the RSI coating. Since RSI is somewhat translucent, the possiblity of detecting gross anomalies by illuminating the material with bright light was examined. This method has been used to examine other low-density foam composites of a translucent nature (Reference 6).

Three thicknesses of uncoated material were examined. Each sample was examined using a 500-W light source for back illumination. None of the voids, cracks, or delaminations in the 2- and 1-in.-thick samples were detectable with this light source. Holes 0.128 and 0.064 in. in diameter and 0.125 in. deep were detectable in the 1/4-in.-thick uncoated material. Generally, this approach is not adequate for internal defects since access to two surfaces is required and the sensitivity is much less than that of x-ray radiography.

Two thicknesses of coated material containing coating defects were examined. None of the defects in the 2-in.-thick material were detectable. Coating defects were detectable in the 1/4-in.-thick material, as shown in Figure 2-71. Holes as small as 0.013 in. in diameter and very fine cracks were detectable.

CR86

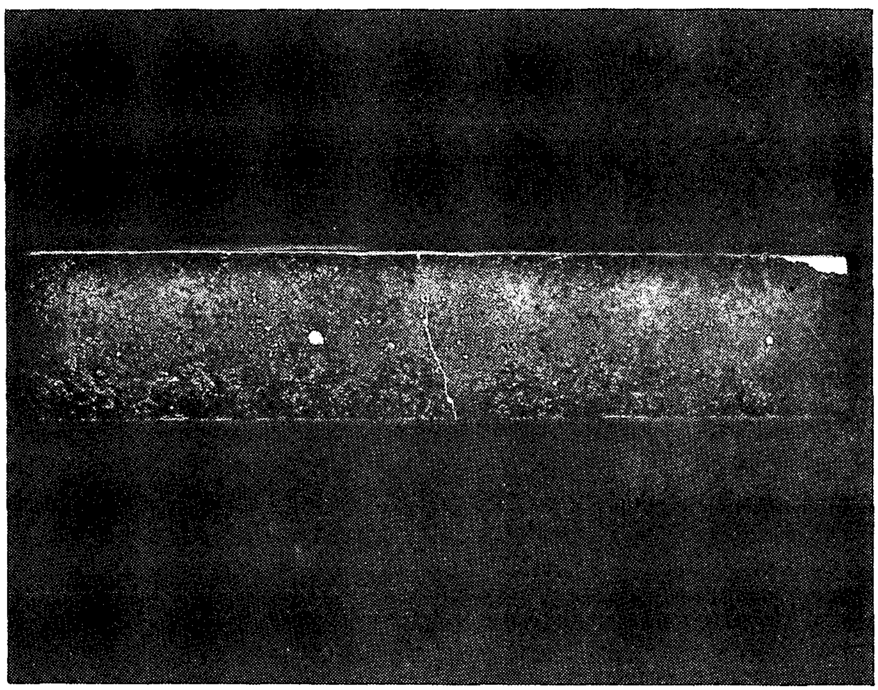

Figure 2-71. Backlighted 1/4-In.-Thick Coated RSI

Section 3
APPLICATION OF NONDESTRUCTIVE TEST TECHNIQUES

Selected nondestructive test techniques were applied to several samples which contained density variations. The material supplied by MDAC-E for these tests were selected through preliminary x-ray radiography screening. Density variations were the only type of naturally occurring defect available from the material screened. One sample, referred to as the material screening sample, was approximately 9 in. in diameter and 2 in. thick. Sixteen additional samples, referred to as the natural defect samples, were approximately 3 in. long, 2-3/4 in. wide, and 3-1/4 in. thick. X-ray radiographs were taken of all samples. Regions of higher and lower density were identified for the material screening sample as shown in Figure 3-1. Top- and side-view radiographs of the natural defect samples revealed a low-density layer centered between the top and bottom surfaces. Five of these

CR86

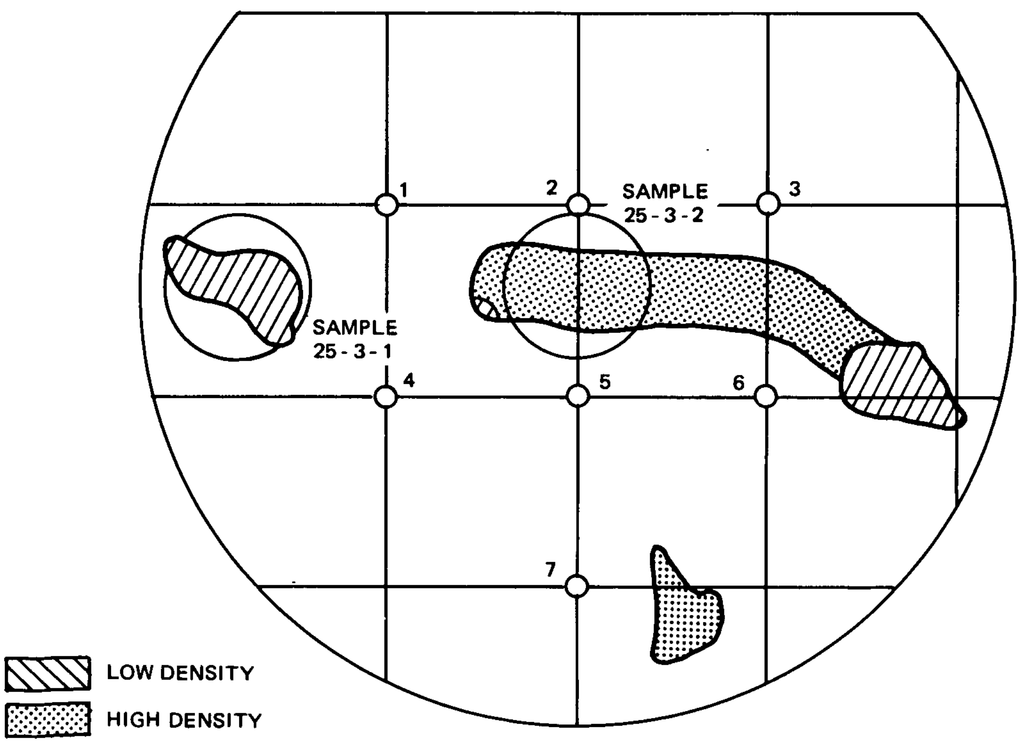

Figure 3-1. Material Screening Sample

samples were selected (to represent the range of bulk densities present) for further inspection.

Besides x-ray radiography, microwave reflection was the only other technique evaluated capable of detecting density variations. Microwave-reflection measurements were taken at 9 and 15 GHz for each of the five selected natural defect samples and for seven different locations (as shown in Figure 3-1) on the material screening sample. A plot of the reflected amplitude versus the bulk density for the natural defect samples is shown in Figure 3-2. These curves suggest that microwave reflection measurements may be used to determine sample density. The results for the material screening sample were nearly identical for each of the different locations. This agrees with the fact that the radiograph of this sample shows the densities in these areas to be the same. Unfortunately, the material screening sample was not large enough to allow application of the microwave technique to more than the number of locations used, and did not have a large range of density variations.

CR86

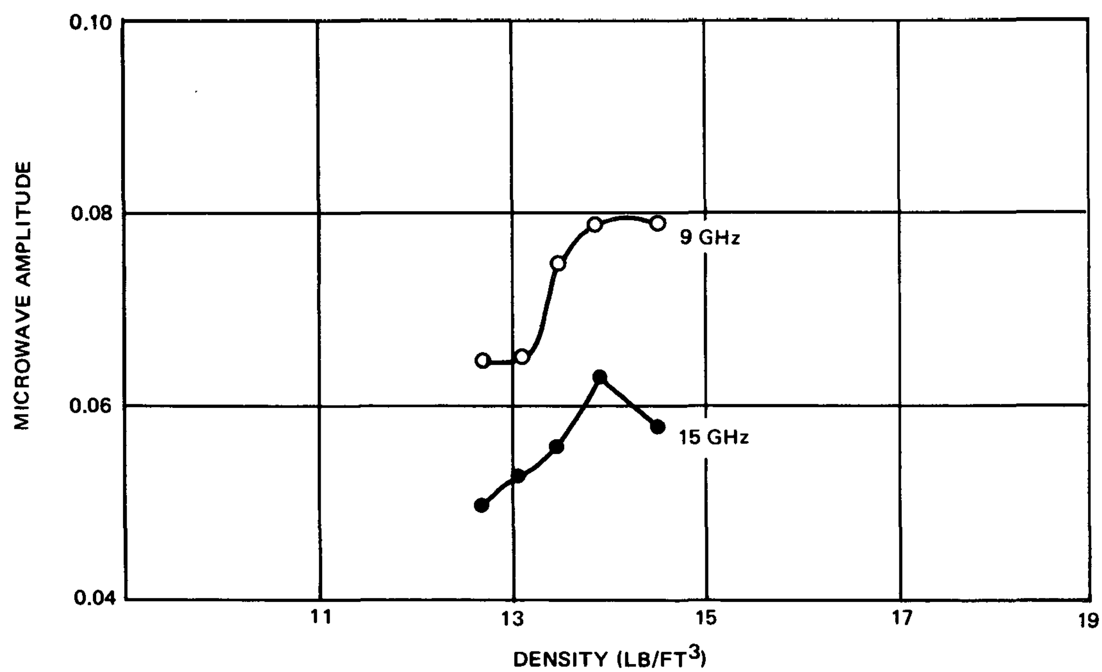

Figure 3-2. Microwave Amplitude Versus Density for Natural Defect Samples

Seven tensile specimens were machined from these samples, two from the material screening sample and one each from the natural defect samples. The tensile specimens were 1-1/2 in. in diameter and 1 in. thick, with axis of the specimen parallel to the thickness direction of the defect samples. The location of the specimens selected from the material screening sample are shown in Figure 3-1. The specimens taken from the natural defect samples were machined from the center of the samples. The bulk densities of the machined tensile specimens and the ultimate tensile strengths are given in Table 3-1. Unfortunately, of the seven specimens, the results for four specimens are uncertain due to the presence of high bending strains at failure. Using the results for which high bending strains were not present, a possible relationship between the microwave amplitude readings and the tensile strength is shown in Figure 3-3. This figure merely displays a possible trend; further work would be necessary to better define the limits of such a relationship.

Table 3-1

TENSILE TEST RESULTS

Specimen No.	Density (lb/ft^3)	Strength (psi)
1	12.7	19.5*
2	11.3	18.3*
7	10.8	23.0
10	10.9	22.3
16	12.6	43.0
25-3-1	15.9	35.8*
25-3-2	17.8	30.7*

*High bending strains present at failure

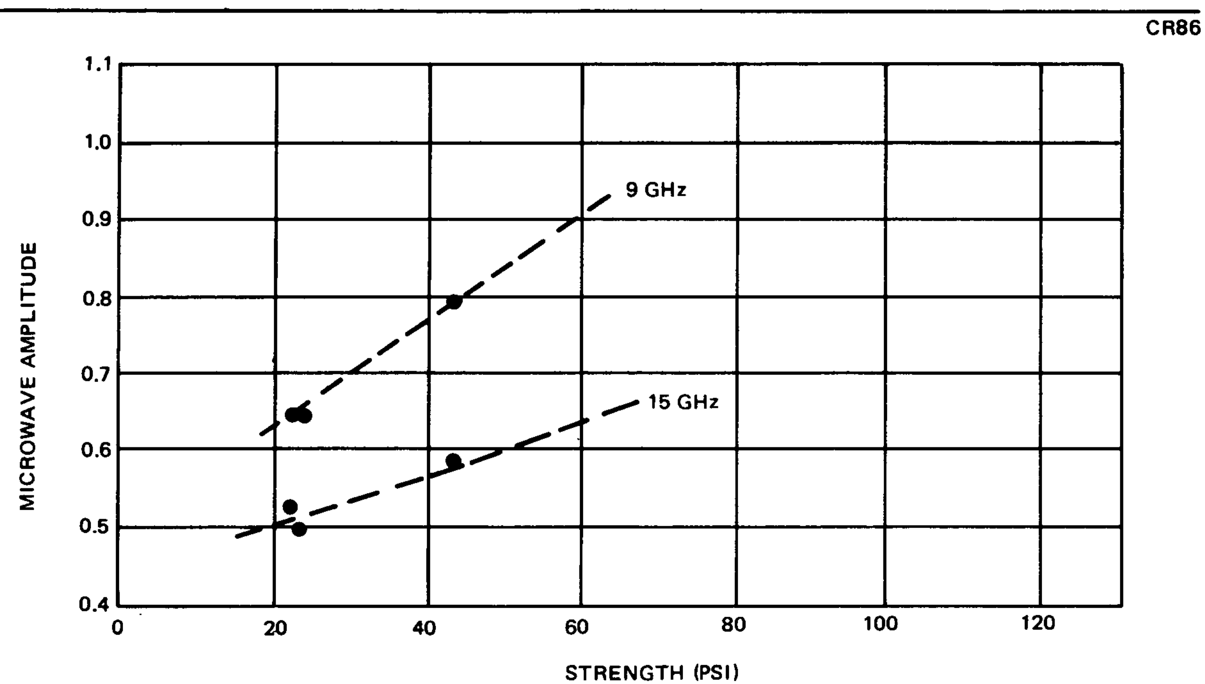

Figure 3-3. Possible Trend Between Microwave Amplitude and Strength for Uncoated RSI

Section 4
SUMMARY OF RESULTS

A summary of the results for each of the nondestructive analysis techniques as a function of the material condition and defect type is presented in Table 4-1. A YES or NO is used to indicate whether a given technique was successful or not for a given defect type. A dash is used to indicate that the given technique was not applied for that particular defect type. When required, additional information for a specific YES or NO is supplied as a series of notes numbered sequentially for each technique as shown. These notes provide sensitivities, resolutions, and qualifications as required. Comments are also supplied in the REMARKS column as to the relative merits of the various techniques for a given material condition and defect type.

The results for the application of NDT techniques for the natural defect and material screening samples suggest that a possible relationship may exist between microwave reflection measurements (or x-ray-radiography density measurements) and the tensile strength. More data would be required to verify that the relationship is valid.

Table 4-1

SUMMARY OF RESULTS (Page 1 of 3)

Material Condition	Defect Type	X-ray Radiography	Acoustic Transmission	Acoustic Reflection	Micro-wave	High-Frequency Ultrasonics	Beta Back-scatter	Thermal	Holo-graphy	Visual	Remarks
Uncoated	Void	Yes[1]	Yes[1]	Yes[1]	Yes[1]	—	—	—	—	Yes[1]	X-ray best
	Cracks	Yes[2]	—	—	—	—	—	—	—	No	
	Delamination	Yes[3]	Yes[2]	Yes[2]	Yes[2]	—	—	—	—	No	X-ray best followed by acoustic transmission and contact microphone as a check
	Density	Yes[4]	No[3]	No[3]	Yes[3]	—	—	—	—	—	X-ray best
	Moisture	—	—	—	Yes[4]	—	—	—	—	—	Microwave very sensitive
Coating	Hole	Yes[5]	—	—	—	—	No	No	—	Yes[2]	X-ray best
	Cracks	Yes[6]	—	—	—	—	No	No	Yes[1]	Yes[3]	Holography best
	Coating thickness	Yes[7]	—	—	No[5]	—	—	—	—	—	None applicable when applied to coating
	Loss of adhesion	Yes[8]	No[4]	Yes[4]	No[6]	—	—	No	Yes[2]	—	Holography best
Coated	Void	Yes[9]	No[5]	Yes[5]	No	—	—	—	—	—	X-ray best
	Cracks	Yes[10]	—	—	—	—	—	—	—	—	
	Delamination	—	No[6]	Yes[6]	No	—	—	—	—	—	More work needed for acoustic reflection
	Moisture	—	—	—	Yes[7]	—	—	—	—	—	Microwave less sensitive than for uncoated
Bonded	Bondline void	Yes[11]	Yes[7]	Yes[7]	Yes[8]	Yes[1]	—	No	Yes[3]	—	More work needed for acoustic and microwave reflection
	Unbond	No[12]	Yes[8]	Yes[8]	Yes[9]	Yes[2]	—	No	No	—	
	Moisture	—	—	—	Yes[10]	—	—	—	—	—	

Key:

Yes ( ) Successful

No ( ) Unsuccessful

— Not applied

(Number in parentheses refers to accompanying notes)

Table 4-1

SUMMARY OF RESULTS (Page 2 of 3)

Notes:

X-ray Radiography

1. Detected all voids corresponding to sensitivities of 1.6 percent for 2-in.-thick material, 2.2 percent for 1-in.-thick material, and 6.4 percent for 1/4-in.-thick material with a resolution of at least 0.020 in. between voids.

2. Detected all cracks used (as small as 25 percent of thickness deep, 0.002 in. wide).

3. Detected all delaminations corresponding to sensitivities of 2.4 percent for 2-in.-thick material, 2.2 percent for 1-in.-thick material, and 4.8 percent for 1/4-in.-thick material.

4. Detected density variations of ±0.25 lb/ft^3 for 2-in.-thick material, ±0.33 lb/ft^3 for 1-in.-thick material, and ±1.20 lb/ft^3 for 1/4-in.-thick material.

5. Detected all holes used (as small as 0.013-in. dia).

6. Was not possible to create controlled cracks. Should be able to detect crack widths of at least 0.013 in., based on results with holes.

7. Detected using edge exposure—thicknesses larger than those obtained visually.

8. Detected using edge exposure—width larger than that obtained visually.

9. Detected all voids corresponding to sensitivity of 1.6 percent for 2-in.-thick material with resolution of at least 0.0125 in. between voids.

10. Was not possible to create controlled cracks. Should be able to detect crack widths of at least 0.016 in., based on results with holes.

11. Detected all bondline voids (as small as 3/4 in. in diameter).

12. Detected all unbonds (as small as 3/4 in. in diameter), but probably was sensitive to presence of Mylar film rather than unbond condition itself. Would probably not detect more realistic simulation of unbond.

Acoustic Transmission

1. Detectable using air coupling, 1-in. dia microphone.

2. Detectable using air coupling, 1-in. dia microphone. Contact microphone coupling useful as a check.

3. Suggest that the average response be determined for samples covering the allowable range in density. Differences then due to defects other than density (the effect of which is small).

4. The amplitude of the difference in response was very small. Additional measurements to establish the variation in response due to material density variations is needed to determine whether or not the loss of adhesion defect was detected.

5. Results similar to those for the loss-of-adhesion defect.

6. Results similar to those for the loss-of-adhesion defect.

7. Significant differences below 14,000 Hz. Differences small compared to those for reflections.

8. Results similar to those for the bondline void defect.

Acoustic Reflection

1. Detected using air coupling, 1-in.-dia microphone for void defects in 1- and 1/4-in.-thick material. Differences due to density variations were too great to allow detection for the 2-in.-thick material.

2. Results similar to those for the void defect.

3. Variation in response due to density smaller for 1-in.-thick material than for 1/4-in.-thick material.

4. Amplitude of difference in response greater than that obtained using transmission. Difference in response may be large enough for detection. Information on the variation due to sample density is needed to determine whether or not loss-of-adhesion defect was detected.

5. Results similar to those for loss-of-adhesion defect.

6. Results similar to those for loss-of-adhesion defect.

7. Significant differences below 10,000 Hz. Difference in response larger than those for transmission.

8. Difference in response substantially below zero for unbonds in 2-in.-thick material and above zero for unbonds in 1/4-in-thick material.

Microwave

1. Different phase and amplitude for voids as compared to control, delaminations, and density variations. (The differences were greater at 15 GHz.) More work needed to determine reason for difference and to develop scanning techniques.

2. Different phase and amplitude for delaminations as compared to control, voids, and density variations. (The differences were greater at 15 GHz.) More work needed to determine reason for difference and to develop scanning techniques.

3. Different phase and amplitude for density variations as compared to defect free, voids, and delaminations. The differences were greater at 15 GHz. More work needed to determine reason for difference and to develop scanning techniques.

4. Amplitude of reflected microwaves is proportional to the percentage of moisture present. The results at 15 GHz are more sensitive and uniform than those at 9 GHz.

Table 4-1

SUMMARY OF RESULTS (Page 3 of 3)

Microwave (Continued)

5. Very little difference in phase and amplitude as compared to control. Suggests possibility that further work for uncoated and coated may not be successful.

6. Very little difference in phase and amplitude as compared to control. Suggests possibility that further work for uncoated and coated may not be successful.

7. Results similar to those for moisture content in uncoated material except that the results were not as conclusive for the 2-in. -thick material.

8. Results suggest that the phase, not the amplitude, may be related to the presence of a bondline void. More work is needed to determine reason for relationship and to develop scanning techniques.

9. Results suggest that the phase, not the amplitude, may be related to the presence of an unbond. More work is needed to determine reason for relationship and to develop scanning techniques.

10. Results suggest that the phase, not the amplitude, may be related to the presence of water. More work is needed to develop scanning techniques.

High-Frequency Ultrasonics

1. Fokker Bond Tester, ultrasonic pulse-echo, and Sondicator detected all the voids used (as small as 3/4 in. in diameter) when applied to the metallic side. These techniques were either not applicable or were not successful for application from the RSI side.

2. Fokker Bond Tester and Sondicator detected all the unbonds used (as small as 3/4 in. in diameter) except the 3/4 in. in diameter unbond in 2-in. -thick material when applied to the metallic side. Ultrasonic pulse-echo did not detect any of the unbonds used. These techniques were either not applicable or were not successful for application from the RSI side.

Holography

1. Very sensitive detection of cracks using either mechanical or thermal stressing. Mechanical stressing, unlike thermal stressing, displayed all the cracks present.

2. Detectable in real time using thermal stressing but not detectable using mechanical stressing.

3. Not detectable from the RSI side. Detectable from the metallic side using either mechanical or thermal stressing.

Visual

1. Not detectable (as large as 0.128 in. in diameter by 50 percent of the thickness in depth) for 2- or 1-in. -thick material using 500-W backlighting. Detectable (as small as 0.064 in. in diameter by 50 percent of the thickness in depth) for 1/4-in. -thick material. Less sensitive than x-ray radiography.

2. Detectable using low-power magnification but time consuming and difficult.

3. Large cracks in the coating detectable but time consuming and difficult. Very fine cracks undetectable (especially for thicker material). Less sensitive than holography.

Section 5
CONCLUSIONS AND RECOMMENDATIONS

X-ray radiography was found to be the best technique of those considered for the detection of voids, cracks, delaminations, and density variations in uncoated material; holes and thickness variations in the coating; voids and cracks in coated material; and voids in the bondline of coated and bonded material. Interferometric holography was better for cracks in the coating and coating loss of adhesion. From a practical standpoint, radiography will not be applicable for coating-thickness variations (because edge exposures are required) or voids in the bondline (because current Space Shuttle configurations limit access to the RSI side only). The sensitivity required for the detection of defects in the RSI was found to be 1.6 percent for 2-in.-thick material, 2.2 percent for 1-in.-thick material, and 4.8 percent for 1/4-in.-thick material. A resolution of at least 0.0125 in. between voids was observed. These sensitivities and resolutions were obtained for selected exposure parameters using the lowest applied kilovoltage consistent with exposure durations of 150 sec or less.

X-ray radiography is recommended for both uncoated and coated material as part of an in-process quality control program. The radiographs should be taken in the conventional manner, using exposure parameters selected for the best sensitivity. Radiography often tends to be a time-consuming and expensive approach. Only exposure durations up to a maximum of 180 sec were investigated in this program as a reasonable upper limit. If considerably shorter exposures are required in the interests of economy, additional work should be performed to determine if the sensitivity and resolution remain acceptable. The use of new, easily processed paper instead of film should be investigated as a means of saving time and money.

Acoustic techniques showed promise for detection of voids and delaminations in both uncoated and coated material, and voids and unbonds in the bondline of coated and bonded material. Where access to both sides is possible, radiography was far superior to the acoustic techniques. Further work on acoustic-reflection techniques for coated and bonded material is recommended as this technique showed promise for detection of bondline defects and can be applied when access is limited to the RSI side only. Emphasis should be placed on the possibility of using air coupling for scanning techniques. Further studies should be performed to determine the type, size, and placement of the receiving microphone for the best sensitivity. An attempt should be made to develop an acoustic-reflection-scanning technique using a single narrow band of frequencies in order to keep the necessary associated electronics and analysis to a minimum. Conceptually, the final probe configuration might consist of a small speaker and microphone enclosed in a five-sided acoustic chamber (designed to minimize background noise and attenuate the sound transmitted by the speaker through the chamber), equipped with pneumatic wheels to provide the proper separation of the probe from the surface and to allow easy scanning.

Microwave techniques were successful for moisture detection in uncoated, coated, and coated and bonded material. The nature of the response to moisture shifted from primarily a change in amplitude for the uncoated and coated material to primarily a change in phase for the coated and bonded material due to the presence of a metal backing. The results at 15 GHz were more sensitive and uniform than those at 9 GHz. Microwave-reflection techniques are recommended as part of an in-process quality control program for moisture detection. Further work is recommended for moisture detection in coated and bonded material to determine a means of maintaining a constant horn-to-metal-plate separation in combination with a scanning approach. The microwave techniques also showed some promise for voids, delaminations, and density variations in uncoated material, but not in coated material. X-ray radiography was better for these defects. Further work is recommended for microwave-reflection techniques for coated and bonded material because this technique, like acoustic reflection, showed promise for detection of bondline defects and can be applied when access is limited to the RSI side only. If compensation cannot be made for the effect of the metal backing, then the technique can at least be used to measure the RSI thickness.

While the high-frequency ultrasonic techniques evaluated were successful for detection of voids (and unbonds in some cases) from the metallic side only, the current Space Shuttle configuration restricts access to the RSI side only. Thus, these techniques will have little applicability unless the RSI is first attached to substructure which, in turn, is then attached to the primary structure.

The beta-backscatter technique was unsuccessful for detection of holes and cracks in the coating. Further work is not recommended for this technique. Even if the technique were successful, application to RSI bonded to primary structure would create radiation safety problems and would be extremely time consuming and expensive.

The application of tape-backed liquid crystals as a thermal technique for the detection of holes and cracks in the coating and voids and unbonds in the bondline (when applied to the metal side) was unsuccessful. In the case of the coating, the surface texture was so rough, any possible defects would be completely masked. The effects of a rough surface texture should be less adverse for radiometer techniques than for liquid-crystal techniques. Radiometer-thermal techniques should be investigated for applicability to coating defects and other sources of nonuniform heat transfer.

Interferometric holography was successful for detection of cracks and coating loss-of-adhesion defects. Fairly crude thermal- and mechanical-stressing techniques were used. Nevertheless, the technique was excellent for the detection of coating cracks, and no doubt further work will reveal better methods of stressing the material (only extremely small stresses are required) to determine the presence of loss-of-adhesion defects more easily. Although not examined in this program, interferometric holography might also be capable of detecting holes in the coating. While this technique was capable of detecting voids in the bondline from the metallic side, the technique was not successful when applied from the RSI side. Further work is recommended to develop the interferometric-holography technique for detection of coating defects and possible bondline defects. Different additional stressing and holographic techniques (such as the use of a pulsed laser) should be investigated.

Visual examination was of limited usefulness. This approach was capable of detecting only relatively large defects in thin material. X-ray radiography and interferometric holography were much more sensitive to defects than could ever be expected of visual inspection.

The attempt at relating NDT measurements to material properties was successful only in establishing a possible trend between microwave reflection measurements (or x-ray-radiography density measurements) to the tensile strength. More data would be required to determine if the trend does indeed exist. This possibility, while interesting, is of considerably less importance at the moment than the problem of simply detecting defects in the material.

The most difficult problem remaining at the conclusion of this program is the inspection of the RSI material and especially the bondline of RSI bonded directly to primary structure. Serious thought should be given to the fact that presently none of the techniques considered provides a satisfactory inspection for bondline defects given access only to the RSI side. Assuming that the integrity of the bond is important, either access to the metallic side will have to be made available or an extensive effort will be required to further develop acoustic reflection, microwave reflection, and holographic techniques for this problem. Using a combination of the techniques evaluated in this program, a possible in-process NDT procedural flow chart is shown in Figure 5-1.

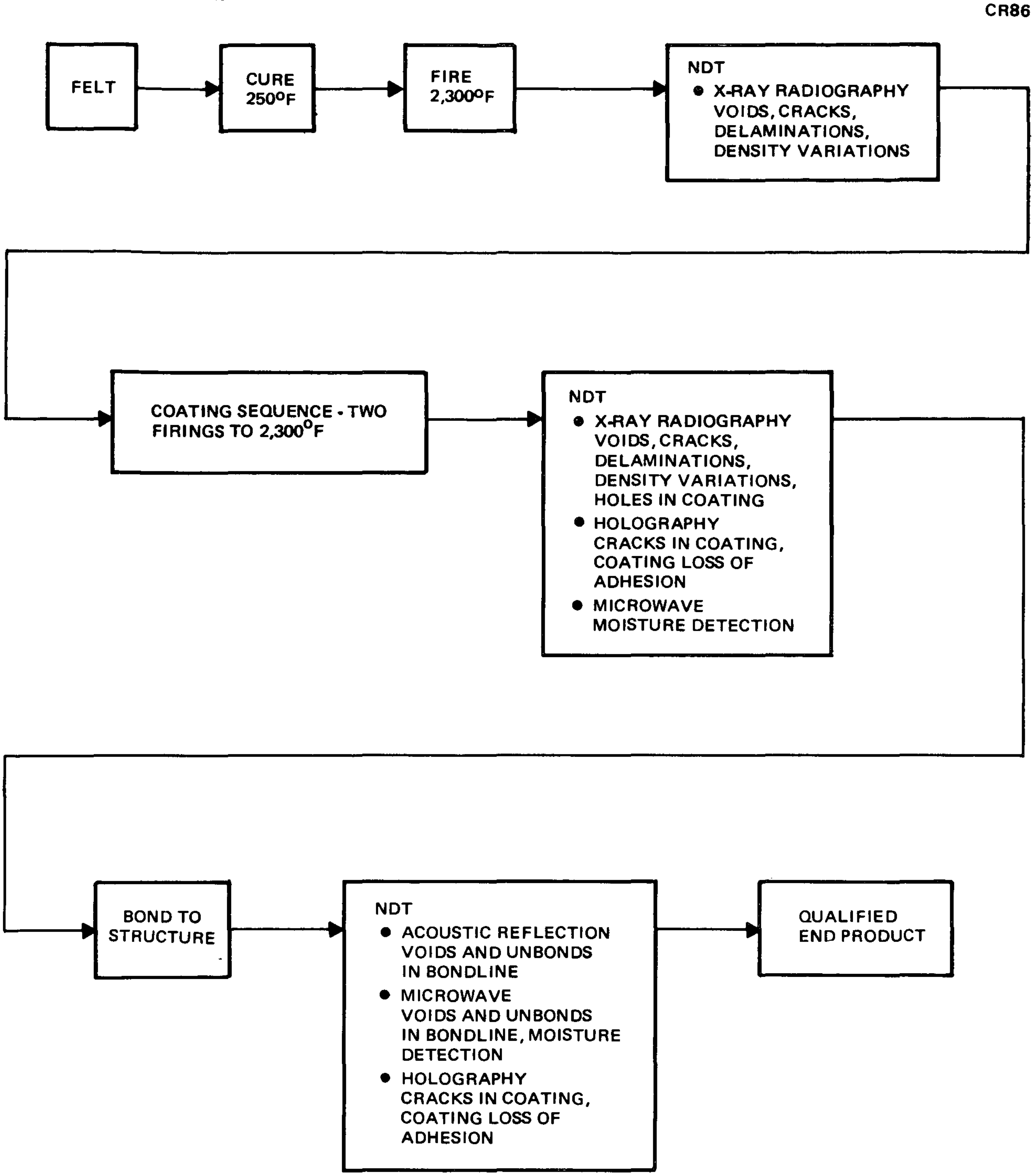

Figure 5-1. In-Process Nondestructive Analysis

PRECEDING PAGE BLANK NOT FILMED

Appendix
THEORETICAL SENSITIVITIES

Theoretical radiographic sensitivity is affected by (1) graininess, (2) unsharpness, and (3) the contrast of the defect image on the film. Graininess is the visual impression of nonuniform density in a uniformly exposed radiographic image. Unsharpness is the width of the band of density change in the image of a sharp edge. Contrast is the change in density across the image of a sharp edge.

Graininess is due to the random, statistical exposure of individual silver particles. A particle of black metallic silver resulting from the development of a single photographic grain is usually less than 0.001 mm (0.00004 in.) wide. For the purposes of this program, the contribution of graininess as a factor affecting sensitivity is insignificant for the extrafine-grain Type M film used.

Unsharpness is composed of (1) geometric unsharpness and (2) inherent unsharpness. The total unsharpness is given by (Reference 19).

$$U^2 = U_G{}^2 + U_I{}^2$$

The geometric unsharpness arises from the finite size of the source and is dependent on the source-film and object-film distances as given by $U_G = \frac{Fx}{D}$ where F is the focal spot size, x is the object-to-film distance, and D is the source-to-film distance. For the exposure parameters and sample thicknesses of this program, the geometric unsharpnesses are

Two-inch material

$$U_{G2} = 0.00437 \text{ in.}$$

One-inch material

$$U_{G1} = 0.00219 \text{ in.}$$

Quarter-inch material

$$U_{G1/4} = 0.00055 \text{ in.}$$

Preceding page blank

Inherent unsharpness is caused by the scattering of secondary electrons in the film emulsion. The incident x-rays excite electrons, which travel a certain distance before coming to rest. This distance is dependent upon the original energy of the x-ray. The inherent unsharpness of Type M film over the 20 to 50-kV range is less than 0.0004 in. Using this value for the inherent unsharpness, the total unsharpnesses are:

Two-inch material

$$U_{T2} = 0.0044 \text{ in.}$$

One-inch material

$$U_{T1} = 0.0022 \text{ in.}$$

Quarter-inch material

$$U_{T1/4} = 0.0007 \text{ in.}$$

The radiographic contrast can be derived from basic principles of the interaction of radiation with matter. Radiographic contrast is a combination of both subject contrast and film contrast.

Subject contrast is the relative change in intensity of radiation as it passes through the subject. Radiation is both scattered and absorbed by materials. Neglecting scattering, which has the effect of reducing the contrast, the transmitted intensity is given by $I = I_o e^{-\mu x}$, where I_o is the initial intensity, μ is the total linear absorption coefficient (characteristics of the incident energy and of the absorbing material), and x is the material thickness. From this equation, the ratio of intensities for different thicknesses is given by

$$\frac{I_2}{I_1} = e^{-\mu(x_2 - x_1)}$$

Film contrast is the relative change in photographic density due to a change in the exposure. The Bunsen-Roscoe reciprocity law states that the exposure is proportional to the product of the radiation intensity I and the duration of exposure t.

The relationship between the photographic density and the exposure depends upon the type of film and is usually given as a characteristic curve of density versus log of relative exposure. For the range of densities employed in this program, the density versus log relative exposure relationship may be approximated by an equation for a straight line. Thus, the photographic density may be given by $D = G \log_{10} (I \times t) + C$, where G is the slope of the characteristic curve over the density range of interest, and C is a constant. The change in film density due to changes in radiation intensity for a given exposure duration t is given by

$$D_2 - D_1 = G \log_{10} \frac{I_2}{I_1} = \frac{G}{2.3} \ln \frac{I_2}{I_1}$$

If the changes in intensity are due to changes in material thickness, the change in density is given by combining the two previous equations.

$$D_2 - D_1 = \frac{-\mu G}{2.3} (X_2 - X_1)$$

The minus sign represents the fact that the density is greater for thinner materials. This may be rewritten as

$$X_2 - X_1 = \frac{-2.3 (D_2 - D_1)}{\mu G}$$

The slope of the density versus log relative exposure curve for a density range of 2.0 to 4.0 for Type M film results in the value G = 5.88.

For an average density of 3.0 and the minimum detectable density change of 1.6 percent, the change in density is given by $D_2 - D_1 = 0.048$. Combining these results,

$$-\Delta X = \frac{0.0188}{\mu}$$

To obtain an estimate of ΔX, the value of μ for the energies and material used must be found. The RSI material is approximately 77 percent by weight Al_2O_3 and 23 percent by weight SiO_2. The material also has a porosity of 87 percent. That is, by volume the material is 87 percent air. The mass attenuation coefficient for RSI is given by

$$\frac{\mu}{\rho} (\text{RSI}) = \sum_i \left(\frac{\mu}{\rho}\right)_i R_i$$

where $\left(\frac{\mu}{\rho}\right)_i$ is the mass attenuation coefficient for an element present in the material and R_i is the relative percentage by weight of that element. The total linear attenuation coefficient for RSI is given by the product of the mass attenuation coefficient and the density. The density of RSI is 15 lb/ft^3 (0.2403 g/cc). Thus, a 1-cc sample of RSI would have a mass of 0.2403 g. Of the 1-cc sample, 0.87 cc is air. The density of air is 0.0013 g/cc. Thus, the mass of air present in a 1-cc sample of RSI is 0.0011 g. Combining these two masses, the effective density of an RSI sample containing air is 0.2414 g. Air consists of 75.6% N, 23.1% 0, and 1.3% A. $Al_2 0_3$ consists of 53% Al and 47% 0. $Si0_2$ consists of 47% Si and 53% 0. Combining these figures, the relative percentages by weight of each of the elements is

Element	Percent
0	48.3
Al	40.6
Si	10.7
N	0.4
A	0.0

The mass attenuation coefficient is also a function of the energy of the incident radiation. The energy of the x-radiation from an x-ray tube varies with the applied voltage. The voltage applied to an x-ray tube is used to accelerate an electron. The kinetic energy an electron acquires as the result of being accelerated across a potential difference of 1 V is 1 eV. The maximum energy of an electron for a 50-kV applied voltage is thus 50 keV. The energy of the x-radiation generated as the electron collides with the target can at most equal the kinetic energy of the electron. Thus, the maximum x-ray energy from an x-ray tube with an applied voltage of 50 kV is 50 keV. In general, x-rays of many energies are emitted with a continuous spectrum. The shorter the wavelength, the higher the energy. The peak in this spectrum occurs for an energy lower than the maximum possible electron energy. For the half wave, self-rectifying tube employed in this program, the peak in the radiation intensity expressed in keV is approximately numerically equal to 2/3 the applied voltage in kV. The mass attenuation coefficients for the exposures used in this program as extrapolated from tables in the NDT Handbook (Reference 19) are:

MASS ATTENUATION COEFFICIENTS

Element	22.5 kV (cm^2/g)	35 kV (cm^2/g)	45 kV (cm^2/g)
0	1.80	0.630	0.371
Al	8.08	2.44	1.13
Si	10.6	3.32	1.44
N	1.20	0.450	0.301

Using these values for the mass attenuation coefficients and the relative percentages of each element, the linear attenuation coefficients for RSI as a function of the applied tube voltages are:

LINEAR ATTENUATION COEFFICIENTS

Voltage (kV)	μ (1/in.)
45	0.486
35	1.013
22.5	3.243

The corresponding values for ΔX are:

Material Thickness (in.)	Voltage (kV)	ΔX (in.)
2	45	0.0386
1	35	0.0185
1/4	22.5	0.0058

Combining these values for ΔX with the values for the unsharpness, the theoretical sensitivities are:

Material Thickness (in.)	Sensitivity (%)
2	2.2
1	2.1
1/4	2.6

PRECEDING PAGE BLANK NOT FILMED

REFERENCES

1. E. L. Rusert. Development of Rigidized, Surface Insulative, Thermal Protection System for Shuttle Orbiter. NASA Report MSC 02565, February 1971.

2. K. N. Lohse. Application of Photographic Extraction Techniques to Nondestructive Testing of Graphite and Other Materials. AFML-TR 70-162 November 1970.

3. J. S. Evangelides and R. A. Meyer. Investigation of the Properties of Carbon-Carbon Composites and Their Relationship to Nondestructive Test Measurements. Annual Report No. MDC G1004, Contract F33615-69-C-1640, June 1970.

4. Radiography in Modern Industry. Eastman Kodak Company, Third Edition, 1969.

5. W. N. Clotfelter, B. F. Bauhston, and P. C. Duren. The Nondestructive Evaluation of Low Density Foam-Aluminum Composite Materials. NASA Report No. 53940, October 1969.

6. J. Haynes. Development of Nondestructive Test Device for Evaluation of 3/4-Inch Thick Polyurethane Spray-On Foam Insulation (SOFI) on the Saturn S-II Stage. N69-35245, May 1969.

7. R. Hochschild. Microwave Nondestructive Testing in One (Not-So-Easy) Lesson. Materials Evaluation, January 1968.

8. R. Hochschild. Applications of Microwaves in Nondestructive Testing. Nondestructive Testing, March-April 1963.

9. T. M. Lavelle. Microwaves in Nondestructive Testing. Materials Evaluation, November 1967.

10. S. Summerhill. Microwaves in the Measurement of Moisture. Instrument Review October 1967.

11. H. B. Taylor. Microwave Moisture Measurement. Industrial Electronics, February 1965.

12. A. D. Lucian and R. W. Cribbs. The Development of Microwave NDT Technology for the Inspection of Nonmetallic Materials and Composites. Aerojet-General Corporation, June 1967.

Preceding page blank

13. A. E. Oaks, Microwave Studies of Bonding. General Electric, Technical Information Series No. 68SD208, 1967.

14. W. L. Shelton. Electron Radiography. AFMC Report No. T6-6214, June 1967.

15. D. K. Wilburn. A Thermal Imaging Technique of Nondestructive Testing. ATAC Technical Report No. 8883, June 1965.

16. E. Sprow. Liquid Crystals—A Film in Your Future. Machine Design, February 1969.

17. D. A. Tiede. Interferometic Holography Inspection of Bond Lines for Teflon Aluminum Structures. McDonnell Douglas Astronautics Co. Report No. MDC G2082, February 1972.

18. K. J. Maxwell and C. E. Wiswall. Application of Pulsed Laser to Holographic NDT. MDAC Report No. 5138-79, June 1970.

19. R. C. McMaster. Nondestructive Testing Handbook, 1959.